



Technische Universität München

Max-Planck-Institut für Physik
(Werner-Heisenberg-Institut)

Techniques for higher order corrections and their application to LHC phenomenology

Johannes Kaspar Schlenk

Vollständiger Abdruck der
von der Fakultät für Physik
der Technischen Universität München
zur Erlangung des akademischen Grades eines
Doktors der Naturwissenschaften (Dr. rer. nat.)
genehmigten Dissertation.

Vorsitzender: Prof. Dr. P. Fierlinger
Prüfer der Dissertation: 1. Hon.-Prof. Dr. W. F. L. Hollik
2. Prof. Dr. A. Weiler

Die Dissertation wurde am 29.08.2016
bei der Technischen Universität München eingereicht und
durch die Fakultät für Physik am 15.09.2016 angenommen.

This thesis is based on the author's work conducted at the Max Planck Institute for Physics (Werner-Heisenberg-Institut) in Munich. Parts of this work have already been presented in the following publications:

Articles

- [1] S. Borowka, N. Greiner, G. Heinrich, S. P. Jones, M. Kerner, J. Schlenk et al., *Full top quark mass dependence in Higgs boson pair production at NLO*, 1608.04798.
- [2] S. Borowka, N. Greiner, G. Heinrich, S. Jones, M. Kerner, J. Schlenk et al., *Higgs Boson Pair Production in Gluon Fusion at Next-to-Leading Order with Full Top-Quark Mass Dependence*, *Phys. Rev. Lett.* **117** (2016) 012001, [1604.06447].
- [3] S. Borowka, G. Heinrich, S. P. Jones, M. Kerner, J. Schlenk and T. Zirke, *SecDec-3.0: numerical evaluation of multi-scale integrals beyond one loop*, *Comput. Phys. Commun.* **196** (2015) 470–491, [1502.06595].
- [4] G. Cullen et al., *GOSAM-2.0: a tool for automated one-loop calculations within the Standard Model and beyond*, *Eur. Phys. J.* **C74** (2014) 3001, [1404.7096].
- [5] M. Argeri, S. Di Vita, P. Mastrolia, E. Mirabella, J. Schlenk, U. Schubert et al., *Magnus and Dyson Series for Master Integrals*, *JHEP* **03** (2014) 082, [1401.2979].
- [6] G. Heinrich, A. Maier, R. Nisius, J. Schlenk and J. Winter, *NLO QCD corrections to $W^+W^-b\bar{b}$ production with leptonic decays in the light of top quark mass and asymmetry measurements*, *JHEP* **06** (2014) 158, [1312.6659].
- [7] S. Alioli et al., *Update of the Binoth Les Houches Accord for a standard interface between Monte Carlo tools and one-loop programs*, *Comput. Phys. Commun.* **185** (2014) 560–571, [1308.3462].

Proceedings

- [1] S. Borowka, G. Heinrich, S. Jahn, S. P. Jones, M. Kerner, J. Schlenk et al., *Numerical multi-loop calculations: tools and applications*, in *17th International workshop on Advanced Computing and Analysis Techniques in physics research (ACAT 2016) Valparaiso, Chile, January 18-22, 2016*, 2016. 1604.00267.
- [2] J. Schlenk and T. Zirke, *Calculation of Multi-Loop Integrals with SecDec-3.0*, in *Proceedings, 12th International Symposium on Radiative Corrections (Radcor 2015) and LoopFest XIV (Radiative Corrections for the LHC and Future Colliders)*, 2016. 1601.03982.
- [3] P. Mastrolia, M. Argeri, S. Di Vita, E. Mirabella, J. Schlenk, U. Schubert et al., *Magnus and Dyson Series for Master Integrals*, *PoS LL2014* (2014) 007.
- [4] H. van Deurzen et al., *Automated one-loop calculations with GoSam 2.0*, *PoS LL2014* (2014) 021, [1407.0922].
- [5] J. Schlenk, G. Heinrich and J. Winter, *NLO QCD corrections to $W^+W^-b\bar{b}$ production and top quark observables*, *PoS RADCOR2013* (2013) 033, [1312.5666].
- [6] G. Cullen et al., *GoSam @ LHC: algorithms and applications to Higgs production*, *PoS RADCOR2013* (2013) 029, [1312.1761].
- [7] G. Cullen et al., *NLO QCD Production of Higgs plus jets with GoSam*, *PoS EPS-HEP2013* (2013) 446, [1311.5191].
- [8] G. Cullen et al., *GoSam applications for automated NLO calculations*, *J. Phys. Conf. Ser.* **523** (2014) 012056, [1309.3741].

Abstract: Tools and techniques for higher order corrections and their application to LHC phenomenology are presented.

The process $pp \rightarrow W^+W^-b\bar{b}$ with leptonic decays of the W -bosons is calculated at NLO QCD. It is used for a phenomenological study of the effect of higher order and non-factorizable contributions on top quark mass measurements based on the m_b observable. The required one-loop amplitudes are calculated with the publicly available program GOSAM. New features of GOSAM-2.0 are presented, which extend its range of applicability and make the code faster and more stable.

A strategy to bring differential equations, which are used for the analytical integration of multi-loop Feynman integrals, in a canonical form is introduced. It is applied to the calculation of two-loop QED vertex integrals.

Sector decomposition is a method for the numerical calculation of multi-loop and multi-scale integrals. A new sector decomposition algorithm based on convex geometry is presented which is guaranteed to terminate, and leads to a small number of sectors and fast runtimes. The geometric algorithm is implemented in the public program SECDEC-3.0.

NLO QCD corrections to the production of a Higgs boson pair in gluon fusion are presented. The full top quark mass dependence is retained throughout the calculation. For the generation of the two-loop virtual amplitude an extended version of GOSAM is used. The appearing two-loop integrals are calculated with SECDEC-3.0. Substantial differences with respect to various calculations which contain only partial top quark mass corrections are found, emphasising the importance of the full top quark mass dependence at NLO.

Zusammenfassung: Es werden Methoden für Korrekturen höherer Ordnung und deren Anwendung auf LHC Phänomenologie präsentiert.

Der Prozess $pp \rightarrow W^+W^-b\bar{b}$ mit leptonischen Zerfällen der W -Bosonen wird in NLO QCD berechnet. Er wird verwendet für eine phänomenologische Studie der Effekte von NLO und nichtfaktorisierbaren Korrekturen auf Bestimmungen der Top Quark Masse durch die $m_{t\bar{t}}$ Observable. Die beitragenden Einschleifenamplituden werden mit dem öffentlichen Programm GOSAM berechnet. Version 2.0 von GOSAM wird präsentiert, in der die Anwendungsmöglichkeiten erweitert und Schnelligkeit und Stabilität des Programms erhöht wurden.

Eine Strategie, um Differentialgleichungen, die fuer die analytische Berechnung von Mehrschleifenintegralen verwendet werden, in eine kanonische Form zu bringen, wird vorgestellt. Diese wird auf die Berechnung von Zweischleifenintegralen angewendet, die zum QED Vertex beitragen.

Sector Decomposition ist eine Methode fuer die numerische Berechnung von Mehrschleifenintegralen mit mehreren Skalen. Ein neuer Sector Decompositionsalgorithmus, der auf konvexer Geometrie basiert, wird präsentiert. Es wird gezeigt, dass dieser Algorithmus immer terminiert, er führt darüber hinaus zu einer kleinen Zahl von Sektoren und hat eine geringe Laufzeit. Der geometrische Algorithmus ist in dem öffentlichen Programm SECDEC-3.0 implementiert.

Die NLO QCD Korrekturen zu der Produktion eines Paares von Higgs Bosonen durch Gluon Fusion werden präsentiert. In der Rechnung wird die exakte Top Quark Massenabhängigkeit berücksichtigt. Für die Erzeugung der Zweischleifenamplitude wird eine erweiterte Version des Programms GOSAM verwendet. Die auftretenden Zweischleifenintegrale werden mit SECDEC-3.0 numerisch berechnet. Es werden substanzielle Unterschiede zu verschiedenen Rechnungen gefunden, die nur genäherte Top Quark Massenkorekturen enthalten. Dies hebt die Wichtigkeit der exakten Behandlung von Top Quark Masseneffekten hervor.

Contents

1	Introduction	13
2	Calculations for hadron colliders	17
2.1	Factorization and parton distribution functions	17
2.2	Hard scattering and perturbation theory	19
2.3	Divergences	20
2.3.1	Ultraviolet divergences	21
2.3.2	Infrared divergences	21
2.4	Parton shower and hadronization	23
I	NLO phenomenology	25
3	Calculation of one-loop amplitudes	27
3.1	General amplitude structure	27
3.2	Master integral basis	28
3.3	Reduction methods	29
3.3.1	Passarino-Veltman reduction	29
3.3.2	OPP reduction	30
4	GoSam	33
5	NLO QCD corrections to $W^+W^-b\bar{b}$ production	37
5.1	Introduction	37
5.2	Computational framework	39
5.3	Treatment of top quarks	40
5.4	General input parameters	41
5.5	Numerical results for the LHC at 7 TeV	42
5.6	Study of theoretical uncertainties in top quark mass measurements	45
5.6.1	Top quark mass definition	45
5.6.2	Mass measurement using the $m_{t\bar{b}}$ observable	46

II	Beyond the one-loop order	55
6	Calculation of multi-loop amplitudes	57
6.1	Form factor decomposition	57
6.2	Integration by parts reduction	58
6.2.1	Quasi-finite basis	59
6.3	Differential equations	61
6.3.1	Two-loop QED vertex	63
7	Sector decomposition	69
7.1	Feynman parameter integrals	69
7.2	Singularities of Feynman parameter integrals	71
7.3	Sector decomposition	72
7.3.1	Iterated decomposition	73
7.4	Geometric decomposition	75
7.4.1	Convex geometry	75
7.4.2	The geometric algorithm	78
7.5	Contour deformation	83
7.6	Subtraction	85
7.7	Numerical integration	86
8	SecDec-3.0	89
8.1	Program structure	90
8.2	New features of SECDEC-3.0	90
8.2.1	Improved user interface	90
8.2.2	Implementation of geometric decomposition algorithms	93
9	Higgs boson pair production in gluon fusion	97
9.1	The Higgs sector	97
9.2	The process $gg \rightarrow hh$	98
9.3	Form factor decomposition	100
9.4	NLO cross section	102
9.4.1	Parton distribution functions	102
9.4.2	LO cross section	103
9.4.3	Virtual two-loop contributions	103
9.4.4	Real radiation	105
9.5	Top quark mass expansion	106
9.6	Numerical results	106

10 Conclusion and outlook

111

1 Introduction

Elementary particle physics is the study of nature at the highest energies, or equivalently smallest distance scales. The best currently available tool for this study is the Large Hadron Collider (LHC), where protons are accelerated and brought to collision with a center of mass energy of 13 TeV. The collision events are recorded by the four big detectors ATLAS [1], CMS [2], LHCb [3], ALICE [4]. In 2012 the two LHC experiments ATLAS [5] and CMS [6] discovered a scalar boson. Its measured properties have so far been consistent with the Standard Model Higgs boson. Until then the Higgs boson which was predicted already in the 1960s [7–12] had been the last unobserved particle of the Standard Model of particle physics.

The Standard Model of particle physics (SM) is a Quantum Field Theory which currently provides our most complete description of the interactions between elementary particles. It is a gauge theory based on a $SU(3)_C \times SU(2)_L \times U(1)_Y$ gauge symmetry which is broken by the Higgs mechanism to the group $SU(3)_C \times U(1)_{em}$. The $SU(3)_C$ subgroup is the gauge symmetry of quantum chromodynamics (QCD), while $SU(2)_L \times U(1)_Y$ is the gauge symmetry of the electroweak (EW) theory. While the SM is very successful for many observed phenomena, it is clear that it is not a complete description of nature at a fundamental level. The most important experimental observations not described by the SM are the matter-antimatter asymmetry, dark matter, the accelerated expansion of the universe, and gravity. Neutrino masses are also not included in the SM, however neutrino mass terms can be added. There are also theoretical issues with the SM such as the hierarchy problem and the strong CP -problem.

The investigation of the mechanism of electroweak symmetry breaking and the search for physics beyond the Standard Model (BSM) are among the main goals of the LHC. To achieve these goals precise theoretical predictions for signal and background processes are required. Theoretical uncertainties should be of the

same order as the experimental uncertainties achieved by the LHC experiments. Predictions for the LHC are mainly obtained as a perturbative expansion in the SM couplings. In this thesis we concentrate on higher order corrections in the expansion of the QCD coupling, nevertheless EW corrections and an improved understanding of nonperturbative effects are also necessary to achieve the required precision.

The Les-Houches wishlist is a list of processes whose calculation to a given precision is desired by experimentalists and is achievable with current technology. After all processes on the first wishlist [13, 14], which consisted mainly of next to leading order (NLO) QCD corrections, had been calculated, a new wishlist containing NNLO QCD, NLO EW, and mixed QCD+EW corrections was recently proposed [15].

The calculation of the processes on the first list was possible due to the high level of automation achieved in the computation of NLO QCD corrections. To calculate the list of processes on the new wishlist, a similar level of automation as for NLO QCD corrections will be required beyond NLO.

In this thesis methods and tools for higher order theoretical predictions in the SM, and their application to Higgs boson and top quark processes at the LHC are presented.

In Chapter 2 a short introduction to the calculation of higher order calculations in perturbative QCD at hadron colliders is given.

The first part of the thesis then gives details on a NLO QCD calculation of production and decay of a pair of top quarks including non-resonant effects. The top quark is the heaviest particle in the SM and was discovered in 1995 at the Tevatron collider [16, 17]. Its mass is an important parameter in the SM, and the uncertainty on its experimentally measured value limits the precision of many theoretical predictions.

The calculation is performed using the one-loop program GOSAM [18, 19] and the Monte-Carlo generator SHERPA [20]. In Chapter 3 methods for the calculation of one-loop amplitudes are presented. The program GOSAM, which is a public tool for the automated calculation of one-loop amplitudes, is introduced in Chapter 4, and details on its most recent version 2.0 are given [19]. Its range of applicability is increased by the implementation of higher rank tensor integrals and an improved interface to Monte-Carlo event generators [21]. Furthermore the code generation is improved and a rescue system for numerically unstable points is added.

In Chapter 5 the process $pp \rightarrow W^+W^-b\bar{b}$ at NLO in QCD is presented [21]. Similar calculations appeared previously in [22–24]. The effect of higher or-

der corrections and non-factorizable contributions on theoretical uncertainties of top quark mass measurements based on the m_{tb} observable at the LHC is studied. Sizeable corrections are found with respect to the calculation in the narrow width approximation with LO top quark decays commonly used in experimental analyses.

The second part of the thesis is concerned with calculations beyond the one-loop order.

In Chapter 6 details on the method of differential equations for the analytic integration of multi-loop Feynman integrals [25–28] are given. A method to bring the differential equations in a canonical form identified by Henn [28], where the dependence on the dimensional regularization parameter factorizes, is introduced. It is applied to the calculation of two-loop integrals contributing to the QED vertex [29].

Sector decomposition is a method for the (numerical) calculation of multi-loop Feynman integrals and more general parameter integrals in dimensional regularization [30–33]. Chapter 7 contains a review of the method. A new sector decomposition algorithm which uses convex geometry is presented. The geometric decomposition method is guaranteed to terminate, and usually leads to a smaller number of sectors and a lower runtime compared to other decomposition algorithms. It is based on the original geometric decomposition method developed by Kaneko and Ueda [34, 35].

The public program SECDEC [36, 37] implements the sector decomposition algorithm. Its most recent version SECDEC-3.0 [38] contains the new geometric decomposition algorithm (Chapter 8). In the new version phase-space points can be evaluated in parallel on a computer cluster. Furthermore the communication with integral reduction programs was simplified by including support for inverse and pinched propagators and by improving the user interface.

In Chapter 9 SECDEC-3.0 and an extension of the program GOSAM to multi-loop amplitudes are used to calculate the cross section for the production of a Higgs boson pair in gluon fusion at NLO in QCD including the full top quark mass dependence [39]. This process is of interest, since it can be used for a direct measurement of the triple Higgs self-coupling at hadron colliders. It is part of the updated Les-Houches wishlist, and was previously only known at LO with full top quark mass dependence [40] and to higher order in various approximations. A measurement of the coupling, which in the SM is fixed by the Higgs mechanism, will give insight into the mechanism of electroweak

symmetry breaking.

Already at LO the process proceeds via a top quark loop, which means that the NLO correction requires the calculation of a two-loop amplitude. Since most of the contributing two-loop integrals are not known analytically, they are calculated numerically using `SECDEC-3.0`. It is found that the inclusion of the full top quark mass dependence leads to important deviations from the commonly used approximations in the heavy quark limit, which are known up to NNLO QCD.

The methods and tools used for most parts of the calculation are automated and process independent, representing a step towards the automation of multi-loop corrections.

2 Calculations for hadron colliders

2.1 Factorization and parton distribution functions

At hadron colliders such as the LHC and Tevatron high energy collisions of hadrons are studied. The final state of these collisions generically contains collimated jets of hadrons as well. Hadrons are states of quarks and gluons bound together by long range QCD interactions.

The strength of the QCD coupling α_s depends on the energy scale. At small energies the coupling is strong, which leads to the confinement of colored particles in hadrons. At high energies on the other hand the coupling becomes small, a property of QCD which is known as asymptotic freedom. Fig. 2.1 shows measurements of the strong coupling constant α_s at different energy scales Q .

In QCD it is possible to calculate scattering processes of hadrons, because short and long distance interactions factorize [42, 43]. The factorization of hadron-hadron collisions (Fig. 2.2) is given by

$$d\sigma(P_1, P_2) = \sum_{a,b} \int dx_1 dx_2 f_a(x_1, \mu_F^2) f_b(x_2, \mu_F^2) d\hat{\sigma}_{ab}(x_1 P_1, x_2 P_2, \mu_F^2) + \mathcal{O}((\Lambda/Q)^p) \quad (2.1)$$

here $f_{a,b}$ are the parton distribution functions (PDFs) which encode the non-perturbative structure of the incoming hadrons. The partonic scattering cross section $d\hat{\sigma}_{ab}$ describes the hard scattering of partons and can be calculated with perturbative methods. The integration is over the fraction of the hadron momentum carried by the partons involved in the hard scattering x_i . The summation is over all partons in the initial state hadrons. The factorization procedure introduces the unphysical factorization scale μ_F , which divides the process into perturbative and nonperturbative parts. It is usually set to a characteristic scale of the process.

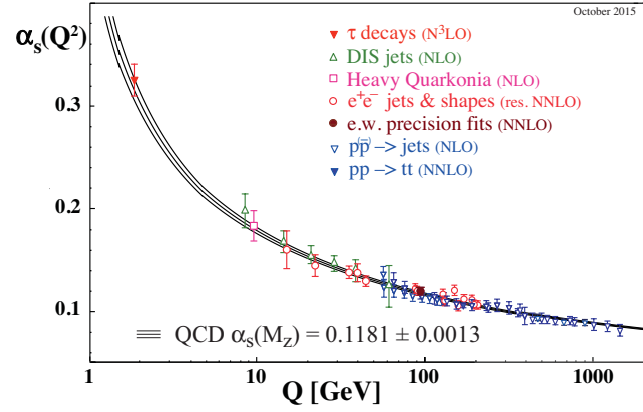


Figure 2.1: Summary of measurements of α_s as a function of the energy scale Q [41].

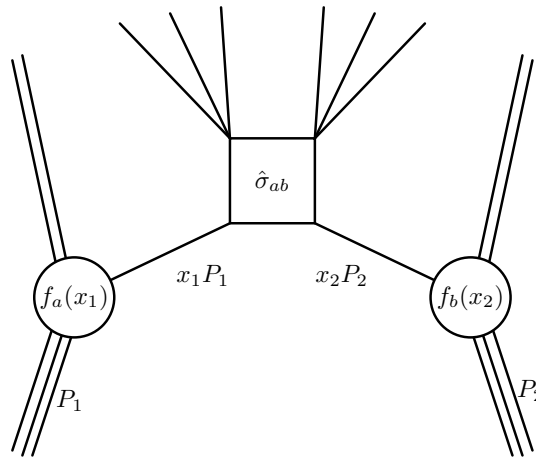


Figure 2.2: Factorization of parton distribution functions and partonic cross section.

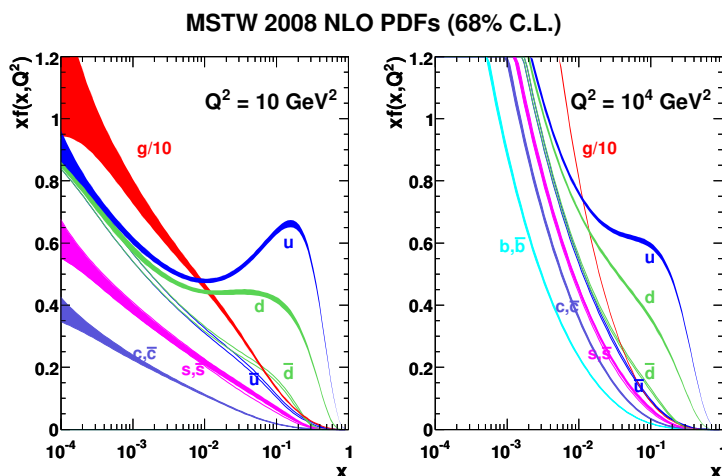


Figure 2.3: Parton distribution functions of the MSTW collaboration [49] at two energy scales $\mu_F^2 = Q^2$.

(2.1) is strictly valid only in the limit $Q^2 \rightarrow \infty$ where Q^2 is the energy exchanged in the scattering. A rigorous proof exists only for specific processes like deep inelastic scattering [44] and Drell-Yan [45]. Factorization is also not guaranteed for more exclusive final states.

The nonperturbative PDFs $f_a(x, \mu_F^2)$ describe the structure of the incoming hadrons. They have to be fitted from experimental data. However it is possible to calculate their evolution between different energy scales perturbatively using the Dokshitzer-Gribov-Lipatov-Altarelli-Parisi (DGLAP) equations [46–48]. These are obtained by the requirement that the physical cross section $d\sigma$ has to be independent of the unphysical scale μ_F . Fig. 2.3 shows the MSTW 2008 NLO PDFs at two different scales.

2.2 Hard scattering and perturbation theory

The differential cross section $d\hat{\sigma}_{ab}$ in (2.1) is defined as the modulus square of the scattering amplitude \mathcal{A}_n in the following way:

$$d\hat{\sigma}_{ab} = |\mathcal{A}_n|^2 d\phi_n. \quad (2.2)$$

Here the n -particle phase-space measure is denoted $d\phi_n$. The scattering amplitude \mathcal{A}_n describes the scattering of initial state partons a and b into a final

state of n particles. It is a complex-valued function on the domain of external particle momenta, and depends on the type and quantum numbers of the external particles. For sufficiently high momentum exchange it can be approximated by the first terms in the expansion in the strong coupling constant $\alpha_s = \frac{g_s^2}{4\pi}$

$$\mathcal{A}_n = \left(\frac{g_s}{\sqrt{4\pi}} \right)^k \sum_{i=0}^k \alpha_s^i \mathcal{A}_n^{(i)}, \quad (2.3)$$

where k denotes the number of couplings g_s appearing in the first term of the expansion of the amplitude. Here an expansion in the strong coupling constant is given. For precision predictions it is also necessary to include electroweak corrections. The scattering amplitude can be calculated perturbatively as the sum over all Feynman diagrams with given initial and final state and a specified order of the coupling constant. The calculation of higher order Feynman diagrams is the main focus of this thesis.

Following from (2.3) the perturbative expansion of the differential cross section is

$$d\hat{\sigma}_{ab} = \alpha_s^k \sum_{i=0}^k \alpha_s^i \left[\sum_{j=0}^i \mathcal{A}_n^{(i-j)*} \mathcal{A}_n^{(j)} \right] d\phi_n. \quad (2.4)$$

The first term in the series is called the leading order approximation (LO) involving only $\mathcal{A}_n^{(0)}$. To make quantitative predictions for a process it is usually necessary to go at least to the next to leading order (NLO).

2.3 Divergences

The calculation of the i -th term in the expansion of \mathcal{A}_n involves an integration over at least i unconstrained four dimensional momenta. The integration generically diverges due to the singular behaviour of the integrand at large and small momentum.

The standard procedure of regularizing these divergences is to use dimensional regularization [50]. Dimensional regularization is based on the observation that the appearing integrals can become convergent in dimensions different from four. One continues the dimension of the loop momentum away from four by choosing $D = 4 - 2\epsilon$. The divergences in $D = 4$ dimensions are then regulated by the parameter ϵ and show up as $\frac{1}{\epsilon^n}$ singularities when expanding the integrals as a Laurent expansion in ϵ .

2.3.1 Ultraviolet divergences

The large momentum divergences are called ultraviolet divergences. They can be understood by considering the Standard Model as an effective theory parametrising our knowledge of particle physics at low energy.

The UV divergences can be removed order-by-order in perturbation theory through a redefinition of fields and parameters of the theory. This process is called renormalization.

There is some freedom in the redefinition which affects the renormalized parameters. Different choices are known as renormalization schemes, the most common ones are the minimal subtraction (MS) scheme, the modified minimal subtraction ($\overline{\text{MS}}$) scheme, and the on-shell scheme. In the MS scheme only the divergent part is subtracted, in the $\overline{\text{MS}}$ scheme an additional factor of $-\gamma_E + \log(4\pi)$ where γ_E is the Euler-Mascheroni constant is included, which simplifies appearing expressions. The on-shell scheme relates the renormalized parameters to physical observables, for example a coupling at a certain energy scale or the pole of the renormalized propagator for the on-shell mass.

In schemes other than the on-shell scheme, a dependence of the renormalized theory parameters on the renormalization scale μ_R is introduced. The scale dependence is constrained by renormalization group equations, differential equations obtainable by requiring μ_R independence of observable quantities. An example is the energy scale dependence of the strong coupling constant α_s as shown in Fig. 2.1.

The terms $\mathcal{A}_n^{(i)}$ in the expansion of the scattering amplitude also depend on μ_R which leads to a renormalization scale dependence of the perturbative cross section. This dependence can be used to estimate the uncertainty introduced by truncating the expansion in (2.4) at a finite order since the full cross section should be independent of the unphysical scale μ_R . It is customarily obtained by varying the renormalization scale by a factor two up and down.

2.3.2 Infrared divergences

The second type of singularities due to small loop momentum behaviour are called infrared divergences. Here infrared divergence is used as a general term for soft and collinear divergences. They arise in theories with massless particles and are connected to singularities of cross sections with additional massless particles in the final state. Final states with extra massless partons become

indistinguishable from the original final state when the additional partons become soft or collinear.

Consequently one has to augment the perturbative expansion in (2.4) by cross sections with additional massless particles in the final state up to a fixed order in α_s . The NLO cross sections for an observable F then corresponds to

$$\frac{d\hat{\sigma}^{NLO}}{dF} = \alpha_s^k \int \left[(|\mathcal{A}_n^{(0)}| + \alpha_s 2\text{Re}(\mathcal{A}_n^{(0)*} \mathcal{A}_n^{(1)})) F_n d\Phi_n + \alpha_s |\mathcal{A}_{n+1}^{(0)}| F_{n+1} d\Phi_{n+1} \right] \quad (2.5)$$

$$= \int_n (d\hat{\sigma}^B + d\hat{\sigma}^V) + \int_{n+1} d\hat{\sigma}^R. \quad (2.6)$$

The terms in the preceding equation correspond to leading order (LO) or Born, virtual, and real correction respectively. While the Born and virtual term are integrated over a n -particle phase-space, the real correction has to be integrated over a $n + 1$ -particle phase-space due to the extra massless particle in the final state. The real correction diverges in phase-space regions where the extra massless particle becomes soft or collinear. Starting from NNLO there are also mixed real-virtual contributions.

Here an observable F was introduced which is a function of the final state particle momenta. F has to behave in the following way when one massless particle becomes soft or two massless particles become collinear:

$$F_{n+1}(p_1, \dots, p_i, \dots, p_{n+1}) \xrightarrow{p_i \rightarrow 0} F_n(p_1, \dots, \hat{p}_i, \dots, p_{n+1}) \quad (2.7)$$

$$F_{n+1}(p_1, \dots, p_i, p_{i+1}, \dots, p_{n+1}) \xrightarrow{p_i \parallel p_{i+1}} F_n(p_1, \dots, p_i + p_{i+1}, \dots, p_{n+1}). \quad (2.8)$$

This requirement is called soft and collinear safety or generally infrared safety. As a result of the Kinoshita-Lee-Nauenberg (KLN) theorem [51, 52] the perturbative cross section for infrared safe observables is finite. Infrared singularities cancel between real and virtual corrections. In hadron collisions there is an additional divergence due to real radiation becoming collinear to initial state partons which is not cancelled by the virtual corrections. It is absorbed into a redefinition of the parton distribution functions (Section 2.1) or in the case of identified hadrons in the final state into the fragmentation function.

The cancellation only takes place after the phase-space integrations have been performed. Real and virtual corrections can not be combined on the integrand level since they live in phase-spaces of differing dimensions. The infrared singularities of the virtual part are usually resolved using dimensional regularization and show up as poles in ϵ . For the real part on the other hand it would be

necessary to perform the integration over the D -dimensional phase-space analytically to resolve the singularities which is possible in very simple cases only. Usually Monte-Carlo methods are used for the phase-space integration which is possible only for integrals finite in $D = 4$.

Subtraction and phase-space slicing are the two main methods solving this problem. The slicing method [53, 54] relies on finding an observable that separates the phase-space into a hard region in which the real radiation is resolved and a soft region with the n -particle phase-space. One then introduces a cut-off parameter in this observable to split up the two regions. In the hard region a lower order real radiation calculation can be used, while factorization theorems are used in the soft region. Finally the independence of the result on the slicing parameter has to be checked. Slicing is mainly used at NNLO as q_T -subtraction [55] for color singlet final states and N -jettiness [56–58] for arbitrary colored final states. Its advantage is that lower order (NLO) calculations can be reused for the hard region, the drawback is that for small cut-off parameters large cancellations are expected.

The subtraction method introduces counter-terms that reproduce the real and collinear behaviour of the real correction:

$$\frac{d\hat{\sigma}^{NLO}}{dF} = \int_n d\hat{\sigma}^B + \int_n \left[d\hat{\sigma}^V + \int_1 d\hat{\sigma}^A \right] + \int_{n+1} \left[d\hat{\sigma}^R - d\hat{\sigma}^A \right]. \quad (2.9)$$

This makes the the $n + 1$ -particle phase-space integration finite such that it can be integrated in $D = 4$ numerically. The subtraction terms $d\hat{\sigma}^A$ are chosen to be process and observable independent, and should be analytically integrable over the one-particle unresolved phase-space. At NLO there are several fully automated subtraction strategies such as Catani-Seymour dipole subtraction [59–61] and Frixione-Kunszt-Signer subtraction [62, 63]. Besides the slicing schemes N -jettiness and q_T -subtraction, the subtraction schemes Antenna subtraction [64, 65], sector decomposition [32, 66–68], sector improved residue subtraction [69, 70], and colorful NNLO [71, 72] subtraction are used at NNLO. For specific processes like Higgs boson production in vector boson fusion the projection to Born method can be used [73, 74].

There is no fully automated process independent scheme beyond NLO yet.

2.4 Parton shower and hadronization

The main missing steps towards a realistic description of hadron collider events as observed in an experiment are parton shower and hadronization.

The parton shower adds QCD radiation to colored external particles of a process in an approximate way. It is perturbative and can be used down to scales of ~ 1 GeV, at which point the final state contains a large number of quarks and gluons.

Below this scale partons in the final state are clustered into hadrons, which is a nonperturbative process. There are two main phenomenological models: the string model [75, 76] implemented in the Monte-Carlo generator PYTHIA [77, 78] and the cluster model [79] implemented in HERWIG [80, 81] and SHERPA [20]. The produced hadrons are in general too short-lived to be measured directly and have to be decayed into stable hadrons for which hadron decay data is used.

After correcting for detector effects like finite resolution and acceptance one obtains predictions that can be compared to experimental data.

Part I

NLO phenomenology

3 Calculation of one-loop amplitudes

3.1 General amplitude structure

Here details on the one-loop amplitude $\mathcal{A}_0^{(1)}$ in (2.3) are given. The explicit form of a N -point one-loop amplitude $\mathcal{A}_0^{(1)}$ (Fig. 3.1) is

$$\mathcal{A}_0^{(1)} = \int \frac{d^D k}{i\pi^{D/2}} \frac{\mathcal{N}(k)}{\prod_{i=1}^N D_i} \quad (3.1)$$

where the propagators are defined as $D_i = q_i^2 - m_i^2$ with $q_i = k + \sum_{j=1}^i p_j$. The integration over the loop momentum k is in general divergent (see Section 2.3). The loop momentum is therefore continued away from four dimensions to $D = 4 - 2\epsilon$ dimensions, where the parameter ϵ regulates the divergences.

The numerator $\mathcal{N}(k)$ is polynomial in the loop momentum k and can therefore be written as

$$\mathcal{N}(k) = C + C_{\mu_1} k^{\mu_1} + C_{\mu_1 \mu_2} k^{\mu_1} k^{\mu_2} + \dots \quad (3.2)$$

For renormalizable theories the powers of the loop momentum that can appear in (3.2) are bounded by the number of external particles N .

The integrals that have to be calculated are then tensor integrals of the form

$$I_N^{D, \mu_1 \dots \mu_r}(S) = \int \frac{d^D k}{i\pi^{D/2}} \frac{k^{\mu_1} \dots k^{\mu_r}}{\prod_{i \in S} D_i} \quad (3.3)$$

with tensor rank r . Here S is a subset of the set of propagator labels $\{1, \dots, N\}$.

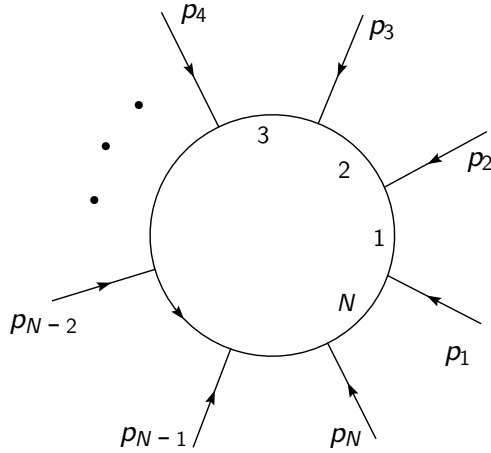


Figure 3.1: One-loop Feynman diagram with N external legs.

3.2 Master integral basis

At the one-loop order it is possible to reduce all appearing integrals to a basis of scalar master integrals. A general one-loop amplitude can be expressed in the master integral basis as

$$\mathcal{A}_0^{(1)} = d \text{ (box) } + c \text{ (triangle) } + b \text{ (bubble) } + a \text{ (tadpole) } + \mathcal{R}. \quad (3.4)$$

The master integrals are scalar integrals with up to four propagators (tadpoles, bubbles, triangles, and boxes). The coefficients d , c , b , and a depend on kinematic invariants built from the external momenta and internal masses. In dimensional regularization the rational part \mathcal{R} is generated from $D - 4$ dimensional components of the amplitude, but it also appears in other regularization schemes [82]. (3.4) is simplified in that there are usually several master integrals with a fixed number of propagators differing in offshell external momentum assignments and internal masses.

Integrals with five or more propagators can be reduced to a linear combination of box integrals if terms of order ϵ are neglected. This is due to space-time being four dimensional which makes the decomposition of any momentum into a basis of four independent external momenta possible.

There are libraries implementing expressions for all scalar master integrals with vanishing, real, and complex masses at one-loop [83–89].

In the next section two methods for the reduction of a one-loop amplitude to master integrals are introduced.

3.3 Reduction methods

3.3.1 Passarino-Veltman reduction

The Passarino-Veltman tensor reduction introduced in [90] can be used to reduce rank r tensor integrals from (3.3) to integrals with tensor rank $r - 1$ and integrals with a lower number of propagators. It relies on a form factor decomposition of the tensor integrals which follows from Lorentz invariance. The form factor decomposition of a rank one tensor integral for example would be

$$I_N^{D,\mu}(S) = \sum_{i=1}^{N-1} c_i p_i^\mu \quad (3.5)$$

since the external momenta are the only rank one tensors appearing in the integral. More details on the form factor decomposition can be found in Section 6.1.

In the next step the step both sides of the form factor decomposition are contracted with the external momenta. The scalar products of the form $k \cdot p_i$ are rewritten as linear combinations of propagators and a constant factor. The propagator factors can then be cancelled leading to integrals with pinched propagators. After this one can solve the system of equations for the coefficients c_i which are expressed in terms of simpler integrals. Inverting the system introduces the inverse of the Gram determinant $\det(p_i p_j)$ in the solution which becomes zero when external momenta are not linear independent. This leads to spurious singularities.

The problem of vanishing Gram determinants can be avoided by stopping the reduction before divergences are introduced. This leaves tensor integrals which have to be calculated by other methods. They can for example be expressed as finite scalar integrals in shifted dimensions, which can then be integrated numerically. The approach is implemented in Golem95 [84, 91].

Furthermore it is possible to avoid Gram determinants in the reduction of

integrals with $N > 5$ external legs by basing the reduction on the Cayley determinant [92].

3.3.2 OPP reduction

A different reduction method was introduced by Ossola, Papadopoulos, and Pittau [93]. In this method the coefficients of the master integrals are obtained by sampling the integrand of the loop amplitude at special values of the loop momentum.

It requires knowledge of the integrand level form of the master integral basis given by

$$\begin{aligned}
 \mathcal{N}(k) = & \sum_{i_0 < i_1 < i_2 < i_3}^N \left[d(i_0 i_1 i_2 i_3) + \tilde{d}(i_0 i_1 i_2 i_3; k) \right] \prod_{i \neq i_0, i_1, i_2, i_3}^N D_i \\
 & + \sum_{i_0 < i_1 < i_2}^N \left[c(i_0 i_1 i_2) + \tilde{c}(i_0 i_1 i_2; k) \right] \prod_{i \neq i_0, i_1, i_2}^N D_i \\
 & + \sum_{i_0 < i_1}^N \left[b(i_0 i_1) + \tilde{b}(i_0 i_1; k) \right] \prod_{i \neq i_0, i_1}^N D_i \\
 & + \sum_{i_0}^N \left[a(i_0) + \tilde{a}(i_0; k) \right] \prod_{i \neq i_0}^N D_i.
 \end{aligned} \tag{3.6}$$

The coefficients $\tilde{d}, \dots, \tilde{a}$ are spurious terms which evaluate to zero upon integration over the loop momentum. Their loop momentum dependence is given in [93].

The coefficients can be determined analytically or numerically by sampling the integrand on cuts of the amplitude. The box coefficients are obtained by evaluating the amplitude on the four particle cut given by

$$D_1 = D_2 = D_3 = D_4 = 0. \tag{3.7}$$

These equations have two solutions k_0^\pm . By evaluating the numerator at the solutions one can determine the box coefficients d and \tilde{d} as

$$\mathcal{N}(k_0^\pm) = \left[d(1234) + \tilde{d}(1234; k_0^\pm) \right] \prod_{i \neq 1, 2, 3, 4} D_i(k_0^\pm). \tag{3.8}$$

All other terms in (3.6) are set to zero for k_0^\pm .

To obtain the lower point coefficients one subtracts the box terms from (3.6).

Then the triangle coefficients can be determined by three particle cuts. This procedure is iterated until all coefficients in (3.6) are fixed.

The rational part has to be calculated using other methods. There is also a generalization of the OPP method to D dimensions which gives the rational part directly [94, 95].

4 GoSam

It is observed that LO calculations in QCD are often not precise enough for meaningful comparisons to experimental data. For this reason NLO predictions are becoming the standard for phenomenology and experimental data analyses at the LHC. This requires automated and fast tools for the calculation of NLO cross sections.

GOSAM is a public program for the automated calculation of one-loop amplitudes [18, 19]. One-loop amplitudes $\mathcal{A}_n^{(1)}$ are needed for the calculation of NLO cross sections as given in (2.9) and constitute the most difficult part of their computation. The Born and real radiation contributions in (2.9) involve only tree-level diagrams and can be provided by Monte-Carlo event generators.

The program is available at <http://gosam.hepforge.org>.

Other programs that provide one-loop amplitudes in an automated way are BLACKHAT [96], HELAC-NLO [97], FEYNARTS/FORMCALC [85], MADLOOP [98], NJET [99], OPENLOOPS [100] and RECOLA [101]. The programs MCFM [102, 103], VBFNLO [104], and POWHEG-BOX [105] implement hardcoded one-loop matrix elements.

GOSAM can be called from a Monte-Carlo generator via the Binoth-Les-Houches-interface [106, 107], which is a standardized interface for the communication between one-loop amplitude providers like GOSAM and Monte-Carlo generators. In Fig. 4.1 an overview over the interface is given. This would be the typical way of using GOSAM to obtain NLO results. Alternatively GOSAM can be called directly from an input card. A minimal example card for the process $e^+e^- \rightarrow t\bar{t}$ is

```
process_path=eett
in=e-,e+
out=t, t~
order=QCD, 0, 2
```

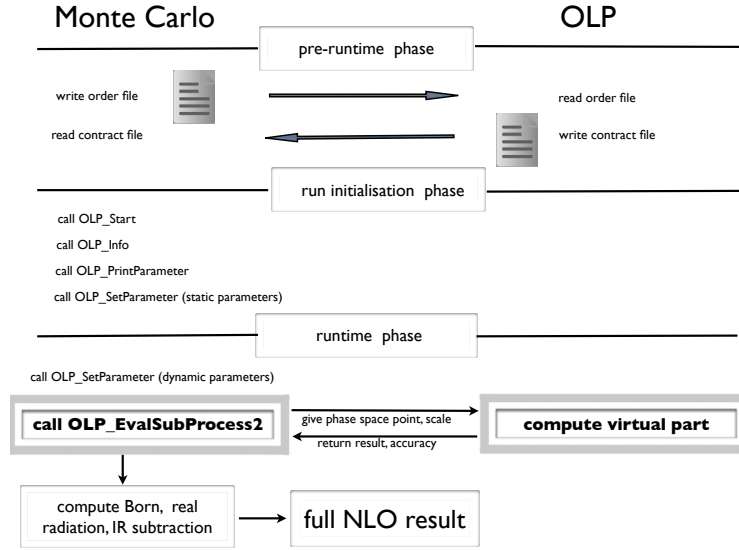


Figure 4.1: Overview over the communication between Monte-Carlo event generators and one-loop amplitude providers via the BinOth-Les-Houches-interface.

Here the name of the process directory is given, the external particles are specified, and the α_s order of the tree level and one-loop corrections for the process is defined.

The structure of the program is shown in Fig. 4.2. A process is read in from the input card and QGRAF [108] is used to list all contributing Feynman diagrams. Using `python` the diagrams are filtered and grouped. After substituting the Feynman rules in the diagrams, the resulting expressions are processed using FORM [109, 110]. The program SPINNEY [111] performs the Dirac algebra calculations using the spinor helicity formalism. At this stage the algebraic expression for the one-loop amplitude is turned into optimized FORTRAN90 code with FORM.

It is possible to choose between the interfaced reduction libraries GOLEM95C [84, 112], NINJA [113, 114], and SAMURAI [115] at runtime.

GOLEM95C is a tensor integral library based on an improved version of the Passarino-Veltman reduction method. It avoids spurious divergences due to vanishing Gram determinants and implements fast numerical expressions for

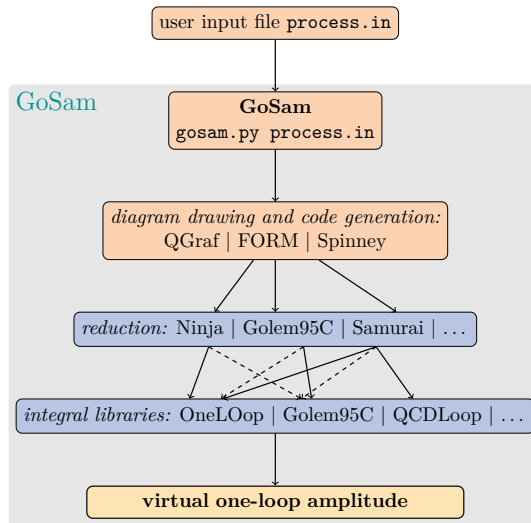


Figure 4.2: Flowchart showing the main steps GOSAM performs to produce the virtual amplitude.

form factors of tensor integrals.

The programs SAMURAI and NINJA are both based on the D -dimensional generalization of the OPP method. NINJA uses reduction via Laurent series expansion [116] which allows the determination of the coefficients in (3.6) with a small number of integrand evaluations.

The reduction programs determine the coefficients of the master integral basis and call master integral libraries for the evaluation of the scalar master integrals. The libraries ONELOOP [86], GOLEM95C [84, 112], QCDDLOOP [87, 88], or LOOPTOOLS [85] can be used.

At runtime GOSAM takes a phase-space point and returns the coefficients of the Laurent expansion of the interference $2\text{Re}(\mathcal{A}_n^{(0)*} \mathcal{A}_n^{(1)})$ up to the finite part in ϵ . In GOSAM the renormalization of QCD corrections is automatized, and therefore the returned expression is renormalized and only contains singularities due to infrared divergences. For electroweak corrections and calculations in BSM theories only the unrenormalized result can be returned. Nevertheless GOSAM has been used for the calculation of electroweak corrections in [117, 118] and of SUSY-QCD corrections to neutralino pair production in association with

a jet in [119].

GoSAM-2.0 [19] is the most recent version of the program. The code generation is improved by grouping and summing diagrams with similar propagator structure and by using the new features provided by FORM version ≥ 4 [110]. Higher rank tensor integrals, with tensor rank $r = N + 1$ where N is the number of propagators are supported. The implementation of higher rank tensor integrals in GOLEM95C was presented in [112]. These integrals are absent in renormalizable theories, but appear in effective field theories and BSM theories. A rescue system automatically identifies numerically unstable points and tries to rescue them. By default NINJA is used for the reduction. If the stability test fails for a phase-space point, it is reevaluated with GOLEM95C which usually gives more stable results. GoSAM-2.0 also fully supports the complex mass scheme for unstable gauge bosons and fermions [120]. To include their width the masses of the unstable particles are changed according to

$$m^2 \rightarrow \mu^2 = m^2 - im\Gamma, \quad (4.1)$$

where Γ is the decay width.

Several electroweak scheme choices are implemented. Different sets of electroweak parameters can be taken as input, and the remaining ones are derived from them. Finally the second version of the Binoth-Les-Houches-accord for the communication between one-loop providers and Monte-Carlo programs is fully implemented [107].

5 NLO QCD corrections to $W^+W^-b\bar{b}$ production

5.1 Introduction

The top quark is the heaviest particle in the Standard Model. It was first observed at the Tevatron in 1995 [16, 17]. The precise determination of the top quark properties is an important goal of the LHC. Knowledge of the top quark properties is required since top quarks constitute an important background for new physics searches. The top quark mass m_t is also needed as an input parameter in many precision calculations, for example the determination of the stability of the SM vacuum [121].

A recent combination of top quark mass measurements at Tevatron and LHC finds [122]

$$m_t = 173.34 \pm 0.27 (\text{stat}) \pm 0.71 (\text{syst}) \text{ GeV}.$$

To match this precision on the theoretical side, it is necessary to consider higher order effects and to go beyond the approximation of factorizing top quark production and decay. The NLO QCD corrections to top quark pair production in hadronic collisions are known for a long time [123–127]. Electroweak corrections were determined in [128], the QED corrections were given in [129], for recent developments see [130]. More recently the NNLO QCD corrections became available [131, 132].

In all of these calculations top quarks are treated as stable on-shell particles. Top quarks decay predominantly into a b -quark and a W -boson:

$$t \rightarrow W^+b. \tag{5.1}$$

The decay can be attached to the top quarks in the narrow width approximation (NWA), where production and decay factorize. In most applications, these decays are calculated only at the leading order. One however makes use

of spin density matrix or reweighting techniques to preserve the spin correlations between particle production and decay. This, especially, is the standard in multi-purpose Monte-Carlo event generators. At parton level, NLO calculations using the NWA were further improved by including the top quark decays at NLO. Parton level here means that the calculation is performed at fixed order and no parton shower or hadronization effects are added. The complete evaluation of the NLO QCD corrections to $t\bar{t}$ production and decay based on the NWA including spin correlations and NLO decays is given in [133–135].

The process $pp \rightarrow W^+W^-b\bar{b}$ describes top quark pair production and decay, and also includes irreducible backgrounds due to singly resonant and non-resonant contributions (see Fig. 5.1 for representative tree-level diagrams).

The first NLO QCD calculations were presented in [22, 23]. Non-resonant effects in the decay of the W -bosons were included and studied in [24]. The previous calculations are in the 5-flavour scheme and treat b -quarks as massless particles. In [136, 137] the same process was calculated with massive b -quarks in the 4-flavour scheme. These calculations include single top production and its irreducible background in a natural way. In the 5-flavour scheme potentially large logarithms $\log(Q^2/m_b^2)$ due to gluons splitting into b -quark pairs in the initial state are resummed into the b -quark PDF, where Q^2 is the hard scale of the process. This makes it necessary to include subprocesses with initial state b -quarks and to treat b -quarks as massless particles in the matrix element. In the 4-flavour scheme there is no b -quark PDF, which means that the logarithms appear explicitly in the calculation and are not resummed. Its advantage is that the b -quarks can be treated as massive particles in the matrix element.

The process was also matched with a parton shower at NLO in [138].

Recently NLO electroweak corrections to offshell top quark pair production with leptonic decays became available [139].

In the following the NLO QCD corrections to the $2 \rightarrow 4$ process $pp \rightarrow W^+W^-b\bar{b} \rightarrow (e^+\nu_e)(\mu^-\bar{\nu}_\mu)b\bar{b}$ are presented [21, 140]. Resonant semi-leptonic decays of the W -bosons are included and the b -quarks are treated as massless particles.

The calculation is used to study offshell and higher order effects on top quark mass measurements.

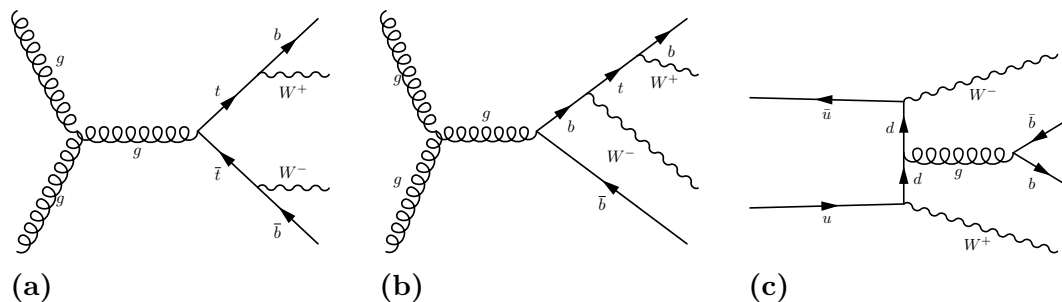


Figure 5.1: Representative tree-level Feynman diagrams for resonant (5.1a), singly resonant (5.1b) and non-resonant (5.1c) contributions.

5.2 Computational framework

The calculation is performed using the programs GOSAM [18, 19] and SHERPA [20]. Both programs communicate via the Binoth-Les-Houches-interface [106] (see Chapter 4).

SHERPA is a multi-purpose Monte-Carlo event generator. In this calculation it is used to generate tree-level matrix elements for the Born and real radiation contributions via the included matrix element generators AMEGIC [141] and COMIX [142]. Real radiation and virtual contributions are combined with the implementation of the Catani-Seymour dipole subtraction [59] included in SHERPA [60] (see Subsection 2.3.2). Finally SHERPA is also used to perform the numerical integration over the final state phase-space.

The only missing piece is the virtual contribution which is provided by the one-loop provider GOSAM, described in Chapter 4. Finally the program RIVET [143] is used to define observables and to plot differential distributions.

The process $pp \rightarrow W^+W^-b\bar{b}$ provides a full description of top quark pair production and decay including singly resonant and non-resonant contributions, which constitute an irreducible background, see Fig. 5.1. Diagrams including Higgs bosons are neglected, due to their small effect on the cross section. The calculation is in the 5-flavour scheme with massless b -quarks. The complex mass scheme [120] is used to take into account the width of the top quark by replacing the top quark mass by

$$\mu_t^2 = m_t^2 - im_t\Gamma_t \quad (5.2)$$

where Γ_t is the top quark width.

The renormalization is automatically performed by GOSAM. It uses the $\overline{\text{MS}}$

scheme for gluons and massless quarks, for the renormalization of the top quark mass the on-shell scheme is used (see Subsection 2.3.1).

The virtual amplitude was compared with the result of [24] at a given phase-space point and agreement was found. The validity of the dipole subtraction was verified by varying the parameter α_{dip} over a certain range. The parameter α_{dip} is used to limit the phase-space region in which the dipole subtraction terms are applied [144].

5.3 Treatment of top quarks

As already mentioned above there are different ways of adding decays to top quark pair production. The narrow width approximation relies on approximating the resonant top quark propagators as

$$\lim_{\Gamma_t/m_t \rightarrow 0} \frac{1}{(p_t^2 - m_t^2)^2 + m_t^2 \Gamma_t^2} = \frac{\pi}{m_t \Gamma_t} \delta(p_t^2 - m_t^2) + \mathcal{O}\left(\frac{\Gamma_t}{m_t}\right). \quad (5.3)$$

Due to the δ -function the full process factorizes into on-shell top quark pair production and decays as $pp \rightarrow t\bar{t} \rightarrow W^+W^-b\bar{b}$.

Each top quark resonance introduces a factor of $\frac{1}{\Gamma_t}$. Therefore singly resonant and non-resonant diagrams can be neglected in the $\Gamma_t \rightarrow 0$ limit.

Two examples of non-factorizable and non-resonant one-loop diagrams that are neglected in the NWA but contribute to the full calculation are shown in Fig. 5.2.

The contributions beyond the NWA are suppressed by powers of $\frac{\Gamma_t}{m_t} \lesssim 1\%$. Nevertheless in certain regions of the phase-space the effects can become important as can be seen for example in the m_{lb} distribution discussed in Section 5.6.

To investigate off shell effects we differentiate between three types of calculations for the $W^+W^-b\bar{b}$ final state in the following. The calculations are schematically shown in Fig. 5.3.

The full or $WWb\bar{b}$ calculation gives a complete description of the $WWb\bar{b}$ final state. Finite width effects and non-resonant contributions are fully taken into account.

In the NWA approach (5.3) is used to factorize the process into top quark pair production and subsequent decays. NLO corrections to production and decay are included in a consistent way [133–135].

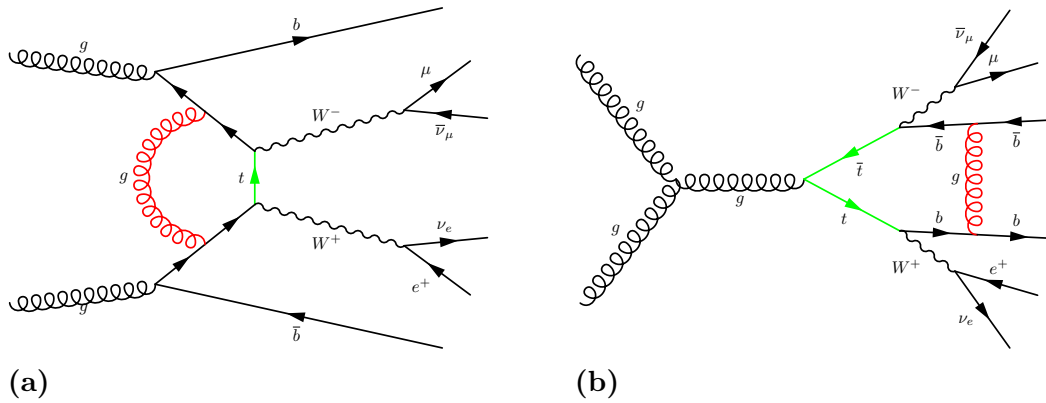


Figure 5.2: Examples of one-loop Feynman diagrams contributing to the full calculation: a non-resonant diagram (5.2a) and a non-factorizable virtual contribution (5.2b).

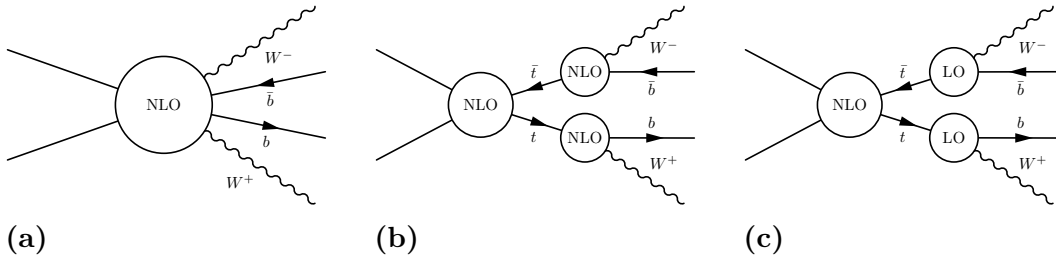


Figure 5.3: Form of the full (5.3a), NWA (5.3b), and factorized (5.3c) calculations at NLO.

The factorized approach is used in most Monte-Carlo generators and therefore in experimental analyses. It also uses the NWA but in contrast to the strict NWA approach one includes NLO corrections to the production only. The decays are added at LO.

5.4 General input parameters

Here the input parameters of the calculation are listed. For the (N)LO calculations, the MSTW2008(N)LO parton distributions [49] are used, relying on the strong coupling constant, α_s , as provided by these PDF parametrizations. The PDFs are interfaced using the LHAPDF library [145]. The evolution equation for the strong coupling is taken from [146]. The electroweak parameters are

given in the G_μ scheme where the weak coupling constant is derived from the Fermi constant G_μ :

$$\begin{aligned} G_\mu &= 1.16637 \cdot 10^{-5} \text{ GeV}^{-2}, \\ M_W &= 80.399 \text{ GeV}, & \Gamma_W &= 2.0997 \text{ GeV}, \\ M_Z &= 91.1876 \text{ GeV}, & \Gamma_Z &= 2.5097 \text{ GeV}. \end{aligned} \quad (5.4)$$

Measured values are used for the gauge boson masses and the Fermi constant [147], for the gauge boson widths the NLO QCD values are taken from [24]. All quarks other than the top quark are taken to be massless. For the top quark mass, we use $m_t = 172.0$ GeV. From the parameters given above, it is possible to derive the value of the top quark decay width at LO and NLO using the expressions given in [148]. The numerical values used are

$$\begin{aligned} \Gamma_t^{\text{LO}} &= 1.4426 \text{ GeV}, \\ \Gamma_t^{\text{NLO}} &= 1.3167 \text{ GeV}. \end{aligned} \quad (5.5)$$

5.5 Numerical results for the LHC at 7 TeV

Here results for the full $WWb\bar{b}$ calculation with semi-leptonic decays at a center of mass energy of 7 TeV are given. We require at least two jets containing one or more b -quarks in the final state. The jets are clustered using the anti- k_T [149, 150] algorithm implemented in FastJet [151] with a jet separation

$$\Delta R = \sqrt{\Delta\phi^2 + \Delta\eta^2} > 0.5. \quad (5.6)$$

They have to obey the conditions

$$p_{T,b} > 30 \text{ GeV} \quad \text{and} \quad |\eta_b| < 2.5. \quad (5.7)$$

The requirements on the leptons in the final state are

$$p_{T,l} > 20 \text{ GeV}, \quad |\eta_l| < 2.5 \quad \text{and} \quad \not{p}_T > 20 \text{ GeV}. \quad (5.8)$$

The variable \hat{H}_T , defined as

$$\hat{H}_T = \sum_i p_{T,i}, \quad (5.9)$$

where the sum runs over all final state particles is used to define the dynamical renormalization scale. The central scale is chosen as $\mu_R = \mu_F = \hat{H}_T/2$. This choice leads to small differences between LO and NLO cross section, and to small uncertainties due to scale variations. Recently a NNLO study of scale choices for top quark pair production appeared, which suggests that this scale might not be optimal [152]. A similar scale choice was also in [136].

With the given parameters and phase-space constraints the LO and NLO cross sections are

$$\begin{aligned}\sigma_{\text{LO}} [\text{fb}] &= 638.4^{+38.5\%}_{-24.8\%} (\text{scale}) \pm 0.03\% (\text{stat}) , \\ \sigma_{\text{NLO}} [\text{fb}] &= 758.5^{+2.5\%}_{-5.3\%} (\text{scale}) \pm 0.2\% (\text{stat}) ,\end{aligned}\tag{5.10}$$

corresponding to a K -factor of about 1.2.

The statistical error is the usual Monte-Carlo error from the numerical integration over the final state phase-space. The scale variation error is obtained by varying the renormalization and factorization scales by a factor of two around the central scale $\hat{H}_T/2$. The scale dependence of the cross section is shown in Fig. 5.4a.

Fig. 5.4b shows the transverse momentum of the leading b -jet p_{T,b_1} . The blue and red bands denote the scale variation by a factor $x = \frac{1}{2}$ and $x = 2$ where $x = 2 \mu/\hat{H}_T$ and $\mu = \mu_R = \mu_F$ at LO and NLO respectively. The scale variation uncertainty is significantly reduced at NLO. In the ratio plot a rise in the NLO distribution at high transverse momentum is visible. This is due to the additional real radiation against which the b -jet can recoil.

Fig. 5.5 shows two observables built from the charged leptons in the final state. They are the ΔR separation and the relative angle in the plane perpendicular to the beam axis ϕ between e^+ and μ^- . For these observables the K -factor varies at most by 20% and the NLO distribution stays inside the LO scale uncertainty band.

The distributions in Fig. 5.6 are the transverse momenta of the (e^+, μ^-) system $p_{T,e^+\mu^-}$ and the (b, b) system $p_{T,b\bar{b}}$. The NLO corrections have a similar behaviour for both observables. While the corrections are small for low transverse momenta, they become large above $p_T \gtrsim 150$ GeV. In the tail the K -factor becomes as large as ~ 3 for the $p_{T,b\bar{b}}$ distribution, and lies far outside the LO scale variation band. This is again due to the real radiation which in-

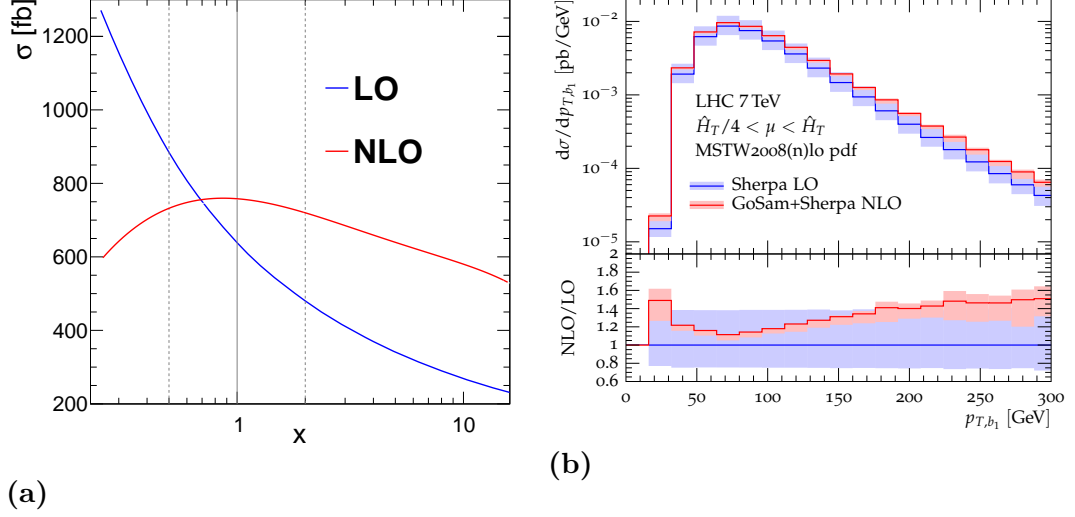


Figure 5.4: Scale variation of the LO and NLO cross sections in the full approach (5.4a) between $x = 1/4$ and $x = 16$ where $x = 2\mu/\hat{H}_T$ and $\mu = \mu_R = \mu_F$. (5.4b) shows the transverse momentum of the leading b -jet at LO (blue lines) and NLO (red lines). The bands denote the uncertainty due to scale variations by a factor of two around the central scale $\hat{H}_T/2$.

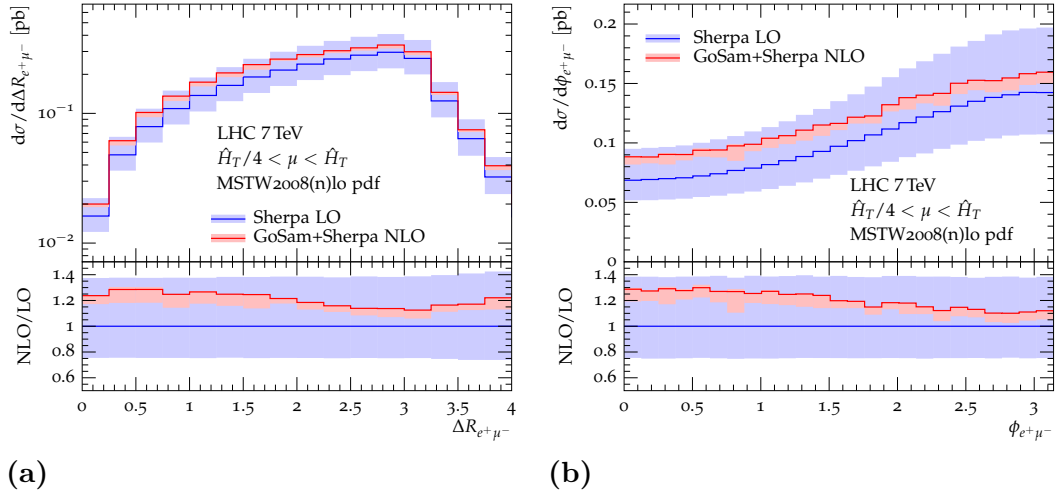


Figure 5.5: ΔR separation (5.5a) and relative azimuthal angle (5.5b) between the two charged leptons in the final state.

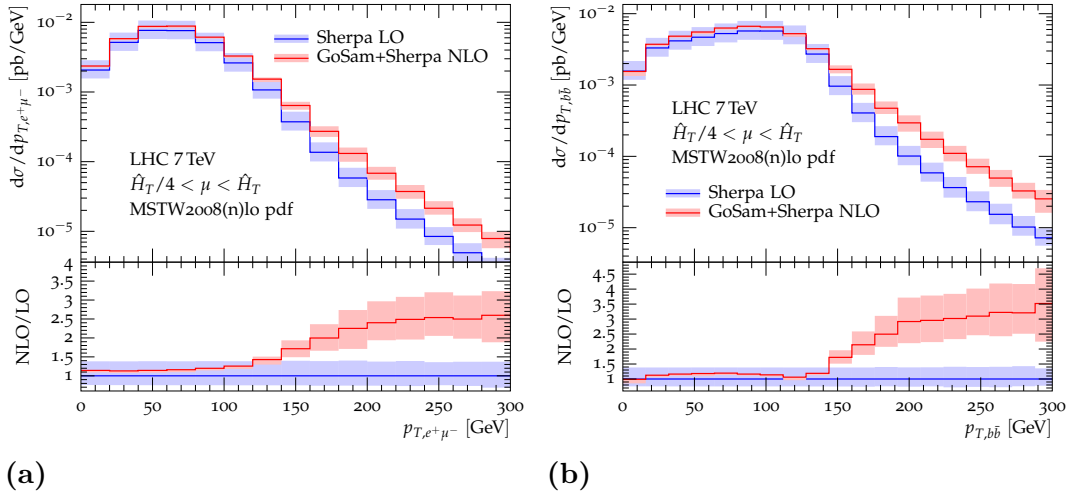


Figure 5.6: Transverse momentum of the (e^+, μ^-) system (5.6a) and the system of the two leading b -jets (5.6b).

duces a transverse momentum imbalance between the (b, \bar{b}) and the (W^+, W^-) system.

5.6 Study of theoretical uncertainties in top quark mass measurements

5.6.1 Top quark mass definition

The top quark mass m_t is a parameter in the SM Lagrangian. Therefore it is not a physical observable and is dependent on the renormalization scheme, see Subsection 2.3.1. Most commonly the pole mass and the modified minimal subtraction ($\overline{\text{MS}}$) mass are used. The relation between the two mass definitions is known up to the four loop order [153].

The pole mass scheme is a long distance scheme. One defines the pole mass as the real part of the pole of the top quark propagator, see (5.3). Since the top quark is colored, it is subject to confinement, which means that nonperturbatively there is no pole in the top quark propagator and the pole mass can only be defined perturbatively. There is an irreducible uncertainty of the order of

70 MeV [154] on the pole mass due to the infinite sum of self-energy insertions, which is known as the renormalon ambiguity [155, 156].

The $\overline{\text{MS}}$ mass scheme on the other hand is a short distance scheme. Only the divergent parts of the self-energy insertions are absorbed into the renormalized $\overline{\text{MS}}$ mass, see Subsection 2.3.1. In contrast to the pole mass, the $\overline{\text{MS}}$ mass is not affected by the renormalon ambiguity.

Experimental measurements of the top quark mass are performed by comparing kinematic observables of top quark decay products with predictions from Monte-Carlo generators. The exact relation between the top quark mass m_t^{MC} used in Monte-Carlo generators and a well defined top quark mass definition is not known [157–160]. In [157] the difference between m_t^{MC} and the pole mass is estimated to be about 1 GeV.

It is also possible to obtain the $\overline{\text{MS}}$ mass directly from measurements of the total $t\bar{t}$ cross section, when comparing with the calculated $t\bar{t}$ cross section where the top quark mass is renormalized in the $\overline{\text{MS}}$ scheme. The drawback of this method is the comparably large experimental uncertainty. There is also a residual dependence of cross section measurements on the Monte-Carlo mass m_t^{MC} [161].

5.6.2 Mass measurement using the m_{lb} observable

An observable that is commonly used for top quark measurements is the invariant mass of the charged lepton and b -jet system $m_{lb}^2 = (p_l + p_b)^2$ from a semi-leptonic top quark decay. The observable was recently used in ATLAS analyses of 7 TeV [162] and 8 TeV [163] data, and also in a CMS analysis [164]. Using the m_{lb} observable, the ATLAS analysis [162] finds a top quark mass of

$$m_t = 173.09 \pm 0.64 (\text{stat}) \pm 1.50 (\text{syst}) \text{ GeV} . \quad (5.11)$$

The main systematic uncertainty is due to the jet energy scale uncertainty. Theoretical uncertainties contribute about 0.8 GeV.

Since we generate events in the dilepton decay channel, there is one m_{lb} per top quark. Because the charge information of the b -jet is lost, there is no obvious way to find the combinations of leptons and b -jets which originate from the same top quark. In [162] a combination criterion based on a Monte-Carlo study is

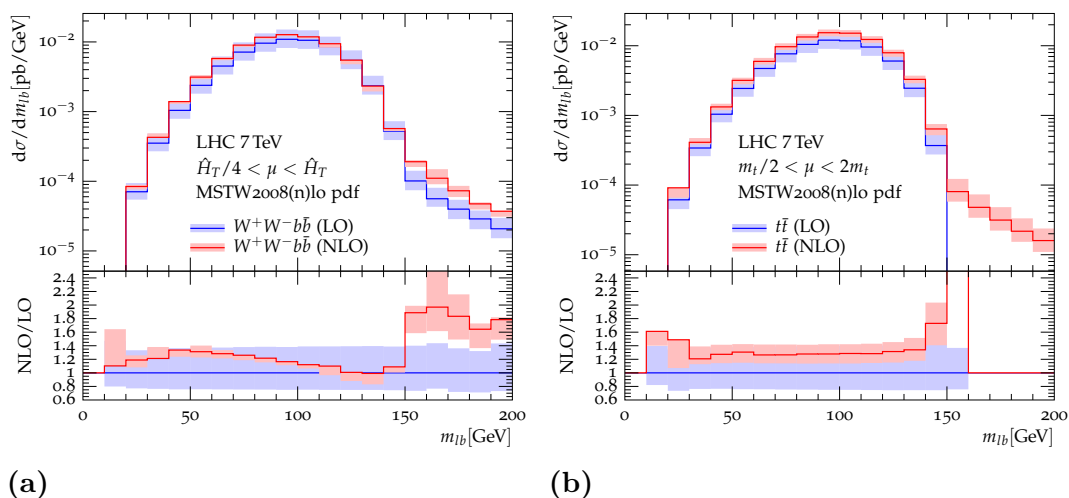


Figure 5.7: Distribution of m_{lb} at LO and NLO for the full $WWb\bar{b}$ calculation (5.7a) and the factorized calculation (5.7b). The central scale for the full calculation is $\mu = \hat{H}_T/2$, while for the factorized calculation $\mu = m_t = 172.5$ GeV is used.

given, which will be used in the following. The pairing (l^+b, l^-b') is chosen which minimizes the sum of the two m_{lb} values obtained from the combination. Finally the m_{lb} observable shown below is the average of the two m_{lb} values.

Parton level m_{lb} predictions at NLO

For the calculation of the m_{lb} distribution, we follow the ATLAS procedure as outlined above. We use $m_t = 172.5$ GeV as the default top quark mass and employ the ATLAS kinematic requirements for 7 TeV LHC pp collisions: we require exactly two oppositely charged leptons (electrons with $p_T > 25$ GeV, and muons with $p_T > 20$ GeV) in the pseudo-rapidity range $|\eta_l| < 2.5$, and two b -jets with $p_{T,b} > 25$ GeV, $|\eta_b| < 2.5$ and $\Delta R > 0.4$, using the anti- k_T algorithm. The leptons have to be isolated from the jets with $\Delta R_{l,j} > 0.4$. Lastly, H_T defined as the sum over the transverse momenta of charged leptons and jets has to be larger than 130 GeV.

In Fig. 5.7 the m_{lb} distribution at LO and NLO is shown for the full $WWb\bar{b}$ calculation and the factorized calculation. The full calculation uses $\mu = \hat{H}_T/2$

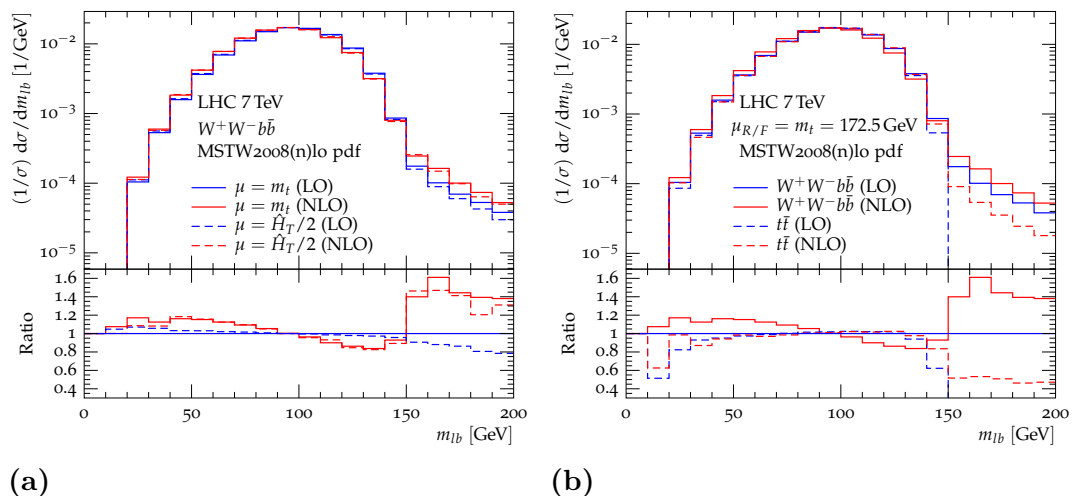


Figure 5.8: Comparison of the normalized m_{lb} distribution using the dynamical scale $\mu = \hat{H}_T/2$ and the fixed scale $\mu = m_t$ in the full approach (5.8a). Normalized m_{lb} distribution comparing the full and the factorized calculation using the fixed scale $\mu = m_t$ (5.8b). In the ratio plot all distributions are normalized to the factorized LO calculation.

as central scale, while for technical reasons in the factorized calculation $\mu = m_t$ is used.

The K -factor for the factorized calculation in Fig.5.7b is flat over most of the m_{lb} region. At LO the distribution has a cut-off at $m_{lb} = \sqrt{m_t^2 - m_W^2} \simeq 150 \text{ GeV}$ due to on-shell constraints. The NLO distribution on the other hand develops a tail above the cut-off, because of real radiation contributions. In the full calculation the K -factor varies more and a tail is already present at LO. The NLO corrections in the tail region exceed the LO scale variation bands.

The top quark mass measurement in [162] is mostly affected by shape changes close to the peak of the distribution. The shape changes due to NLO corrections are more pronounced in the full calculation, while the corrections for the factorized calculation are almost flat. To verify that this is not due to the different scale choices used in the two calculations, a comparison of the full calculation evaluated at the two scales is shown in Fig. 5.8a. This shows that the shape of the m_{lb} distribution is similar for the scales $\mu = \hat{H}_T/2$ and $\mu = m_t$. Another difference between the two calculation is the behaviour under scale variations. The scale variation bands of both LO calculations and factorized NLO calcu-

lation are symmetric around the central scale, while the full NLO calculation exhibits asymmetric uncertainty bands.

Fig. 5.8b shows a comparison of the shapes of the m_{lb} distributions obtained in the full and the factorized approach using a fixed scale $\mu = m_t$. The only distribution with a shape significantly different from the rest in the peak region is the full $WWb\bar{b}$ NLO distribution. The shape of the factorized NLO distribution on the other hand is similar to the shape of the LO distributions.

Investigation of theoretical uncertainties in the m_t measurement

In [162, 163] a template method is used to determine the top quark mass from data. Details on the method can also be found in [165, 166]. Template distributions for different input top quark masses m_t^{in} are generated. The m_{lb} distributions are then fitted using a fit function. All parameters of the fit function depend linearly on m_t^{in} in the region around the expected top quark mass, which is verified in [162]. After fixing the parameters in the linear relation using the templates, the only free parameter is the top quark mass. In the experiment a likelihood fit of the function to data is performed which fixes the free parameter in the fit function, leading to the measured top quark mass m_t^{out} . In the experimental analysis templates are generated at detector level. The following analysis on the other hand is performed at parton level. Effects of parton shower, hadronization, and detector simulation can therefore not be addressed

In Fig. 5.9 normalized m_{lb} distributions for three different top quark masses are shown. Also shown is the LO distribution for $m_t = 172.5$ GeV to illustrate the shape change due to NLO corrections.

To assess theoretical uncertainties, NLO distributions are used to generate pseudo-data corresponding to an integrated luminosity of 4.7/fb. Two sets of templates are obtained from LO and NLO distributions respectively. The impact of the NLO corrections is then assessed by comparing m_t^{out} obtained with the LO templates to the value obtained with NLO templates.

The scale uncertainty on m_t^{out} is estimated by generating pseudo-data from NLO distributions at a shifted scale while keeping the templates at the central scale.

Since there are sizeable shape differences in the m_{lb} distribution for the full and the factorized prediction, the analysis is performed for both calculations

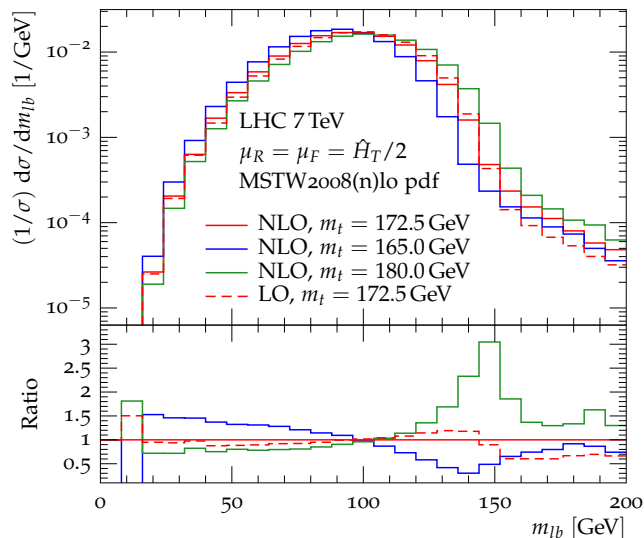


Figure 5.9: Normalized m_{lb} distributions at NLO in the full approach generated with three different top quark masses. The dashed line is the LO prediction obtained with $m_t = 172.5$ GeV.

separately.

In Fig. 5.10 the top quark mass analysis for the full calculation is presented. Fig. 5.10a shows the NLO m_{lb} distribution with $m_t^{\text{in}} = 172.5$ GeV as a black histogram. A pseudo-data set corresponding to an integrated luminosity of 4.7/fb, generated from the distribution, is given by the data points. The red line finally shows the result of the template fit using NLO templates to the pseudo-data. From the fit one obtains a top quark mass of $m_t^{\text{out}} = 172.3 \pm 0.52$ GeV consistent with the m_t^{in} used to generate the pseudo-data, demonstrating the internal consistency of the method.

Fig. 5.10b shows the difference between the input top quark mass m_t^{in} used for the generation of the pseudo-data and the output top quark mass m_t^{out} measured from the pseudo-data using the template method. Pseudo-data is generated with three different input masses m_t^{in} . The red dots correspond to NLO pseudo-data measured with a fit based on NLO templates. The statistical error due to the assumed luminosity is given by the error bars of the points. The error bands are obtained by using scale varied NLO distributions as input for the pseudo-data while keeping the original templates. The scale variation

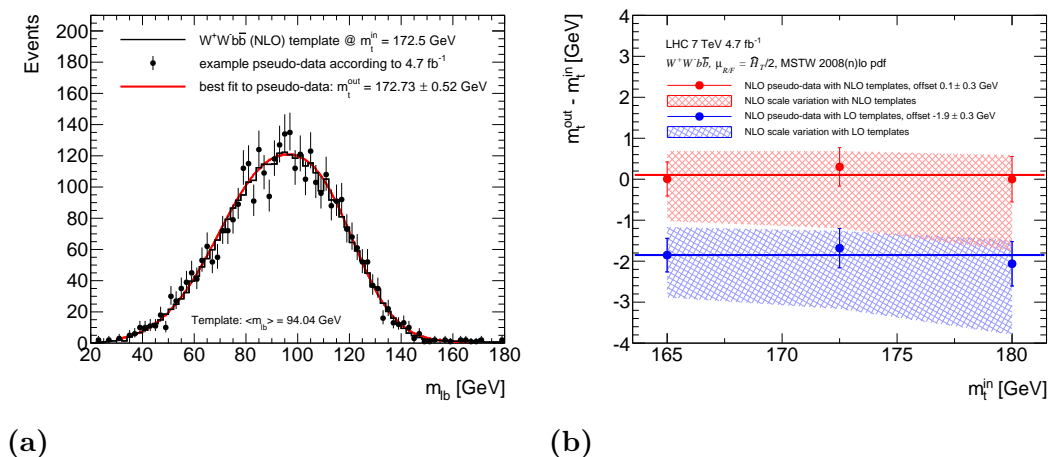


Figure 5.10: In (5.10a) a NLO m_b distribution (black histogram) and the pseudo-data set (black points) generated from it are shown. A fit of the pseudo-data based on NLO templates is given by the red line.

In (5.10b) the difference $m_t^{\text{out}} - m_t^{\text{in}}$ based on NLO templates (red) and LO templates (blue) is shown. The error bars denote the statistical uncertainty due to a luminosity of 4.7/fb. The bands are obtained by varying renormalization and factorization scale in the calculations used for the generation of the pseudo-data, while keeping the templates at the central scale $\mu = \hat{H}_T/2$. The horizontal lines stem from a fit of the three points to a constant, displaying the average offset.

error on m_t^{out} is significantly larger than the statistical uncertainty and of similar size as the theoretical systematic uncertainty assigned to the experimental result in [162]. This is due to the asymmetric scale variation bands of the NLO distribution in Fig. 5.7a.

The blue data points and error band are obtained by replacing the NLO templates with LO templates. Using LO templates introduces a difference between m_t^{in} and m_t^{out} of about -1.9 GeV since the pseudo-data is still generated with NLO distributions. This shift is a measure of the effect of NLO corrections on this top quark mass analysis.

The same analysis is repeated with templates and pseudo-data obtained from the factorized calculation. Results are shown in Fig. 5.11. The scale variation band in Fig. 5.11b is reduced compared to the full calculation. It shrinks from $^{+0.6}_{-1.0}$ GeV for the full calculation to ± 0.2 GeV. This is a consequence of the dif-

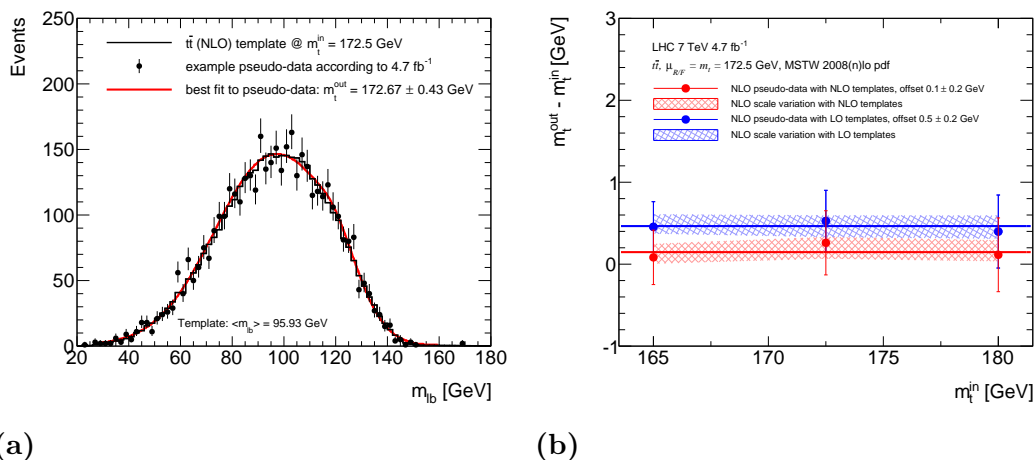


Figure 5.11: Same as Figure 5.10, but pseudo-data as well as templates for the fit are based on the factorized calculation using $\mu = m_t$ instead of the full calculation. The range of the vertical axis in (5.11b) differs from (5.10b).

ferent shapes of the NLO scale variation bands in Fig. 5.7a and Fig. 5.7b. The shift between using NLO templates and LO templates is also reduced, since the shapes of LO and NLO m_{lb} distributions are very similar in the factorized calculation (see Fig. 5.8b).

NLO factorized calculations matched to a parton shower are the standard tool used in experimental top quark analyses such as [162]. This parton level study shows that there can be sizeable differences between the factorized and full calculation, in particular for the magnitude of the scale variation errors.

The large differences between the full and factorized calculation can come from NLO corrections to the top quark decays and from non-resonant contributions. To separate the two contributions it is necessary to repeat the analysis in the strict NWA which includes NLO decays but no non-resonant contributions. Fig. 5.12 shows a comparison between the strict NWA calculation [135, 167] and the full $W^+W^-b\bar{b}$ calculation at NLO. The good agreement in the peak region suggests that the differences between full and factorized calculation are mostly due to NLO corrections to the top quark decays. A more thorough investigation of this issue is in progress.

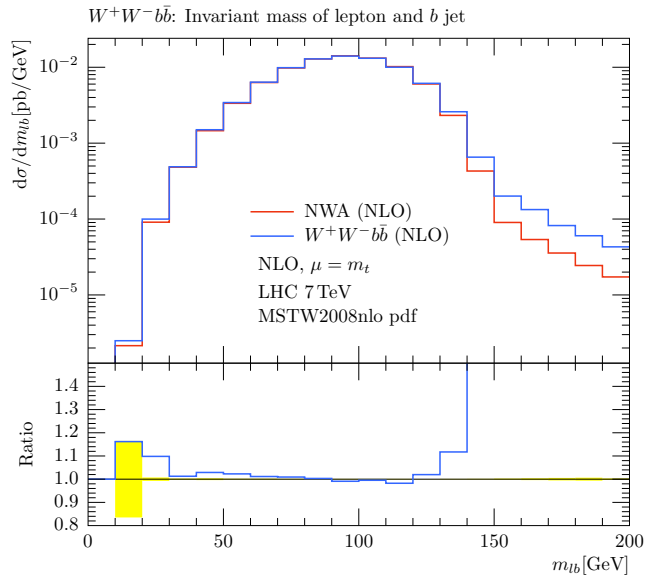


Figure 5.12: Comparison between the full $W^+W^-b\bar{b}$ prediction and the strict NWA approximation including NLO decays for the m_{lb} observable. Renormalization and factorization scale are set to the top quark mass $m_t = 172.5$ GeV.

Part II

Beyond the one-loop order

6 Calculation of multi-loop amplitudes

6.1 Form factor decomposition

The calculation of one-loop amplitudes was described in Chapter 3. Here amplitudes with $L > 1$ are discussed, which appear either in NNLO and higher order calculations or already at lower orders for loop induced processes.

In the form factor approach one strips the polarization vectors of external vector bosons off the amplitude. For an amplitude, as defined in Section 2.2, with m external particles out of which n are vector bosons this leads to

$$\mathcal{A}(p_1, \epsilon_1, \dots, p_n, \epsilon_n, p_{n+1}, \dots, p_m) = \epsilon_{1,\mu_1} \dots \epsilon_{n,\mu_n} \mathcal{A}^{\mu_1 \dots \mu_n}(p_1, \dots, p_n, p_{n+1}, \dots, p_m), \quad (6.1)$$

where the dependence on the quantum numbers of the remaining $m - n$ particles is suppressed. The amplitude can then be rewritten as a linear combination of tensor structures $T_i^{\mu_1 \dots \mu_n}$ with coefficients F_i which are called form factors:

$$\mathcal{A}^{\mu_1 \dots \mu_n} = \sum_i F_i T_i^{\mu_1 \dots \mu_n}. \quad (6.2)$$

As a consequence of the Lorentz covariance of the amplitude, the tensors $T_i^{\mu_1 \dots \mu_n}$ are built from products of external momenta p_i^μ and the metric tensor $g^{\mu\nu}$. For QCD processes with external fermions, they also include generalized Gamma matrices, i.e. structures like $\bar{u}\gamma^\mu u$ [168]. The number of independent form factors can be reduced by exploiting the symmetries of the process, for example transversality conditions, Ward identities, and Bose symmetry [169]. In order to isolate the form factors from the amplitude, one builds projection operators $\mathcal{P}_{i,\mu_1 \dots \mu_n}$ as linear combinations of the independent tensors structures:

$$\mathcal{P}_{i,\mu_1 \dots \mu_n} \mathcal{A}^{\mu_1 \dots \mu_n} = F_i(\{s_{ij}\}, \{m_i\}). \quad (6.3)$$

The form factors are functions of the kinematic parameters s_{ij} and internal masses m_i . Offshell external momenta are included in the s_{ij} as $s_{ii} = p_i^2 \neq 0$. The decomposition depends on the external particles of the process, but it is independent of the loop order of the amplitude. An example for a form factor decomposition is given in Chapter 9.

The numerator of the form factors depends on scalar products of loop and external momenta. One introduces linearly independent sets of propagators $\{D_j\}$ to define integral families with

$$N = \frac{L(L+1)}{2} + L(n-1) \quad (6.4)$$

elements for an n -point L -loop scattering amplitude. All scalar products involving the loop momenta, i.e. $k_i \cdot k_j$ and $k_i \cdot p_j$, can be expressed as linear combinations of the propagators D_j in the integral family and a loop momentum independent term. The integrals appearing in the form factors can then be brought to the form

$$I(\{s_{ij}\}, \{m_i\}) = \int \left(\prod_{i=1}^L \frac{d^D k_i}{i\pi^{D/2}} \right) \frac{1}{\prod_j^N D_j^{\nu_j}}, \quad (6.5)$$

where some of the ν_j can be zero or negative. In general several integral families, corresponding to different topologies and massive propagators, are required for the calculation of a multi-loop amplitude.

6.2 Integration by parts reduction

A multi-loop amplitude contains a large number of loop integrals of the kind given in (6.5), which are in general difficult to calculate. It is therefore advantageous to find relations between the appearing integrals, and to reduce them to a basis of master integrals. The approaches for the reduction of one-loop amplitudes described in Chapter 3 are not applicable at higher loop orders. Integration by parts reduction [170–172] is the most commonly used integral reduction method beyond one-loop. It is implemented in several public computer codes [173–176].

Feynman integrals in dimensional regularization are invariant under linear transformations of the loop momenta or equivalently

$$\int \left(\prod_{i=1}^L \frac{d^D k_i}{i\pi^{D/2}} \right) \frac{\partial}{\partial k_i^\mu} \frac{v^\mu}{\prod_j^N D_j^{\nu_j}} = 0, \quad (6.6)$$

where $v^\mu(k, p)$ depends on loop and external momenta. After taking the derivative explicitly, relations between integrals with changed ν_j are obtained. The coefficients in the relations are rational functions of kinematic invariants, internal masses and the space-time dimension D . The vectors v^μ can be chosen in such a way that no higher propagator powers are introduced in the reduction ($\nu_j \leq 1$) [177, 178], which is useful for unitarity based approaches. There is also progress in understanding the geometric structures underlying the IBP relations [179, 180], relying on the Baikov representation of Feynman integrals [181].

It is possible to use finite field methods for solving the systems of equations in the reduction, which avoids problems due to the large size of intermediate expressions [182, 183]. For a different application of finite field methods in the context of integral reduction see [184].

One obtains a large number of relations in this way, and a systematic algorithm to employ these relations for a reduction to master integrals is needed. This can be achieved by heuristic approaches [174, 185] and the Laporta algorithm [172, 186] implemented in [173, 175, 176]. The Laporta algorithm operates on relations between integrals with numeric ν_i and amounts to Gaussian elimination for the system of linear equations based on a lexicographic ordering of the integrals. For an efficient reduction, it is also important to exploit symmetry relations between Feynman integrals.

There is also progress in alternative multi-loop reduction methods, including integrand level reduction methods using Groebner bases [187–190], and applications of generalized unitarity and on-shell methods beyond the one-loop order [191–194].

6.2.1 Quasi-finite basis

While the number of master integrals for a specific process is fixed, there is some freedom in which integrals to choose as masters. For certain methods of

calculating Feynman integrals, specific basis choices are convenient or even necessary, see for example the canonical basis choice for the differential equation method in Section 6.3.

A different basis choice is motivated by integration methods based on linear reducibility [195–199], which can only be applied to finite integrals. In [199] a method was proposed to express divergent integrals in terms of finite integrals with shifted dimension and propagator powers ν_i . The drawback of the method was the large number of integrals, that it produced. In [200, 201] it was combined with IBP reduction and dimension shift relations [202–204], leading to the quasi-finite basis method. The master integrals are chosen to be quasi-finite (an overall UV divergence from the prefactor is allowed), which can always be achieved by dimension shifts and changing propagator powers. One can test integrals for finiteness by rescaling subsets of Feynman parameters and calculating the degree of divergence [199]. Constraints on dimension and propagator powers for finite integrals can also be derived from the geometric decomposition algorithm (see Section 7.4).

Here the reduction of the two-loop massless nonplanar on-shell box to a quasi-finite basis is shown:

$$\begin{aligned}
 \text{Box}_{4D} &= \frac{c_1}{\epsilon} \text{Box}_{8D} + \frac{c_2}{\epsilon} \text{Box}_{6D} + \frac{c_3}{\epsilon} \text{Box}_{6D} + \frac{c_4}{\epsilon^2} \text{Box}_{6D} \\
 &+ \frac{c_5}{\epsilon^2} \text{Box}_{6D}^{t \leftrightarrow u} + \frac{c_6}{\epsilon^2} \text{Box}_{6D} + \frac{c_7}{\epsilon^2} \text{Box}_{6D}^{t \leftrightarrow u} + \frac{c_8}{\epsilon^2} \text{Box}_{6D}^{s \leftrightarrow u} \\
 &+ \frac{c_9}{\epsilon^4} \text{Box}_{8D} + \frac{c_{10}}{\epsilon^4} \text{Box}_{8D} + \frac{c_{11}}{\epsilon^4} \text{Box}_{8D}^{s \leftrightarrow t} + \frac{c_{12}}{\epsilon^4} \text{Box}_{8D}^{s \leftrightarrow u}.
 \end{aligned} \tag{6.7}$$

Dots on propagators denote an increased exponent of the corresponding propagator, i.e. k dots on propagator i stand for $\nu_i = 1 + k$ in (6.5). The notation for the dimension the integrals live in is nD , which means that the integral is to be calculated in $D = n - 2\epsilon$ dimensions. The $4D$ integral on the left side contains up to ϵ^{-4} poles, while the integrals on the right-hand side of the equation are quasi-finite (integrals 6,7 and 8 contain an overall UV divergence). In the limit $D \rightarrow 4$ the c_i coefficients are finite, all $\frac{1}{\epsilon}$ factors are explicit. Only simple integrals contribute to the leading poles. The coefficient of the first integral is

$$c_1 = \frac{16(2\epsilon - 3)(2\epsilon - 1)(4\epsilon - 3)(2x - 1)(2x - 2x^2 - 3 + \epsilon(9 - 4x + 4x^2))}{s^2(x - 1)x(9 - 6x + \epsilon(10x - 9))}, \tag{6.8}$$

where $x = -\frac{t}{s}$. It contains the thresholds of the nonplanar box $s = 0$, $x = 0$ and $x = 1$. Some of the other coefficients also contain the thresholds of their corresponding master integrals. It would be interesting to investigate this apparent feature of the quasi-finite basis further.

In the limit $D \rightarrow 4$ there is also an additional unphysical divergence at $x = \frac{3}{2}$ which appears in all coefficients c_i . Since it is not present in the $4D$ nonplanar box, it has to cancel between the integrals. This could be a sign that there is a better basis choice that avoids the unphysical threshold.

The fact that the quasi-finite integrals are free of dimensional regularization divergences and seem to have an improved threshold behaviour, makes them well suited for numerical integration approaches such as sector decomposition (see Chapter 7).

6.3 Differential equations

In the following the differential equation method, developed by Kotikov, Remiddi and Gehrmann is described [25–27]. The derivative of a Feynman integral with respect to a kinematic invariant can be written as a linear combination of Feynman integrals in the same integral family. Using IBP reduction the appearing integrals are reduced to a basis of master integrals. This leads to a system of linear differential equations for the master integrals

$$\partial_{x_i} f(\mathbf{x}, \epsilon) = \mathbf{A}_i(\mathbf{x}, \epsilon) f(\mathbf{x}, \epsilon) \quad (6.9)$$

in the kinematic variable x_i , where f is a vector of master integrals.

In [28] it was observed that the system of differential equations can be brought to the simpler form

$$\partial_{x_i} f(\mathbf{x}, \epsilon) = \epsilon \mathbf{A}_i(\mathbf{x}) f(\mathbf{x}, \epsilon) \quad (6.10)$$

or written as a total differential

$$df(\mathbf{x}, \epsilon) = \epsilon d\tilde{\mathbf{A}} f(\mathbf{x}, \epsilon) \quad (6.11)$$

by choosing a suitable basis of master integrals. Here the dependence on the dimensional regularization parameter ϵ is explicit. The kinematic dependence can be made explicit as

$$\mathbf{A}_i(\mathbf{x}) = \sum_j \frac{\mathbf{a}_{ij}}{\alpha_j(\mathbf{x})} \quad (6.12)$$

$$\tilde{\mathbf{A}} = \sum_j \tilde{\mathbf{a}}_j \log(\alpha_j(\mathbf{x})) \quad (6.13)$$

where the function alphabet $\alpha_j(\mathbf{x})$ is determined by the thresholds and pseudothresholds of the integrals. The matrices \mathbf{a}_{ij} or $\tilde{\mathbf{a}}_j$ are independent of the kinematic variables and ϵ containing only rational numbers.

There is no general algorithm to find a basis of integrals that obeys the canonical form of the differential equation. For certain special cases however methods were found [29, 205–209].

In [29] it was found that if the differential equation has a linear ϵ dependence $\mathbf{A}_i(\mathbf{x}, \epsilon) = \mathbf{A}_i^0(\mathbf{x}) + \epsilon \mathbf{A}_i^1(\mathbf{x})$, it can be brought into the canonical form by transforming the \mathbf{A}_i^0 part away. The transformation can be found by solving the differential equation for the ϵ -independent part \mathbf{A}_i^0 or by using the Magnus exponential [210, 211]. It is assumed that the differential equation can be brought to a form linear in ϵ by some other method. The Magnus exponential can also be used to solve the differential equation as an expansion in ϵ . Furthermore in [29] the method was applied to recalculate the previously known two-loop QED vertex [212, 213] and non-planar box integrals [214, 215] in the canonical basis formalism. More advanced applications of this method can also be found in [216, 217].

The solution of (6.11) can be expressed in terms of Chen iterated integrals [218]

$$f(\mathbf{x}, \epsilon) = \mathcal{P} \exp \left[\epsilon \int_{\gamma} d\tilde{\mathbf{A}} \right] f(\mathbf{x}_0, \epsilon) \quad (6.14)$$

where \mathcal{P} denotes path ordering and the path γ starts at \mathbf{x}_0 and terminates at \mathbf{x} . In cases where the function alphabet $\alpha_j(\mathbf{x})$ consists of rational functions in one kinematic parameter, the ϵ -expansion of the integral can be written in terms of hyperlogarithms [219] (also called Goncharov polylogarithms and generalized harmonic polylogarithms) defined by

$$G(a_1, \dots, a_n; z) = \int_0^z \frac{dt}{t - a_1} G(a_2, \dots, a_n; t), \quad (6.15)$$

$$G(a_n; z) = \int_0^z \frac{dt}{t - a_n}. \quad (6.16)$$

Integrals in the canonical basis have the property of uniform weight. With the weight assignments $w(G(a_1, \dots, a_n; z)) = n$ and $w(\epsilon) = -1$ all terms in the ϵ -expansion of uniform weight integrals have the same weight [220].

Another important issue to address is the fixing of the boundary vector $f(\mathbf{x}_0, \epsilon)$ in (6.14). Naively this requires the knowledge of all master integrals at some

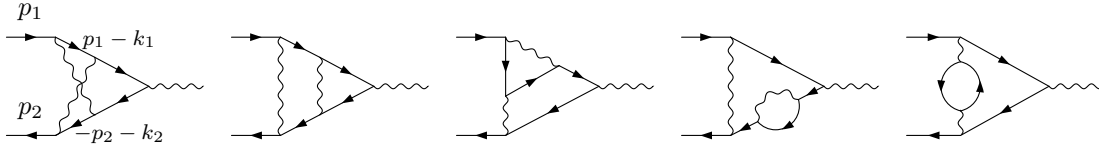


Figure 6.1: Feynman diagrams appearing in the two-loop corrections to the QED vertex. The first diagram shows the momentum routing of the integral family.

kinematic point \mathbf{x}_0 . Using the canonical basis this can be avoided by requiring that the solution is regular in the unphysical pseudo-thresholds of (6.13). This gives additional constraints on the boundary vector. Often these constraints are sufficient to fix the boundary up to a small set of simple integrals [28]. For integrals where no unphysical pseudo-thresholds are available one can fix the boundary by an asymptotic expansion encoded in the differential equation [220].

6.3.1 Two-loop QED vertex

The master integrals contributing to the two-loop QED form factor with massive electrons were first calculated in [212, 213]. Some appearing diagrams are listed in Fig. 6.1. The first diagram also shows the momentum routing of the integral family. Here the master integrals are given in the canonical form, a result which was first presented in [29].

The process depends on the kinematic scales $s = (p_1 + p_2)^2$ and $p_1^2 = p_2^2 = m^2$. From these scales one can build the variable x defined by

$$s = -\frac{m^2(1-x)^2}{x}. \quad (6.17)$$

This change of variables maps the pseudo-thresholds of the integral family in the following way:

$$\begin{aligned} s = 0 & \quad \rightarrow \quad x = 1 \\ s = 4m^2 & \quad \rightarrow \quad x = -1 \\ s = \infty & \quad \rightarrow \quad x = 0. \end{aligned} \quad (6.18)$$

We start with a set of master integrals \mathcal{T}_i shown in Fig. 6.2. In a first step the masters are rescaled with powers of the dimensional regularization parameter

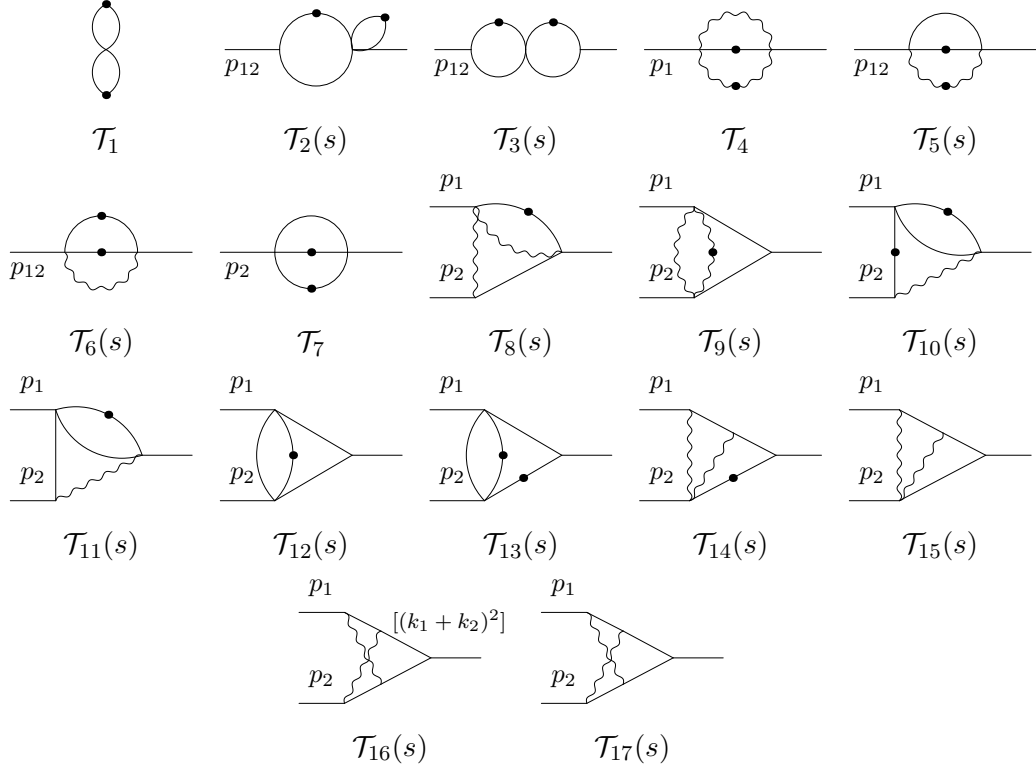


Figure 6.2: Master integrals of the two-loop QED vertex.

ϵ in order to make them finite in the limit $\epsilon \rightarrow 0$:

$$\begin{aligned}
 f_1 &= \epsilon^2 \mathcal{T}_1, & f_2 &= \epsilon^2 \mathcal{T}_2, & f_3 &= \epsilon^2 \mathcal{T}_3, & f_4 &= \epsilon^2 \mathcal{T}_4, & f_5 &= \epsilon^2 \mathcal{T}_5, \\
 f_6 &= \epsilon^2 \mathcal{T}_6, & f_7 &= \epsilon^2 \mathcal{T}_7, & f_8 &= \epsilon^3 \mathcal{T}_8, & f_9 &= \epsilon^3 \mathcal{T}_9, & f_{10} &= \epsilon^2 \mathcal{T}_{10}, \\
 f_{11} &= \epsilon^3 \mathcal{T}_{11}, & f_{12} &= \epsilon^3 \mathcal{T}_{12}, & f_{13} &= \epsilon^2 \mathcal{T}_{13}, & f_{14} &= \epsilon^3 \mathcal{T}_{14}, & f_{15} &= \epsilon^4 \mathcal{T}_{15}, \\
 f_{16} &= \epsilon^4 \mathcal{T}_{16}, & f_{17} &= \epsilon^4 \mathcal{T}_{17}, & & & & & &
 \end{aligned} \tag{6.19}$$

The resulting differential equation in the kinematic variable x has the form

$$\partial_x f(\epsilon, x) = [\mathbf{A}_0(x) + \epsilon \mathbf{A}_1(x)] f(\epsilon, x). \tag{6.20}$$

To bring the differential equation in the canonical form ϵ independent part $\mathbf{A}_0(x)$ has to be transformed away. This is done with the transformation

$$f(\epsilon, x) = \mathbf{B}(x)g(\epsilon, x). \tag{6.21}$$

The matrix $\mathbf{B}(x)$ is determined by solving the differential equation $\partial_x \mathbf{B}(x) = \mathbf{A}_0(x)\mathbf{B}(x)$. The explicit form of the transformation is given by

$$\begin{aligned}
 g_1 &= f_1 , & g_2 &= \lambda_1 f_2 , \\
 g_3 &= (-s)\lambda_2 f_3 , & g_4 &= m^2 f_4 , \\
 g_5 &= \lambda_1 \left(f_5 + \frac{f_6}{2} \right) - \frac{s}{2} f_6 , & g_6 &= (-s)f_6 , \\
 g_7 &= m^2 f_7 , & g_8 &= \lambda_1 f_8 , \\
 g_9 &= \lambda_1 f_9 , & g_{10} &= \lambda_3 (2f_5 + f_6) + m^2 \lambda_2 f_{10} , \\
 g_{11} &= \lambda_1 f_{11} , & g_{12} &= \lambda_1 f_{12} , \\
 g_{13} &= 3 \left(m^2 - \frac{s}{2} \right) f_7 - s\lambda_2 f_{13} , & g_{14} &= (-s)\lambda_2 f_{14} , \\
 g_{15} &= \lambda_1 f_{15} , & g_{16} &= \lambda_1 f_{16} , \\
 g_{17} &= (-s)\lambda_2 f_{17} , & &
 \end{aligned} \tag{6.22}$$

with

$$\lambda_1 = \sqrt{-s}\sqrt{4m^2 - s} , \quad \lambda_2 = (4m^2 - s) , \quad \lambda_3 = \frac{\lambda_1 + \lambda_2}{4} . \tag{6.23}$$

The master integral basis g_i is in the canonical form obeying the differential equation

$$\partial_x g(\epsilon, x) = \epsilon \left[\frac{\mathbf{M}_1}{x} + \frac{\mathbf{M}_2}{1+x} + \frac{\mathbf{M}_3}{1-x} \right] g(\epsilon, x) \tag{6.24}$$

cal threshold to fix the boundary vector of the integration at this point. By requiring the solution to be regular at $x = 1$, one obtains a constraint on the boundary vector $g(x_0 = 1, \epsilon)$. The constraints on the expansion terms of $g(1, \epsilon) = \sum_{n=0}^N \epsilon^n g_n(1)$ turn out to be $\mathbf{M}_3 g_n(1) = 0$ up to the calculated order $N = 5$. This suggests that $\mathbf{M}_3 g(1, \epsilon) = 0$ might be true to all orders in ϵ .

The condition $\mathbf{M}_3 g_n(1) = 0$ fixes the boundary vector up to three simple integrals g_1 , g_4 , and g_7 which do not depend on x . While g_1 and g_4 can be easily computed, the results of [221] are used for the equal mass sunrise graph g_7 . The solution can then be obtained by integrating the differential equation order by order in ϵ in terms of hyperlogarithms with $a_i \in \{-1, 0, 1\}$ (see (6.16)). Agreement was found with the results of [212].

The results in terms of Harmonic Polylogarithms for which the program HPL [222, 223] was used can be found in Appendix B of [29] and in a Mathematica file attached to the Arxiv submission of the same publication.

7 Sector decomposition

7.1 Feynman parameter integrals

In this section parametric representations for the momentum space loop integral in (6.5) are derived. Using the Schwinger trick one can write the propagators as

$$\frac{1}{D_i^{\nu_i}} = \frac{1}{\Gamma(\nu_i)} \int_0^\infty \frac{d\alpha_i}{\alpha_i} \alpha_i^{\nu_i} e^{-\alpha_i D_i} \quad \text{Re}(\nu_i) > 0, \quad (7.1)$$

which is valid for $\text{Re}(D_i) > 0$ achievable by Wick rotating to Euclidean space. Furthermore the condition $\text{Re}(\nu_i) > 0$ has to be fulfilled. For inverse propagators with integer exponents $\nu_i \leq 0$ the relation

$$\frac{1}{D_i^{\nu_i}} = (-1)^{\nu_i} \frac{\partial^{|\nu_i|}}{\partial \alpha^{|\nu_i|}} e^{-\alpha_i D_i} \Big|_{\alpha_i=0} \quad 0 \geq \nu_i \in \mathbb{N} \quad (7.2)$$

can be used. With this transformation the integrand of (6.5) becomes

$$\frac{1}{\prod_i^N D_i^{\nu_i}} = \prod_i^N \left(\frac{1}{\Gamma(\nu_i)} \int_0^\infty \frac{d\alpha_i}{\alpha_i} \alpha_i^{\nu_i} \right) \exp\left(-\sum_i^N \alpha_i D_i\right). \quad (7.3)$$

After integrating out the loop momenta (D -dimensional Gauss integrals), one obtains the Schwinger parameter representation (see for example [224]).

For our purpose the Feynman parameter representation is more useful. Feynman parameters are obtained by introducing a new integration parameter $t = H(\alpha)$ and transforming the Schwinger parameters as $\alpha_i = tx_i$, which leads to

$$\prod_i^N \left(\frac{1}{\Gamma(\nu_i)} \int_0^\infty \frac{dx_i}{x_i} x_i^{\nu_i} \right) \int dt t^\nu \delta(t - H(tx)) \exp\left(-t \sum_i^N \alpha_i D_i\right), \quad (7.4)$$

with $\nu = \sum_i^N \nu_i$. We require $H(\alpha)$ to be a homogeneous weight one function fulfilling the relation $H(tx) = tH(x)$, which makes the argument of the δ -function homogeneous. Furthermore $H(\alpha)$ has to be positive definite for $\alpha \in \mathbb{R}_{>0}^N$ in

order to not change the boundaries of the x_i integrations. These requirements constrain the functional form of H to be $H(\alpha) = \sum_i^N H_i \alpha_i$ with $H_i \geq 0$ and not all H_i zero [225].

Extracting the t variable from the δ -function, one obtains

$$\prod_i^N \left(\frac{1}{\Gamma(\nu_i)} \int_0^\infty \frac{dx_i}{x_i} x_i^{\nu_i} \right) \delta(1 - H(x)) \int \frac{dt}{t} t^\nu \exp(-t \sum_i^N x_i D_i). \quad (7.5)$$

Using (7.1) the integration over t can be performed leading to the Feynman parametrization

$$\frac{1}{\prod_i^N D_i^{\nu_i}} = \Gamma(\nu) \prod_i^N \left(\frac{1}{\Gamma(\nu_i)} \int_0^\infty \frac{dx_i}{x_i} x_i^{\nu_i} \right) \frac{\delta(1 - H(x))}{[\sum_i^N x_i D_i]^\nu}. \quad (7.6)$$

The function H is usually chosen to be $H(x) = \sum_i^N x_i$ and the additional freedom in the choice of $H(x)$ is called the Cheng-Wu theorem [226] and will be important for the geometric decomposition algorithm presented in Section 7.4.

The inverse propagators D_i are defined as $D_i = q_i^2 - m_i^2 + i\delta$, where the q_i are linear combinations of loop momenta k_i and external momenta p_i . With this definition the square-bracket in (7.6) can be written as

$$\sum_i^N x_i D_i = \mathbf{k}^\top \mathbf{M} \mathbf{k} - 2\mathbf{k}^\top \mathbf{Q} + J + i\delta, \quad (7.7)$$

where boldface letters specify vectors and matrices in loop momentum space, e.g. \mathbf{k} is a L -dimensional column vector containing the loop momentum Lorentz vectors as its elements. With the loop momentum transformation $\mathbf{k} = \mathbf{k}' + \mathbf{M}^{-1} \mathbf{Q}$, one eliminates the linear term in (7.7) and obtains

$$\mathbf{k}'^\top \mathbf{M} \mathbf{k}' - \mathbf{Q}^\top \mathbf{M}^{-1} \mathbf{Q} + J + i\delta, \quad (7.8)$$

where $\mathbf{M} = \mathbf{M}^\top$ was used. After Wick rotation the loop momentum integrations can be performed in Euclidean space, and one ends up with the Feynman parametrization of the multi-loop integral in (6.5):

$$I(\{s_{ij}\}, \{m_i\}) = (-1)^\nu \frac{\Gamma(\nu - \frac{LD}{2})}{\prod_i^N \Gamma(\nu_i)} \prod_i^N \int_0^\infty \frac{dx_i}{x_i} x_i^{\nu_i} \delta(1 - H) \frac{\mathcal{U}^{\nu - (L+1)\frac{D}{2}}}{\mathcal{F}^{\nu - L\frac{D}{2}}}, \quad (7.9)$$

$$\mathcal{U}(x) = \det(\mathbf{M}), \quad (7.10)$$

$$\mathcal{F}(x, \{s_{ij}\}, \{m_i\}) = \det(\mathbf{M}) [\mathbf{Q}^\top \mathbf{M}^{-1} \mathbf{Q} - J - i\delta]. \quad (7.11)$$

The graph polynomials \mathcal{U} and \mathcal{F} are polynomials of homogeneous weight L and $L + 1$ respectively. They are also called first and second Symanzik polynomials, and are sometimes denoted ψ and ϕ in the mathematical literature.

There is also a graph theoretical method to obtain the Symanzik polynomials from the associated Feynman diagram [227]. The k -forest \mathcal{T}_k is defined as the partition of a subset of the edges of a graph into k sets with the property that the subsets are connected and contain no loops. For the set of all 1-forests $|\mathcal{T}_1|$ this corresponds to the set of spanning trees of the graph, while the set of 2-forests $|\mathcal{T}_2|$ is obtained by cutting one additional edge in all possible ways. The graph polynomials are then constructed as

$$\mathcal{U} = \sum_{T \in |\mathcal{T}_1|} \prod_{e \notin T} x_e, \quad (7.12)$$

$$\mathcal{F}_0 = \sum_{T \in |\mathcal{T}_2|} (-s_T) \prod_{e \notin T} x_e, \quad (7.13)$$

$$\mathcal{F} = \mathcal{F}_0 + \mathcal{U} \sum_e^N x_e m_e^2, \quad (7.14)$$

where s_T is defined as the squared momentum flowing through the cut of the 2-forest T . This representation shows that \mathcal{U} and \mathcal{F}_0 are homogeneous polynomials linear in the Feynman parameters, while \mathcal{F} can also contain terms which are quadratic in a Feynman parameter corresponding to a massive propagator.

7.2 Singularities of Feynman parameter integrals

The Euclidean region is defined as the kinematic region where all $s_T \leq 0$ and all $m_i^2 \geq 0$. In this region the graph polynomial \mathcal{F} is a positive-semidefinite function of the Feynman parameters.

In the Euclidean region the graph polynomials become zero only in regions where subsets of the Feynman parameters go to zero. Zeroes of the \mathcal{U} polynomial can lead to UV divergences, while $\mathcal{F} = 0$ corresponds to IR divergences (see Section 2.3), all of these singularities are regulated by the dimensional regularization parameter ϵ . An overall UV divergence can come from the $\Gamma(\nu - LD/2)$ prefactor in (7.10).

For general kinematics Feynman integrals develop additional kinematic dependent singularities. The Landau equations constitute necessary conditions for the appearance of divergences [228]. In Feynman parameter space they are given by [229]

$$\mathcal{F} = 0 \quad \text{and} \quad \begin{cases} \text{either} & x_i = 0 \\ \text{or} & \partial_i \mathcal{F} = 0 \end{cases} \quad \text{for each } i. \quad (7.15)$$

A singularity with all $x_i \neq 0$ is called leading Landau singularity. Subleading singularities with $x_i = 0$ for some i correspond to singularities of subgraphs.

7.3 Sector decomposition

The sector decomposition algorithm applies to dimensionally regulated parameter integrals. These integrals can be Feynman integrals, as in (7.10), D -dimensional phase-space integrals [32], or even more general classes of integrals. In the following we will concentrate on its application to Feynman integrals. Sector decomposition was used to disentangle overlapping UV [230, 231] and IR singularities [232, 233], and applied to certain one-loop integrals in [234]. It was generalized to an automatized algorithm for the computation of divergent parameter integrals in dimensional regularization in [30–33].

The sector decomposition algorithm is implemented in the public programs `SECTOR_DECOMPOSITION` [235], `FIESTA` [236–239], and `SECDEC` [36–38].

The goal of sector decomposition is to extract singularities in the dimensional regularization parameter ϵ from an integral before the integration is performed, resulting in an expanded form

$$I(\{s_{jk}\}, \{m_j\}) = \sum_{i=-n}^{n_{\max}} c_i(\{s_{jk}\}, \{m_j\}) \epsilon^i. \quad (7.16)$$

The expansion starts from the leading pole order of the integral n . For an L -loop integral the maximal pole order is $n = 2L$. It is possible to expand to any order n_{\max} . An expansion beyond the finite term $n_{\max} = 0$ is required as an input for the calculation of cross sections beyond NLO and already at NLO for loop-induced processes, such as Higgs boson pair production in gluon fusion presented in Chapter 9. There the one-loop amplitude had to be expanded up to order ϵ^2 to cancel UV and IR singularities in the NLO calculation. The

coefficients $c_i(\{s_{jk}\}, \{m_j\})$ are integrals in the Feynman parameters, which are finite in the $\epsilon \rightarrow 0$ limit. This makes it possible to use numerical integration routines for their evaluation.

To obtain the expansion in ϵ , one considers integrals in the Euclidean region, where all singularities are due to some subset of Feynman parameters going to zero. Now the integration region is split up into sectors in which one can locally transform the Feynman parameters to bring the graph polynomials in the factorized form

$$\mathcal{U} = \mathbf{x}^{\mathbf{v}_0} \left(1 + \sum_i \mathbf{x}^{\mathbf{v}_i} \right) \quad \text{with} \quad \mathbf{v}_i \in \mathbb{N}_{\geq 0}^{N-1}, \quad (7.17)$$

$$\mathcal{F} = \mathbf{x}^{\mathbf{w}_0} \left(s_0 + \sum_i s_i \mathbf{x}^{\mathbf{w}_i} \right) \quad \text{with} \quad \mathbf{w}_i \in \mathbb{N}_{\geq 0}^{N-1}, \quad (7.18)$$

where the integration region in each sector is mapped to an $N - 1$ -dimensional unit hypercube $([0, 1]^{N-1})$. Depending on the decomposition strategy \mathbf{v}_0 and \mathbf{w}_0 can contain negative components. Here and in the following multi-index notation is used, e.g. $\mathbf{x}^{\mathbf{v}_0} = \prod_j x_j^{(\mathbf{v}_0)_j}$. Different strategies for the decomposition are discussed in the next section.

Singularities in the Minkowski region are treated via a deformation of the integration contour described in Section 7.5. In the Euclidean region the expressions in the brackets are nonzero and the only zeros come from the $\mathbf{x}^{\mathbf{v}_0}$ and $\mathbf{x}^{\mathbf{w}_0}$ factors. Due to the simple singularity structure subtraction terms can be introduced which locally cancel the singularities (see Section 7.6). Finally the algebraic expressions for the terms in the ϵ expansion are integrated numerically (see Section 7.7).

7.3.1 Iterated decomposition

Iterated sector decomposition strategies rely on choosing subsets of Feynman parameters $\mathcal{S} = \{x_{\alpha_1}, \dots, x_{\alpha_r}\}$ and partitioning the parameter space into r sectors [30]. In sector i the parameter x_{α_i} is larger than the other $r - 1$ Feynman parameters ($x_{\alpha_i} \geq x_{\alpha_j} \forall j \neq i$). The transformation

$$x_{\alpha_j} = \begin{cases} x'_{\alpha_i} & \text{for } j = i \\ x'_{\alpha_i} x'_{\alpha_j} & \text{for } j \neq i \end{cases} \quad (7.19)$$

is used to map the integration region of sector i back to the unit hypercube. Starting from (7.10) one chooses $\mathcal{S} = \{x_1, \dots, x_N\}$ as the first step of the iteration. This step is called primary sector decomposition. It eliminates the δ -distribution in (7.10) and maps the $N - 1$ remaining Feynman parameter integrations to the unit hypercube. After the primary decomposition one iterates the decomposition with different sets \mathcal{S} until the factorized form of (7.18) is obtained.

There are several different strategies for choosing the subsets \mathcal{S} . The heuristic algorithm implemented in SECDEC chooses the smallest set \mathcal{S} which sets the graph polynomials to zero [30, 36]. It usually produces a small number of sectors with the drawback that it can sometimes run into infinite loops. Often this problem can be circumvented by a reordering of the Feynman parameters. The infinite recursion problem is illustrated in the following example. The function to be decomposed is

$$f = x_1^2 + x_2^2 x_3. \quad (7.20)$$

If one chooses the set $\mathcal{S}_1 = \{x_1, x_3\}$ for the first decomposition step, one obtains in the sector with $x_3 \geq x_1$

$$f' = x_3 (x_3 x_1^2 + x_2^2). \quad (7.21)$$

Since the expression is not yet in the decomposed form of (7.18), one chooses a second set $\mathcal{S}_2 = \{x_2, x_3\}$, leading to

$$f'' = x_3^2 (x_1^2 + x_2^2 x_3) \quad (7.22)$$

in the $x_3 \geq x_2$ sector. The expression in brackets is identical to (7.20), leading to an infinite recursion. In this example the recursion could be avoided by choosing $\mathcal{S}_2 = \{x_1, x_2\}$.

An algorithm which avoids infinite recursion is the original strategy by Hepp [230]. It consists in choosing the maximal set $\mathcal{S} = \{x_1, \dots, x_N\}$ in each decomposition step. This avoids infinite recursion, but produces a very large number of sectors.

Another algorithm solves the recursion issue by choosing decomposition sets according to winning strategies of Hironaka's polyhedra game [235]. The polyhedra game was used to prove resolution of singularities for algebraic varieties in characteristic zero [240]. Sector decomposition can be viewed as a special

case of this more general problem. The algorithms based on different winning strategies of the polyhedra game produce a large number of sectors compared to the heuristic method of [30]. For a comparison see [235].

The strategy implemented in FIESTA is based on geometric information from the exponent vectors of the polynomials, that are to be decomposed [236]. Since the algorithm is not guaranteed to terminate, it is combined with an algorithm based on the polyhedra game [235].

The Speer sector strategy is based on analyzing subgraphs of the Feynman graph under consideration, which gives a graph theoretical interpretation of sector decomposition [231–233]. In [241] it was found that the method implemented in FIESTA produces the same number of sectors as the Speer sector strategy.

7.4 Geometric decomposition

The approach to sector decomposition proposed by Kaneko and Ueda in [34, 35] is based on convex geometry. Here an improved geometric strategy based on their method is presented. The original and the improved geometric method are implemented in SECDEC-3.0 [38].

7.4.1 Convex geometry

In this section the relevant geometric objects are introduced. For more detailed expositions, see [242–246].

A set $X \subset \mathbb{R}^N$ is convex, if a line segment connecting any two points in X is contained in X . The Minkowski sum of two convex sets X and Y , defined as

$$X + Y = \{\mathbf{x} + \mathbf{y} \mid \mathbf{x} \in X, \mathbf{y} \in Y\}, \quad (7.23)$$

is again a convex set.

We are interested in the special case of convex rational polyhedral sets X , which can be defined as intersections of a finite number of affine half-spaces indexed

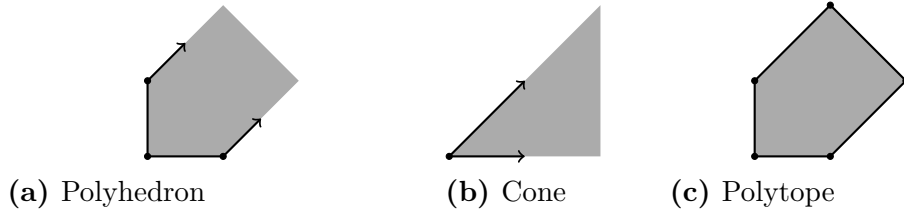


Figure 7.1: Two dimensional examples for geometric sets considered in the text.

by F :

$$X = \bigcap_F \left\{ \mathbf{m} \in \mathbb{R}^N \mid \langle \mathbf{m}, \mathbf{n}_F \rangle + a_F \geq 0 \right\}, \quad (7.24)$$

where $\langle \mathbf{a}, \mathbf{b} \rangle = \sum_{i=1}^N a_i b_i$ is the standard inner product on \mathbb{R}^N . Here the half-spaces are defined by the primitive normal vectors $\mathbf{n}_F \in \mathbb{Z}^N$ and $a_F \in \mathbb{Z}$, since we only consider rational polyhedral sets.

A set X as defined in (7.24) is called a polyhedron. There are two important special cases: cones and polytopes. Every polyhedron can be expressed as the Minkowski sum of a polytope and a cone.

A cone σ is obtained in the case where all half spaces are defined by homogeneous inequalities, i.e. $a_F = 0$ for all F :

$$\sigma = \bigcap_F \left\{ \mathbf{m} \in \mathbb{R}^N \mid \langle \mathbf{m}, \mathbf{n}_F \rangle \geq 0 \right\}. \quad (7.25)$$

The Minkowski-Weyl theorem states that a finite number of vectors $\mathbf{v}_1, \dots, \mathbf{v}_n \in \mathbb{Z}^N$ exists, such that

$$\sigma = \{ a_1 \mathbf{v}_1 + \dots + a_n \mathbf{v}_n \mid a_i \in \mathbb{R}_{\geq 0} \}. \quad (7.26)$$

A cone is pointed if the cone and its negative overlap only in the origin, i.e. the condition $\sigma \cap (-\sigma) = \{0\}$ is fulfilled. For pointed cones (7.26) constitutes a second representation of cones as the convex hull of a set of extreme rays \mathbf{v}_i . The cone σ is simplicial if its extreme rays are linearly independent. Nonsimplicial cones can be decomposed into simplicial cones of the same dimension. This procedure is called triangulation. Triangulations of a three dimensional cone defined by four rays are shown in Fig. 7.2.



Figure 7.2: Cross section of a three dimensional cone defined by four rays. Several possibilities for the triangulation are shown.

A polytope can be defined by (7.24) with the additional requirement of boundedness. This is called the facet representation or \mathcal{H} -representation of a polytope. The vertex or \mathcal{V} -representation is given by

$$P = \text{ConvHull}(\mathbf{v}_1, \dots, \mathbf{v}_n) = \{a_1 \mathbf{v}_1 + \dots + a_n \mathbf{v}_n \mid a_i \in \mathbb{R}_{\geq 0}, \sum_{i=1}^n a_i = 1\}, \quad (7.27)$$

where the convex hull is defined as the minimal convex set containing all \mathbf{v}_i . One can translate one representation into the other using Fourier-Motzkin elimination [245].

The faces of a polyhedron X are defined as the intersection of supporting hyperplanes

$$H_F = \{\mathbf{m} \in \mathbb{R}^N \mid \langle \mathbf{m}, \mathbf{n}_F \rangle + a_F = 0\} \quad (7.28)$$

with X , such that $\langle \mathbf{m}, \mathbf{n}_F \rangle + a_F \geq 0$ for all \mathbf{m} in X . Faces of a cone (polytope) are again cones (polytopes). They are graded by their dimension: Zero dimensional faces are called vertices, one dimensional faces are called edges, and $\dim(X) - 1$ dimensional faces are called facets.

A fan Δ in \mathbb{R}^N is a set of cones σ obeying the following conditions [243]:

1. Each face of a cone σ in Δ is again a cone in Δ .
2. The intersection of two cones is again a cone in Δ .

If $\bigcup_{\sigma \in \Delta} \sigma$, the union of cones σ in a fan Δ , is \mathbb{R}^N , the fan Δ is called complete. The normal fan Δ_P of a polytope P can be constructed by considering cones $\sigma_{\mathcal{F}}$ for each face \mathcal{F} of P , generated by the normal vectors \mathbf{n}_F of all facets F containing the face \mathcal{F} . With this one defines the normal fan of P as [246]

$$\Delta_P = \{\sigma_{\mathcal{F}} \mid \mathcal{F} \text{ is a face of } P\}. \quad (7.29)$$

Every normal fan is complete, the converse statement is generally not true. A polytope and its normal fan are shown in Fig. 7.3.

7.4.2 The geometric algorithm

The general class of integrals that can be treated with geometric sector decomposition is of the form

$$I = \int_{\mathbb{R}_{\geq 0}^N} \left(\prod_i^N \frac{dx_i}{x_i} x_i^{s_i} \right) \left(\prod_j^M f_j(x)^{t_j} \right). \quad (7.30)$$

The functions $f_j(x)$ are Laurent polynomials $f_j(x) = \sum_i^m c_{ji} \mathbf{x}^{\mathbf{v}_{ji}}$ with $\mathbf{v}_{ji} \in \mathbb{Z}^N$. We assume that the coefficients c_{ji} are non-negative, which corresponds to the Euclidean region for Feynman integrals. The exponents s_i and t_j can take arbitrary complex values.

One can bring Feynman integrals as given in (7.10) into this form by integrating out the $\delta(1 - H(x))$ distribution with $H(x) = x_N$.

With the change of variables $z_i = \log(x_i)$ for all i , one obtains

$$I = \int_{\mathbb{R}^N} d\mathbf{z} e^{\langle \mathbf{s}, \mathbf{z} \rangle} \left(\prod_j^M f_j(z)^{t_j} \right), \quad (7.31)$$

with functions $f_j(z) = \sum_i^m c_{ji} e^{\langle \mathbf{v}_{ji}, \mathbf{z} \rangle}$.

The information about singularities in the Euclidean region is completely encoded in the Newton polytopes of the functions $f_j(x)$, that are to be integrated. In the following we specialize to the case of one polynomial f ($M = 1$). The Newton polytope $\mathcal{N}(f)$ is defined as the convex hull of the exponent vectors of the polynomial $f = \sum_i^m c_i \mathbf{x}^{\mathbf{v}_i}$ (see (7.27)):

$$\mathcal{N}(f) = \text{ConvHull}(\mathbf{v}_1, \dots, \mathbf{v}_m). \quad (7.32)$$

The \mathcal{H} -representation of $\mathcal{N}(f)$ as defined in (7.28) is

$$\mathcal{N}(f) = \bigcap_F \left\{ \mathbf{m} \in \mathbb{R}^N \mid \langle \mathbf{m}, \mathbf{n}_F \rangle + a_F \geq 0 \right\}. \quad (7.33)$$

In the following we assume that the polytope $\mathcal{N}(f)$ has full dimension N , lower dimensional polytopes can be treated by adding additional facets normal to the hyperplane the polytope is contained in. The normal fan $\Delta_{\mathcal{N}(f)}$ of the Newton polytope can now be built as in (7.29). For each extreme vertex of $\mathcal{N}(f)$ there is a N -dimensional cone in $\Delta_{\mathcal{N}(f)}$. Each facet normal vector represents

a one-dimensional cone. In general d -dimensional faces of the polytope $\mathcal{N}(f)$ correspond to $N - d$ -dimensional cones in $\Delta_{\mathcal{N}(f)}$.

The rays of a N -dimensional cone $\sigma(\mathbf{v}_i)$ associated to the extreme vertex \mathbf{v}_i are the normal vectors \mathbf{n}_F of the facets incident to \mathbf{v}_i :

$$\text{rays}(\sigma(\mathbf{v}_i)) = \{\mathbf{n}_F \mid \langle \mathbf{n}_F, \mathbf{v}_i \rangle + a_F = 0\}. \quad (7.34)$$

The cones in the fan $\Delta_{\mathcal{N}(f)}$ are in general not simplicial. One obtains the simplicial normal fan $\Delta_{\mathcal{N}(f)}^T$ by splitting the nonsimplicial cones into simplicial cones (see Fig. 7.2). The simplicial fan $\Delta_{\mathcal{N}(f)}^T$ provides a decomposition of \mathbb{R}^N (the integration region of (7.31)) into N -dimensional simplicial cones:

$$\int_{\mathbb{R}^N} \omega = \sum_{\substack{\sigma \in \Delta_{\mathcal{N}(f)}^T \\ \dim(\sigma) = N}} \int_{\sigma} \omega. \quad (7.35)$$

Each N -dimensional simplicial cone is defined by N rays \mathbf{n}_F as

$$\sigma = \left\{ \sum_{F \in \sigma} a_F \mathbf{n}_F \mid a_F \in \mathbb{R}_{\geq 0} \right\}. \quad (7.36)$$

The rays n_F can be used to define local coordinates in the cone. The transformation of the Feynman parameters x_i to the local facet coordinates y_F maps the integration over cones back to the unit hypercube. Its explicit form is

$$x_i = \prod_{F \in \sigma} y_F^{\langle \mathbf{n}_F, \mathbf{e}_i \rangle} \quad (7.37)$$

for the cone σ .

By splitting the integration region of (7.30) according to the simplicial fan $\Delta_{\mathcal{N}(f)}^T$ (see (7.35)) and applying the change of variables for each full dimensional cone σ , one obtains the decomposed form

$$I = \sum_{\substack{\sigma \in \Delta_{\mathcal{N}(f)}^T \\ \dim(\sigma) = N}} |\sigma| \prod_{F \in \sigma} \int_0^1 \frac{dy_F}{y_F} y_F^{\langle \mathbf{n}_F, \mathbf{s} \rangle} \left(\sum_i c_i \prod_{F \in \sigma} y_F^{\langle \mathbf{n}_F, \mathbf{v}_i \rangle} \right)^t, \quad (7.38)$$

where $|\sigma|$ denotes the absolute value of the determinant of the N -by- N matrix built from the facet vectors \mathbf{n}_F of cone σ .

The exponents $\langle \mathbf{n}_F, \mathbf{v}_i \rangle$ can in general be negative. To obtain a polynomial, one factors out a monomial $\prod_{F \in \sigma} y_F^{-a_F}$, which leads to

$$I = \sum_{\substack{\sigma \in \Delta_{\mathcal{N}(f)}^T \\ \dim(\sigma) = N}} |\sigma| \prod_{F \in \sigma} \int_0^1 \frac{dy_F}{y_F} y_F^{\langle \mathbf{n}_F, \mathbf{s} \rangle - ta_F} \underbrace{\left(\sum_i c_i \prod_{F \in \sigma} y_F^{\langle \mathbf{n}_F, \mathbf{v}_i \rangle + a_F} \right)^t}_{=g(y)}. \quad (7.39)$$

The exponents of the monomials in $g(y)$ are $\langle \mathbf{n}_F, \mathbf{v}_i \rangle + a_F$. They are guaranteed to be nonnegative since the \mathbf{v}_i are points in the polytope $\mathcal{N}(f)$, given by (7.33). For the integral to be in sector decomposed form as defined in (7.18), there has to be a constant term in $g(y)$ for each sector σ . Each maximal cone $\sigma(\mathbf{v}_i)$ in $\Delta_{\mathcal{N}(f)}^T$ corresponds to an exponent vector \mathbf{v}_i of $f(x)$. All facets normals \mathbf{n}_F with $F \in \sigma(\mathbf{v}_i)$ are incident to \mathbf{v}_i :

$$\langle \mathbf{n}_F, \mathbf{v}_i \rangle + a_F = 0 \quad \forall F \in \sigma(\mathbf{v}_i). \quad (7.40)$$

This corresponds to the exponent vector of a monomial in $g(y)$ which has to be the zero vector, showing that there is a constant term in each sector.

A convenient way of writing (7.39) is

$$I = \prod_{F \in \Delta_{\mathcal{N}(f)}^T} \int_0^1 \frac{dy_F}{y_F} y_F^{\langle \mathbf{n}_F, \mathbf{s} \rangle - ta_F} \left(\sum_i c_i \prod_{F \in \Delta_{\mathcal{N}(f)}^T} y_F^{\langle \mathbf{n}_F, \mathbf{v}_i \rangle + a_F} \right)^t \sum_{\substack{\sigma \in \Delta_{\mathcal{N}(f)}^T \\ \dim(\sigma) = N}} |\sigma| \prod_{F \notin \sigma} \delta(1 - y_F). \quad (7.41)$$

Here the integration region is viewed as a N -dimensional subspace of the space of facet variables, defined by the δ -distributions. It shows that the different sectors are just projections of a single expression in terms of facet variables.

The case of one function f was discussed above. A generalization to an arbitrary number of functions f_j is possible. Instead of the Newton polytope $\mathcal{N}(f)$, one considers the polytope $\mathcal{N}(\prod_j^M f_j)$ or equivalently the Minkowski sum $\sum_j^M \mathcal{N}(f_j)$. The algorithm works the same, only the step from (7.38) to (7.39) where a monomial is factored out of f changes. Instead of factoring out a monomial $\prod_{F \in \sigma} y_F^{-a_F}$, for each function f_j a monomial $\prod_{F \in \sigma} y_F^{-a_{jF}}$ is factored out. The relation $\sum_{j=1}^M a_{jF} = a_F$ is valid, where a_F is associated to the polytope $\mathcal{N}(\prod_j^M f_j)$.

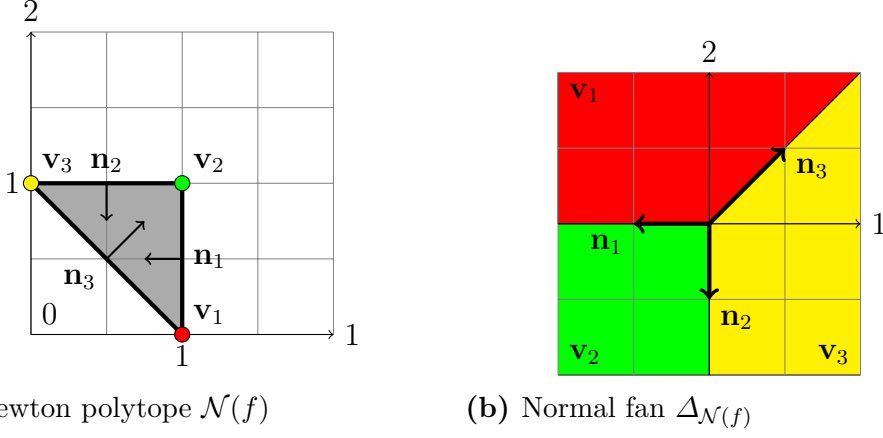


Figure 7.3: Newton polytope $\mathcal{N}(f)$ and normal fan $\Delta_{\mathcal{N}(f)}$ associated to the two-loop vacuum integral of (7.42)

Two-loop vacuum integral

To illustrate the method, here a two-loop vacuum integral will be decomposed using the geometric algorithm. The example was first presented in [247].

The integral under consideration is

$$I = \text{diagram} = \frac{(-1)^\nu \Gamma(\nu - LD/2)}{(m^2)^{\nu - LD/2} \Gamma(\nu_1) \Gamma(\nu_2)} \int_0^\infty \frac{dx_1 dx_2}{x_1 x_2} x_1^{\nu_1} x_2^{\nu_2} (x_1^1 x_2^0 + x_1^1 x_2^1 + x_1^0 x_2^1)^{-\frac{D}{2}}, \quad (7.42)$$

where the Feynman parameter x_3 was integrated out using $\delta(1 - x_3)$. The exponent vectors of $f(x) = x_1^1 x_2^0 + x_1^1 x_2^1 + x_1^0 x_2^1$ are

$$\mathbf{v}_1 = \begin{pmatrix} 1 \\ 0 \end{pmatrix}, \mathbf{v}_2 = \begin{pmatrix} 1 \\ 1 \end{pmatrix}, \mathbf{v}_3 = \begin{pmatrix} 0 \\ 1 \end{pmatrix}. \quad (7.43)$$

They are used to define the Newton polytope $\mathcal{N}(f)$ as the convex hull of the exponent vectors, see Fig. 7.3. The \mathcal{H} -representation of the Newton polytope is given by the facet normal vectors

$$\begin{aligned} \mathbf{n}_1 &= \begin{pmatrix} -1 \\ 0 \end{pmatrix} & \mathbf{n}_2 &= \begin{pmatrix} 0 \\ -1 \end{pmatrix} & \mathbf{n}_3 &= \begin{pmatrix} 1 \\ 1 \end{pmatrix}. \\ a_1 &= 1 & a_2 &= 1 & a_3 &= -1 \end{aligned} \quad (7.44)$$

The normal fan $\Delta_{\mathcal{N}(f)}$ is shown in Fig. 7.3. Here the fan is already simplicial, i.e. $\Delta_{\mathcal{N}(f)} = \Delta_{\mathcal{N}(f)}^T$, since all cones of dimension d are given by exactly d rays. There are three cones of maximal dimension two, corresponding to the extreme vertices \mathbf{v}_1 , \mathbf{v}_2 , and \mathbf{v}_3 . The maximal cones can be defined as in (7.26) by sets of incident facet normal vectors $\{\mathbf{n}_3, \mathbf{n}_1\}$, $\{\mathbf{n}_1, \mathbf{n}_2\}$, $\{\mathbf{n}_2, \mathbf{n}_3\}$ respectively. The change of variables to facet variables y_F is given by

$$\begin{aligned} x_1 &= y_1^{-1} y_3, \\ x_2 &= y_2^{-1} y_3. \end{aligned} \tag{7.45}$$

Using (7.41) one arrives at the decomposed form of the vacuum integral

$$\begin{aligned} I &= \frac{(-1)^\nu \Gamma(\nu - LD/2)}{(m^2)^{\nu - LD/2} \Gamma(\nu_1) \Gamma(\nu_2)} \int_0^1 \frac{dy_1 dy_2 dy_3}{y_1 y_2 y_3} y_1^{-\nu_1 + \frac{D}{2}} y_2^{-\nu_2 + \frac{D}{2}} y_3^{\nu_1 + \nu_2 - \frac{D}{2}} \\ &\quad (y_1 + y_2 + y_3)^{-\frac{D}{2}} [\delta(1 - y_2) + \delta(1 - y_3) + \delta(1 - y_1)], \end{aligned} \tag{7.46}$$

where the sectors correspond to the maximal cones associated to \mathbf{v}_1 , \mathbf{v}_2 , and \mathbf{v}_3 . It is interesting to note that all primary sector decomposition based algorithms (i.e. all other algorithms) produce at least six sectors for this integral.

Finite integrals

It is possible to derive constraints on the propagator powers ν_i and the dimension D for finite integrals as introduced in Subsection 6.2.1 from the decomposed form (7.41). The only divergences in (7.41) come from the monomial $\prod_{F \in \Delta_{\mathcal{N}(f)}^T} y_F^{\langle \mathbf{n}_F, \mathbf{s} \rangle - t a_F}$. The condition for a finite integral is (note the strict inequality)

$$\langle \mathbf{n}_F, \mathbf{s} \rangle - t a_F > 0 \quad \forall F. \tag{7.47}$$

This defines a cone in (\mathbf{s}, t) -space, or equivalently in $(\boldsymbol{\nu}, D)$ -space for scalar Feynman integrals since \mathbf{s} and t are linear homogeneous functions in ν_i and D . All points (\mathbf{s}, t) inside the cone correspond to quasi-finite integrals in the sense of [199–201].

Toric varieties

Here a connection between geometric sector decomposition and the theory of toric varieties is discussed. The following description of toric varieties is based

on [246, 248].

A variety over the complex numbers $V(f_1, \dots, f_m)$ is the subset of \mathbb{C}^N fulfilling polynomial equations $f_j(x) = 0$. General polynomials lead to affine varieties, homogeneous polynomials to projective varieties.

An algebraic torus is defined as $(\mathbb{C}^*)^n$ where $\mathbb{C}^* = \mathbb{C} \setminus \{0\} = \{z \in \mathbb{C} \mid z \neq 0\}$, the n -dimensional complex space with all coordinate hyperplanes removed. A toric variety V is a (irreducible) variety containing the torus $(\mathbb{C}^*)^n$ as a Zariski open subset. Furthermore there is an action of $(\mathbb{C}^*)^n$ on itself which extends to an action on V . For a variety $W \subset V$, a Zariski open subset of V is defined as $V \setminus W = \{v \in V \mid v \notin W\}$.

There is a correspondence between the geometric objects introduced in Subsection 7.4.1 and toric varieties. Affine varieties correspond to fans, and projective varieties to polytopes. The facet variables are homogeneous coordinates in a projective toric variety, the sectors are affine patches covering the projective variety. The decomposition of a fan Δ_P into a simplicial fan Δ_P^T , is a resolution of singularities for the underlying toric variety associated to the polytope P .

The toric variety associated to the two-loop vacuum integral given in (7.42) is the projective space $\mathbb{P}^2 = (\mathbb{C}^3 \setminus 0)/\mathbb{C}^*$. The facet variables y_F in the sector decomposed integral (7.46) correspond to the homogeneous coordinates in \mathbb{C}^3 , while the three sectors define subsets with $y_F = 1$ for $F = 1, 2, 3$. Their union covers all of \mathbb{P}^2 .

Here we also want to mention related constructions used in the theory of generalized hypergeometric functions, which have integral representations similar to Feynman parameter integrals, see for example [249–251].

7.5 Contour deformation

As described in Section 7.2, Feynman integrals can develop kinematic dependent singularities in the physical region. These singularities are not regulated by dimensional regularization. They appear as zeros of the \mathcal{F} -polynomial for some values of the Feynman parameters and kinematic variables, given by the Landau equations (7.15).

To deal with this type of singularity, the real integrations over Feynman parameters are continued to complex integrations. Following from Cauchy's theorem

one has

$$\oint_{\Gamma} \prod_i dz_i f(z) = 0 \quad (7.48)$$

for a closed contour Γ which does not enclose any singularities of $f(z)$. Here $f(z)$ denotes the integrand of a Feynman integral. The contour Γ is split up into an integration from zero to one along the real axis and path γ closing the integration contour:

$$\int_0^1 \prod_i dx_i f(x) + \int_{\gamma} \prod_i dz_i f(z) = 0. \quad (7.49)$$

The path γ is parametrized as $z(x)$ with $z(0) = 0$ and $z(1) = 1$, starting at $x = 1$ and ending at $x = 0$. Singularities on the real line are avoided by the Feynman $i\delta$ -prescription $\mathcal{F}(x) \rightarrow \mathcal{F}(x) - i\delta$ which specifies the direction in which the singularities are moved away from the real line. The first term in (7.49) is the original Feynman integral. The Feynman integral I can therefore be expressed as an integral over the path γ

$$I = \int_0^1 \prod_i dx_i f(x) = \int_0^1 \prod_i dx_i \left| \frac{\partial z}{\partial x} \right| f(z(x)), \quad (7.50)$$

where $\left| \frac{\partial z}{\partial x} \right|$ denotes the Jacobian of the function $z(x)$.

The integration path γ is chosen as

$$z_i(x) = x_i - i\lambda x_i(1 - x_i) \frac{\partial \mathcal{F}(x)}{\partial x_i} \quad (7.51)$$

for each integration variable as proposed in [92, 252, 253]. Here λ is a small positive parameter. The imaginary part is zero at $x = 0$ and $x = 1$ guaranteeing a closed path Γ . Expanding the \mathcal{F} -polynomial around $\lambda = 0$ leads to

$$\mathcal{F}(z(x)) = \mathcal{F}(x) - i\lambda \sum_i x_i(1 - x_i) \left(\frac{\partial \mathcal{F}}{\partial x_i} \right)^2 + \mathcal{O}(\lambda^2). \quad (7.52)$$

The $\mathcal{O}(\lambda)$ term produces a negative imaginary part in agreement with the Feynman $i\delta$ -prescription. Higher order corrections to the imaginary part come in at $\mathcal{O}(\lambda^4)$ and are therefore suppressed for small λ . For large values of λ they can change the sign of the imaginary part.

More details on the contour deformation and on strategies for choosing λ can be found in [254]. The contour deformation has to be performed before the

subtraction of dimensionally regulated divergences, which was shown in [255]. Otherwise it is also possible to change the integration path γ in (7.51) by raising the power of x_i in the imaginary part, which makes it possible to deform the contour after the subtraction [252].

7.6 Subtraction

After the decomposition the singularities of the sector integrals are isolated in an overall monomial (see (7.18)), and appear in the limit $x_i \rightarrow 0$. The goal is to extract the ϵ -dependence from the integrals, singularities in particular have to be isolated. This is done by adding and subtracting terms that behave like the integrand in the singular region, and are analytically integrable.

The form of the integral for one integration parameter is

$$I = \int_0^1 dx x^{-a+b\epsilon} f(x) \quad (7.53)$$

where $f(x)$ implicitly depends on all other integration parameters and ϵ . Assuming Euclidean kinematics the function $f(x)$ is finite in the limit $x \rightarrow 0$. In the case $a < 1$ the integral is finite and one can simply expand in ϵ . For $a \geq 1$ one introduces a subtraction term

$$\int_0^1 dx \sum_{n=0}^{a-1} \frac{x^{-a+n+b\epsilon}}{n!} f^{(n)}(0), \quad (7.54)$$

that reproduces the singularity structure of the integrand in the limit $x \rightarrow 0$ [30]. Here $f^{(n)}(0)$ denotes the n -th derivative of the function $f(x)$ evaluated at $x = 0$.

The subtraction term can be integrated analytically leading to

$$\sum_{n=0}^{a-1} \frac{1}{1-a+n+b\epsilon} \frac{f^{(n)}(0)}{n!}. \quad (7.55)$$

After introducing the subtraction term the integral in (7.53) becomes

$$I = \sum_{n=0}^{a-1} \frac{1}{1-a+n+b\epsilon} \frac{f^{(n)}(0)}{n!} + \int_0^1 dx x^{-a+b\epsilon} \left(f(x) - \sum_{n=0}^{a-1} \frac{x^n}{n!} f^{(n)}(0) \right). \quad (7.56)$$

The integrated terms contain the singularities in ϵ , while the remaining integration is finite and does not contribute further ϵ divergences.

Logarithmic divergences ($a = 1$) are the most common in Feynman integrals and are subtracted in the following way:

$$I = \int_0^1 dx x^{-1+b\epsilon} f(x) = \frac{f(0)}{b\epsilon} + \int_0^1 dx x^{-1+b\epsilon} (f(x) - f(0)). \quad (7.57)$$

This subtraction is equivalent to an expansion of the integrand using the plus distribution

$$x^{-1+b\epsilon} = \frac{\delta(x)}{b\epsilon} + \sum_n \left[\frac{\log^n(x)}{x} \right]_+ \quad (7.58)$$

with

$$\int_0^1 dx \left[\frac{g(x)}{x} \right]_+ f(x) = \int_0^1 dx g(x) [f(x) - f(0)]. \quad (7.59)$$

The subtraction procedure which was shown for one Feynman parameter has to be performed iteratively for all integration variables, in particular the terms $f^{(n)}(0)$ in (7.56) in general still contain singularities in the remaining variables. After subtracting in all Feynman parameters the appearing integrals are finite and can be expanded in a Taylor series around $\epsilon = 0$ to the desired order.

An alternative way of isolating the singularities is to use integration by parts. Details can be found in Appendix A of [256].

7.7 Numerical integration

After subtraction and expansion the Feynman integral is in the form

$$I(\{s_{jk}\}, \{m_j\}) = \sum_{i=-n}^{n_{\max}} c_i(\{s_{jk}\}, \{m_j\}) \epsilon^i. \quad (7.60)$$

The coefficients c_i are finite integrals over a multi-dimensional unit hypercube. They are in general difficult to integrate analytically, since the splitting of the integration region introduces more complicated functions, than are present in

the final result [200].

An example is the vacuum integral calculated in Subsection 7.4.2 which can be expressed in terms of only Γ -functions. After sector decomposition the individual sectors evaluate to integrals over hypergeometric functions, and the result only simplifies after summing up all sector integrals.

For this reason the coefficients c_i are usually integrated numerically. The numerical integration can also be automated to a higher degree, which constitutes an additional advantage. Since the integrations are often of high dimension Monte-Carlo (MC) methods are used. The following discussion of MC integration is based on [257].

The standard MC integration approximates integrals

$$I_s(f) = \int_{[0,1]^s} d\mathbf{x} f(\mathbf{x}) \quad (7.61)$$

via the estimator

$$Q_{n,s}(f) = \frac{1}{n} \sum_{i=0}^{n-1} f(\mathbf{t}_i), \quad (7.62)$$

where the \mathbf{t}_i are points randomly chosen from the s -dimensional hypercube $[0, 1]^s$. The error estimate for square-integrable functions f is

$$\sqrt{E[|I_s(f) - Q_{n,s}(f)|^2]} = \frac{\sigma(f)}{\sqrt{n}}, \quad (7.63)$$

where the standard deviation of f is $\sigma(f) = \sqrt{I_s(f^2) - I_s(f)^2}$. The MC error is independent of the dimension of the integration and scales with the square-root of the number of evaluated points.

In [258] quasi Monte-Carlo (QMC) methods were applied to sector decomposed integrals, and a large increase in efficiency compared to standard MC methods was observed. In QMC methods an estimator as in (7.62) is used, but instead of choosing the \mathbf{t}_i randomly one chooses them deterministically.

There are several ways of choosing the \mathbf{t}_i , here the shifted rank-1 lattice rule is presented. The rank-1 lattice is determined by

$$\mathbf{t}_i = \left\{ \frac{i\mathbf{z}}{n} \right\} \quad i = 0, \dots, n-1 \quad (7.64)$$

where the curly braces denote the fractional part of the argument. The vector \mathbf{z} is the generating vector of the lattice, which depends on the number of lattice points n . Algorithms for its generation are given in [257]. An efficient implementation for large lattices in high dimensions can be found in [259]. The unbiased estimator for the rank-1 shifted lattice rule is

$$\bar{Q}_{n,s,q}(f) = \frac{1}{q} \sum_{k=0}^{q-1} Q_{n,s}^{(k)}(f) \quad (7.65)$$

with

$$Q_{n,s}^{(k)}(f) = \frac{1}{n} \sum_{i=0}^{n-1} f\left(\left\{\frac{i\mathbf{z}}{n} + \Delta_k\right\}\right). \quad (7.66)$$

The rank-1 lattice generated by \mathbf{z} is shifted by q vectors Δ_k randomly chosen from $[0, 1]^s$. For certain classes of 1-periodic functions and generating vectors a linear error scaling $\mathcal{O}(n^{-1})$ in the number of lattice points can be achieved [257]. The scaling in the number of lattice shifts is $\mathcal{O}(q^{-\frac{1}{2}})$. For this reason one usually chooses a small number of shifts q and a high number of lattice points n .

The integrands appearing in the coefficients c_i are usually not periodic. They can be periodized using a Korobov transformation $x_i = \psi(y_i)$ with

$$\psi(y_i) = \int_0^{y_i} du \omega(u), \quad \omega(u) = \frac{u^\alpha(1-u)^\alpha}{\int_0^1 du u^\alpha(1-u)^\alpha}. \quad (7.67)$$

With this transformation and by choosing the parameter α high enough one can map the integrand to zero on the boundary of the hypercube $[0, 1]^s$.

8 SecDec-3.0

The sector decomposition algorithm described in Chapter 7 is implemented in the program SECDEC [36–38]. The program numerically evaluates dimensionally regulated, multi-scale, multi-loop Feynman integrals in general kinematics. Furthermore it is possible to calculate more general parameter integrals of the form given in (7.30). This can for example be used for the calculation of soft functions in soft-collinear effective theory [260] or for phase-space integrals [32]. The program is publicly available at <http://secdec.hepforge.org>.

Version 3.0 of SECDEC [38] features an improved user interface and two geometric decomposition strategies: the original method by Kaneko and Ueda [34, 35], and the improved strategy introduced in Section 7.4. In contrast to the original heuristic SECDEC strategy, the new decomposition strategies are guaranteed to terminate. They also lead to a faster and more compact decomposition for integrals with a complicated singularity structure.

The algebraic and numerical parts of the program were decoupled. Due to this improvement it is possible to run the numerical integration for a large number of phase-space point in parallel on a computer cluster. Submission scripts for the cluster submission systems `Condor`, `pbs`, and `lsf` are provided.

Feynman integrals with inverse and pinched propagators can be treated, i.e. $\nu_i \leq 0$ in (6.5). This makes it easier to interface SECDEC to multi-loop reduction programs like REDUZE [175, 176] where integrals are represented in this form.

Integrals with non-standard propagators which do not have a quadratic but only a linear dependence on the loop momentum can be calculated in the physical region. These propagators occur for example in heavy quark effective theory or in non-covariant gauges. Masses in the propagators can be complex, for details see [247]. In addition to the CUBA library [261, 262], it is now possible to use Mathematica NINTEGRATE [263] and CQUAD [264] for the numerical integration, CQUAD in particular speeds up one dimensional integrations considerably.

In the following an overview over the program structure and details on the implementation of the geometric decomposition are given.

8.1 Program structure

The program consists of two main parts, the loop branch for loop integrals of the form (6.5) and the general branch for more general parameter integrals similar to (7.30), see Fig. 8.1. A loop integral can either be specified by its propagators or by the adjacency list of the Feynman graph. With the userdefined option one can directly specify the Feynman parametrized integral, which can be used to modify the integrand before the decomposition. A contour deformation is only possible in the loop branch, since the Feynman $i\delta$ -prescription is only valid for Feynman integrals. For general parameter integrals the deformation can not be chosen in an automated way, since there is no fixed prescription for the continuation.

The algebraic steps of the sector decomposition method are implemented in Mathematica scripts. The steering of the Mathematica scripts is done in Perl. After the expansion in the dimensional regularization parameter ϵ , the algebraic expressions for the sector integrals are turned into optimized C++ functions. These functions are then integrated using the integrators contained in the CUBA library [261, 262], CQUAD [264], or Mathematica NINTEGRATE [263].

A version of SECDEC written in python is in preparation [265]. It avoids the use of the proprietary software Mathematica, and will be more modular than previous SECDEC versions.

8.2 New features of SecDec-3.0

8.2.1 Improved user interface

The required user input for SECDEC-3.0 is split up into the three files `math.m`, `param.input`, and `kinem.input`. The `math.m` file is in Mathematica syntax. It

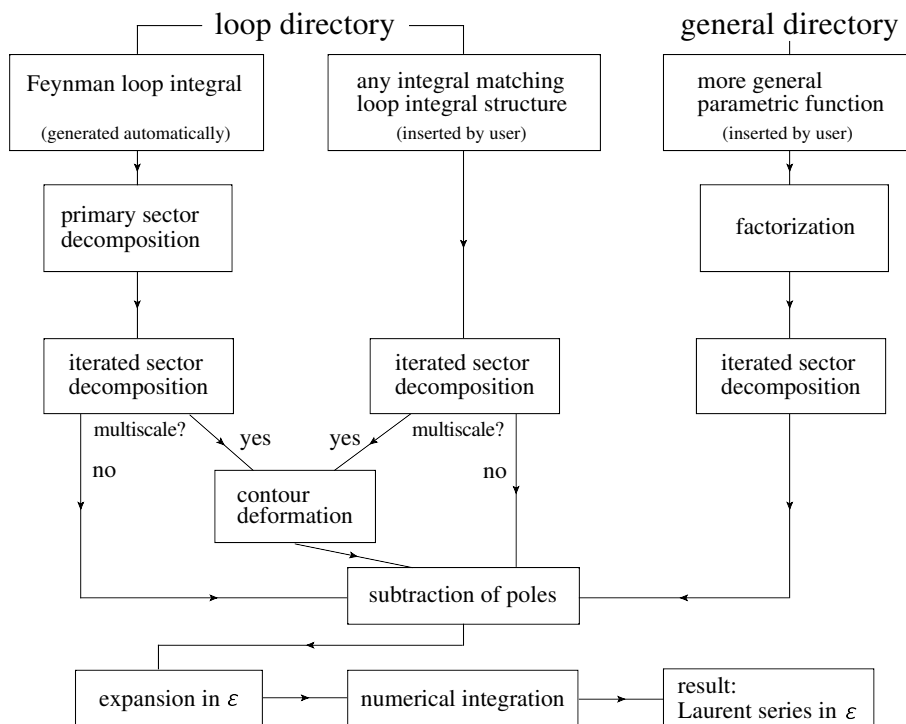


Figure 8.1: Flowchart showing the main steps the program performs to produce the numerical result as a Laurent series in ϵ .

contains the information about the Feynman integral that is to be calculated. Here is the `math.m` input file for a one-loop box integral:

```

momlist={k};
proplist={k^2, (k+p1)^2, (k+p1+p2)^2, (k+p1+p2+p3)^2};
powerlist={1,1,1,1};
Dim=4-2*eps;
prefactor=1;
ExternalMomenta = {p1,p2,p3};
externallegs=4;
KinematicInvariants = {s,t};
Masses={};
ScalarProductRules = {
  SP[p1,p1]->0,
  SP[p2,p2]->0,

```

```
SP[p3,p3]->0,  
SP[p1,p2]->s/2,  
SP[p3,p2]->t/2,  
SP[p1,p3]->-t/2-s/2};
```

The integral is specified by the list of its propagators. The parameter `powerlist` contains the exponents of the propagators. Its entries are usually positive, but it is also possible to set entries to zero thereby pinching the corresponding propagators. Furthermore one can set entries to negative values, which is used to define integrals with inverse propagators. This simplifies communication with reduction programs which often use a similar syntax for the specification of integrals. Tensor integrals can be specified by setting the `numerator` parameter to a scalar product of loop and external momenta.

The on-shell conditions of the Feynman integral and its dimension are also set in the `math.m` file.

The `param.input` contains general options for the sector decomposition:

```
graph=box1L  
epsord=0  
contourdef=True  
integrator=3  
epsrel=1.e-3,1.e-3,1.e-3  
epsabs=1.e-5,1.e-5,1.e-5
```

In this minimal example the name of the integral and the order to which the ϵ -expansion should be performed are given. One also has to specify if contour deformation is required. The remaining options set `DIVONNE` as integrator and set error goals for the numerical integration. For additional options that can be set in the `param.input` file see [38].

The `kinem.input` file contains a list kinematic points that is to be calculated:

```
p1 4 -0.75  
p2 1.2 0.2
```

Here two points `p1` and `p2` are set. The first entry in each line gives the point, the following entries set the numerical values of the kinematic invariants and masses in the order specified in the `math.m` file. The algebraic part of the sector decomposition is independent of the phase-space point. Only for the

numerical integration are specific values for the kinematic invariants needed. For different phase-space points only the numerical integration has to be rerun, which simplifies scans over parameter ranges.

After the input files are prepared, SECDEC can be launched by executing the command `secdec` or `secdec -p <myparam.input> -m <mygraph.m> -k <mykinem.input>` if non-standard names for the input files are used. Additional command line options can be displayed using `secdec -help`. In particular they can be used to only execute certain steps of the sector decomposition.

The output of SECDEC is such that the entire output directory generated by the algebraic part of SECDEC can be transferred as a standalone archive to another machine or cluster, where the numerical evaluation of all kinematic points can be submitted in parallel. Optionally, the user can also evaluate selected pole coefficients individually. The output directory structure which will be created by SECDEC when calculating a loop diagram is depicted in Fig. 8.2.

8.2.2 Implementation of geometric decomposition algorithms

In addition to the iterative heuristic decomposition algorithm (**X**) described in Section 7.3, there are two new algorithms implemented in SECDEC-3.0. These are the original geometric method (**G1**) by Kaneko and Ueda [34, 35] and the geometric algorithm (**G2**) presented in Section 7.4. In contrast to strategy **X** both geometric methods **G1** and **G2** are guaranteed to terminate (see Section 7.3 for an illustration of the problem). The geometric algorithms are only implemented in the `loop` branch, but the upcoming `python` version contains an implementation for general parameter integrals.

For the algorithm **G1** only the iterated sector decomposition step in Fig. 8.1 is replaced, for algorithm **G2** the primary sector decomposition is also switched off. Instead $H = x_N$ is used in (7.10) to integrate out the δ -function (Cheng-Wu). Since the form of the integrals after the decomposition is identical to the form obtained via iterated decomposition methods, all following steps do not have to be changed.

The geometric algorithms themselves are implemented as Mathematica packages interfaced to the program NORMALIZ [245, 266] for geometric calculations. NORMALIZ is used to determine the inequalities defining the facets (\mathbf{n}_F, a_F) of the Newton polytope \mathcal{N} from the exponent vectors \mathbf{v}_i . After calculating the normal fan $\Delta_{\mathcal{N}}$, nonsimplicial full dimensional cones are triangulated by NORMALIZ, leading to the triangulated fan $\Delta_{\mathcal{N}}^T$.

The programs CDD [267], LRS [268], and QHULL [269] were also tested and used for cross-checks of the geometric computations, but turned out to perform worse than NORMALIZ for our applications.

Tab. 8.1 shows the number of produced sectors and the time taken for the decomposition for some example diagrams by the decomposition algorithms implemented in SECDEC-3.0. In most cases algorithm G2 produces a smaller number of sectors than X and G1. For complicated diagrams, where a significant amount of time is spent on the decomposition, method G2 is also faster than the other strategies.

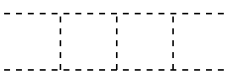
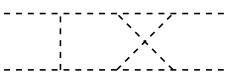
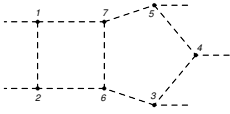
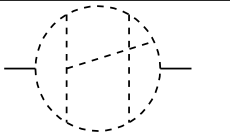
Diagram	X	G1	G2
	282 1 s	266 8 s	166 4 s
	368 1 s	360 9 s	235 5 s
	infinite recursion	72 5 s	76 1 s
	548 3 s	506 15 s	304 4 s
	27336 5510 s	32063 11856 s	27137 443 s

Table 8.1: Number of sectors produced by the implemented decomposition strategies and timings obtained with our implementation of the algorithms. Dashed lines denote massless propagators.

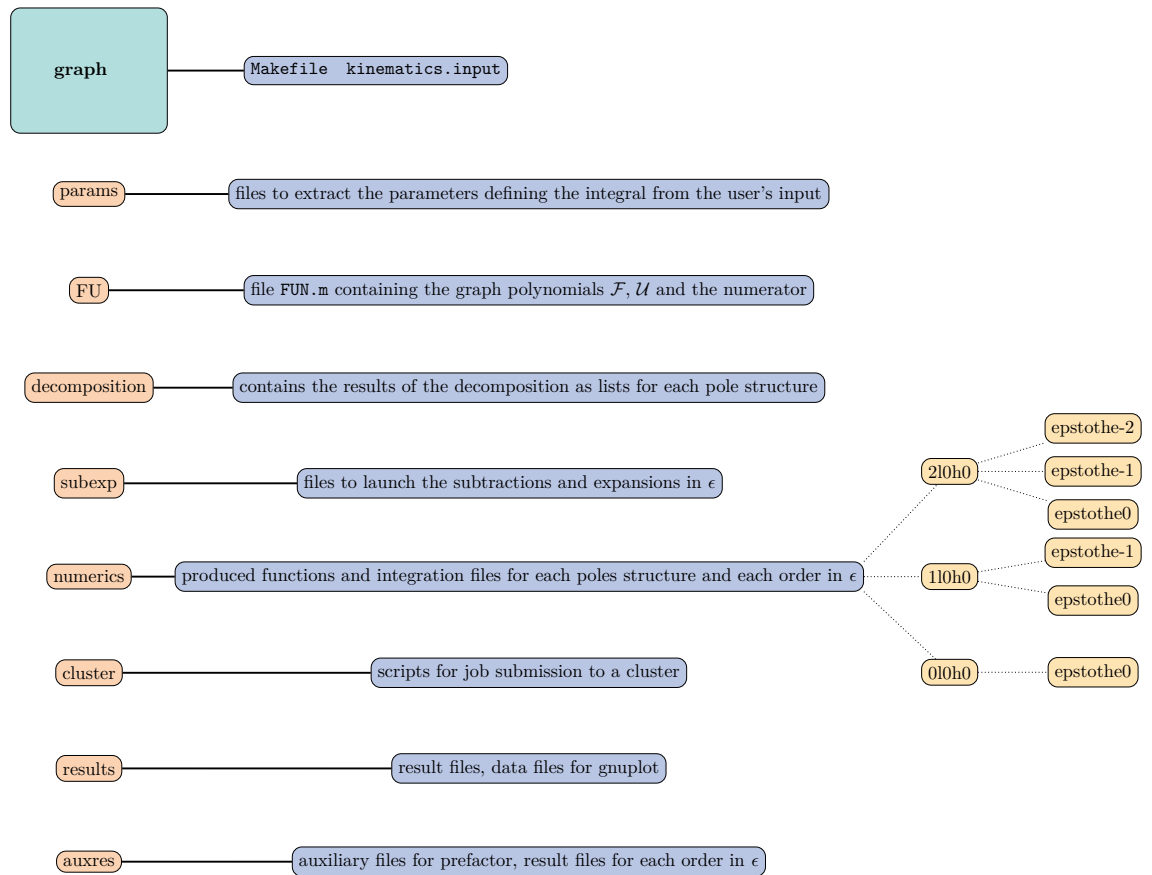


Figure 8.2: Output directory structure generated by the algebraic part of SECDEC, and example of a pole structure in the **numerics** folder containing maximally two logarithmic poles.

9 Higgs boson pair production in gluon fusion

Here the calculation of the NLO QCD corrections to the process $gg \rightarrow hh$ including the full top quark mass dependence is presented [39, 270]. This is an application of the multi-loop techniques that were introduced in the previous chapters, since the process is loop-induced. Already at LO the production of a pair of Higgs bosons in gluon fusion proceeds via a top quark loop, see Fig. 9.1. Therefore the calculation of NLO corrections involves two-loop integrals. Since most of them are not known analytically, sector decomposition is used for their calculation.

The process is phenomenologically relevant, because it can be used for a direct measurement of the triple Higgs coupling at hadron colliders.

9.1 The Higgs sector

The Higgs field in the Standard Model is a complex SU(2) doublet scalar field

$$\Phi = \frac{1}{\sqrt{2}} \begin{pmatrix} \Phi^+ \\ \Phi^0 \end{pmatrix}. \quad (9.1)$$

The Higgs field couples to the electroweak gauge bosons via the covariant derivative and to fermions via Yukawa interactions. The most general renormalizable potential for the Higgs field is

$$V(\Phi) = \mu^2 \Phi^\dagger \Phi + \lambda (\Phi^\dagger \Phi)^2. \quad (9.2)$$

For negative values of μ^2 the Higgs field acquires a nonzero vacuum expectation value that can be chosen as

$$\langle \Phi \rangle = \frac{1}{\sqrt{2}} \begin{pmatrix} 0 \\ v \end{pmatrix} \quad (9.3)$$

with $v^2 = -\frac{\mu^2}{\lambda}$. The vacuum expectation value breaks the $SU(2)_L \times U(1)_Y$ electroweak symmetry group of the Standard Model leaving the $U(1)_{em}$ gauge symmetry of electromagnetism unbroken. This is the mechanism of spontaneous symmetry breaking which generates mass terms for the electroweak gauge bosons in the SM [7–12]. Additionally it leads to mass terms for the SM fermions via the Yukawa couplings. The physical Higgs boson field h is introduced as an scalar excitation around the vacuum expectation value

$$\Phi = \frac{e^{i\vec{\sigma}\cdot\vec{\xi}/2v}}{\sqrt{2}} \begin{pmatrix} 0 \\ v + h \end{pmatrix}, \quad (9.4)$$

where the components of $\vec{\sigma}$ are the three Pauli matrices. The fields $\vec{\xi}$ correspond to the longitudinal polarizations acquired by three of the electroweak gauge bosons after symmetry breaking, leading to the massive W and Z bosons. After symmetry breaking the Higgs potential in (9.2) gives rise to the mass and self-couplings of the Higgs boson h

$$V(h) = V_0 + \frac{m_h^2}{2}h^2 + \frac{\lambda_{3h}}{3!}h^3 + \frac{\lambda_{4h}}{4!}h^4 \quad (9.5)$$

$$= -\frac{m_h^2 v^2}{4} + \frac{m_h^2}{2}h^2 + \frac{m_h^2}{2v}h^3 + \frac{m_h^2}{8v^2}h^4 \quad (9.6)$$

where $m_h^2 = 2\lambda v^2$.

Measuring the Higgs self-couplings is an important test of the mechanism of electroweak symmetry breaking.

9.2 The process $gg \rightarrow hh$

At hadron colliders the triple Higgs coupling can be directly probed by measuring Higgs boson pair production in gluon fusion. The best experimental upper limit on the process is $\sim 70 \times \sigma_{\text{SM}}$ [271, 272] obtained by measurements in the $bb\tau\tau$, $\gamma\gamma WW^*$, $bb\gamma\gamma$, and $bbbb$ decay channels. This is due to fact that the cross section for Higgs pair production is small and the decay channels with large branching fractions suffer from large backgrounds.

In [272] the limit on the cross section was used to constrain possible values of the triple Higgs coupling to $\lambda_{3h}/\lambda_{3h}^{\text{SM}} \in [-17, 22.5]$ in a model where only λ_{3h} is allowed to change from its SM value.

It will be possible to better constrain the Higgs self-coupling via Higgs boson

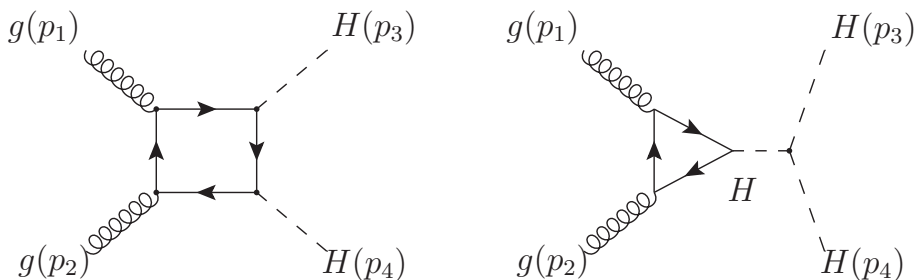


Figure 9.1: Diagrams contributing to the process $gg \rightarrow hh$ at leading order.

pair production at the high luminosity LHC, and at a proposed future hadron collider with a center of mass energy of 100 TeV [273–275].

Other production channels for Higgs boson pairs at hadron colliders, for example vector boson fusion, production in association with a top quark pair, and Higgs strahlung Vhh , have even smaller cross sections than gluon fusion [273, 276].

The process $gg \rightarrow hh$ proceeds through a top quark loop already at LO, for the contributing diagrams see Fig. 9.1. Results for the LO cross section were presented in [40, 277]. The calculation of the NLO corrections requires the evaluation of two-loop integrals with four independent mass scales \hat{s} , \hat{t} , m_h^2 , and m_t^2 . Only a small subset of these integrals is known analytically at present. These are integrals that factorize into two one-loop integrals, integrals with two zero mass legs and one off-shell leg contributing to single Higgs production [278–280], and integrals with two off-shell legs known from the process $h \rightarrow Z\gamma$ [281, 282].

NLO corrections have been calculated in the heavy quark limit $m_t \rightarrow \infty$ [283]. In this limit top quark loops can be integrated out, leading to effective Higgs gluon couplings. NNLO corrections in the heavy top limit are given in [284–287]. Resummed NNLO+NNLL results in the heavy top limit are presented in [288].

There are several approximations which include finite top quark mass effects in an approximate way:

- The Born-improved HEFT (Higgs Effective Field Theory) is used in the

program HPAIR [277, 283]. It relies on the NLO result in the heavy top limit which is reweighted differentially by a factor B/B_{HEFT} . Here B is the LO cross section in the full theory, while B_{HEFT} is the LO cross section in the HEFT.

- In the $\text{FT}_{\text{approx}}$ [289, 290] the full top quark mass dependence is retained in the real radiation. For the virtual corrections the same rescaling as in the HEFT is used.
- The $\text{FT}'_{\text{approx}}$ corresponds to the $\text{FT}_{\text{approx}}$, but the virtual part is augmented with available two-loop corrections with full top quark mass dependence, in particular the contributions known from single Higgs production [290].
- The HEFT result was improved by adding terms in the $1/m_t^2$ expansion of the cross section [286, 291–293]. In [292] the expansion is given up to the sixth order at NLO, and up to the second order for the soft-virtual part at NNLO.

The various approximations suggest $\pm 10\%$ for the size of the top quark mass effects at NLO.

This expectation can be tested with the calculation of the full top quark mass dependent NLO corrections presented in the following.

9.3 Form factor decomposition

Following the description in Section 6.1, the form factor decomposition for the process $g(p_1) + g(p_2) \rightarrow h(p_3) + h(p_4)$ is given. First the gluon polarization vectors and the color dependence are split off as

$$\mathcal{A}_{ab} = \delta_{ab} \epsilon^\mu(p_1) \epsilon_1^\nu(p_2) \mathcal{A}_{\mu\nu}. \quad (9.7)$$

The possible tensor structures that can be built are

$$\mathcal{A}^{\mu\nu} = f_0 g^{\mu\nu} + \sum_{i,j=1}^3 f_{ij} p_i^\mu p_j^\nu \quad (9.8)$$

Using Ward identities, the on-shell conditions for the gluons, and Bose symmetry, the number of independent tensor structures can be reduced to two:

$$\mathcal{A}^{\mu\nu} = F_1(\hat{s}, \hat{t}, m_h^2, m_t^2, D) T_1^{\mu\nu} + F_2(\hat{s}, \hat{t}, m_h^2, m_t^2, D) T_2^{\mu\nu}. \quad (9.9)$$

Here the kinematic invariants are defined as

$$\hat{s} = (p_1 + p_2)^2, \quad \hat{t} = (p_1 - p_3)^2, \quad \hat{u} = (p_2 - p_3)^2. \quad (9.10)$$

Following [40] the two tensors can be chosen as

$$T_1^{\mu\nu} = g^{\mu\nu} - \frac{p_1^\nu p_2^\mu}{p_1 \cdot p_2}, \quad (9.11)$$

$$T_2^{\mu\nu} = g^{\mu\nu} + \frac{m_h^2 p_1^\nu p_2^\mu - 2(p_1 \cdot p_3) p_3^\nu p_2^\mu - 2(p_2 \cdot p_3) p_3^\mu p_1^\nu + 2(p_1 \cdot p_2) p_3^\nu p_3^\mu}{p_T^2 (p_1 \cdot p_2)}, \quad (9.12)$$

with the transverse momentum defined as

$$p_T^2 = \frac{\hat{t}\hat{u} - m_h^4}{\hat{s}}. \quad (9.13)$$

Using the relations

$$T_1 \cdot T_2 = D - 4 \quad \text{and} \quad T_1 \cdot T_1 = T_2 \cdot T_2 = D - 2 \quad (9.14)$$

one can construct projectors that project the amplitude on specific form factors:

$$P_1^{\mu\nu} \mathcal{A}_{\mu\nu} = F_1 \quad (9.15)$$

$$P_2^{\mu\nu} \mathcal{A}_{\mu\nu} = F_2. \quad (9.16)$$

The projectors are given by

$$P_1^{\mu\nu} = \frac{1}{4} \frac{D-2}{D-3} T_1^{\mu\nu} - \frac{1}{4} \frac{D-4}{D-3} T_2^{\mu\nu}, \quad (9.17)$$

$$P_2^{\mu\nu} = -\frac{1}{4} \frac{D-4}{D-3} T_1^{\mu\nu} + \frac{1}{4} \frac{D-2}{D-3} T_2^{\mu\nu}. \quad (9.18)$$

The chosen tensor basis has the property that the form factors correspond to helicity amplitudes [40]:

$$\mathcal{A}^{++} = \mathcal{A}^{--} = -F_1, \quad \mathcal{A}^{+-} = \mathcal{A}^{-+} = -F_2. \quad (9.19)$$

9.4 NLO cross section

The NLO cross section of the process $pp \rightarrow hh$ is

$$\sigma^{\text{NLO}}(pp \rightarrow hh) = \sigma^{\text{LO}} + \sigma^{\text{virt}} + \sum_{i,j \in \{g, q, \bar{q}\}} \sigma_{ij}^{\text{real}}. \quad (9.20)$$

The real radiation is separated into four initial states $\{gg, qg, \bar{q}g, q\bar{q}\}$. Infrared divergences are cancelled between σ^{virt} and σ^{real} using the Catani-Seymour dipole formalism [59] (see Subsection 2.3.2). The integrated dipole term \mathbf{I} which cancels the IR divergences of the virtual contribution as $d\hat{\sigma}^{\text{virt}} - d\sigma^{\text{LO}} \otimes \mathbf{I}$ is given by

$$\mathbf{I} = \frac{\alpha_s}{2\pi} \frac{(4\pi)^\epsilon}{\Gamma(1-\epsilon)} \left(\frac{\mu^2}{\hat{s}} \right)^\epsilon \left\{ \frac{2C_A}{\epsilon^2} + \frac{\beta_0}{\epsilon} + \text{finite} \right\}. \quad (9.21)$$

The LO and virtual amplitudes are calculated in conventional dimensional regularization (CDR) where internal as well as external states are continued to $D = 4 - 2\epsilon$. The strong coupling α_s is renormalized in the $\overline{\text{MS}}$ scheme, while for the top quark mass and the gluon wave function the on-shell scheme is used.

9.4.1 Parton distribution functions

The partonic cross section is combined with the parton distributions f_i using the luminosity function

$$\frac{d\mathcal{L}_{ij}}{d\tau} = \sum_{ij} \int_\tau^1 \frac{dx}{x} f_i(x, \mu_F) f_j\left(\frac{\tau}{x}, \mu_F\right). \quad (9.22)$$

With this definition the total cross section is given as

$$\sigma(pp \rightarrow hh) = \int_{\tau_0}^1 d\tau \frac{d\mathcal{L}_{gg}}{d\tau} \hat{\sigma}(\hat{s} = \tau s), \quad (9.23)$$

where $\tau_0 = 4m_h^2/s$ and s the hadronic center of mass energy.

9.4.2 LO cross section

With the form factors defined in (9.9) the LO partonic cross section is given by

$$\hat{\sigma}^{\text{LO}} = \frac{1}{2^9 \pi \hat{s}^2} \int_{\hat{t}_-}^{\hat{t}_+} d\hat{t} \left\{ |F_1|^2 + |F_2|^2 \right\}, \quad (9.24)$$

where

$$\hat{t}^{\pm} = m_h^2 - \frac{\hat{s}}{2} \left(1 \mp \sqrt{1 - 4 \frac{m_h^2}{\hat{s}}} \right), \quad (9.25)$$

are the boundaries of the allowed kinematic region. Four dimensional expressions for the LO form factors with full top quark mass dependence can be found in [40, 277]. For the NLO corrections the expansion of the LO amplitude up to order ϵ^2 is needed. Therefore the LO contributions are calculated numerically with the same setup as the two-loop corrections. For the finite part agreement with the results of [40] was found.

9.4.3 Virtual two-loop contributions

The Feynman diagrams contributing to the two-loop amplitude are generated with QGRAF [108], and further processed with FORM [109, 110]. After projectors and integral families are supplied the appearing integrals can be mapped to the integral families. These steps are automated in an extension of the program GOSAM to higher loop orders.

At this point the amplitude is written in terms of $\sim 10^4$ two-loop integrals with up to seven propagators and four mass scales \hat{s} , \hat{t} , m_t^2 , and m_h^2 . The numerators of the integrals contain up to four inverse propagators, corresponding to a tensor rank of 8. The amplitude was generated with a second independent setup based on REDUZE [175, 176] and QGRAF, and agreement between the two calculations was found.

To reduce the large number of appearing integrals to a master integral basis the IBP method is used (see Section 6.2). We were not able to achieve a full reduction with the programs FIRE [173], LITERED [174], and REDUZE. After setting the scales m_t^2 and m_h^2 to their numerical values it was possible to reduce the appearing planar integrals to a basis of 145 master integrals with

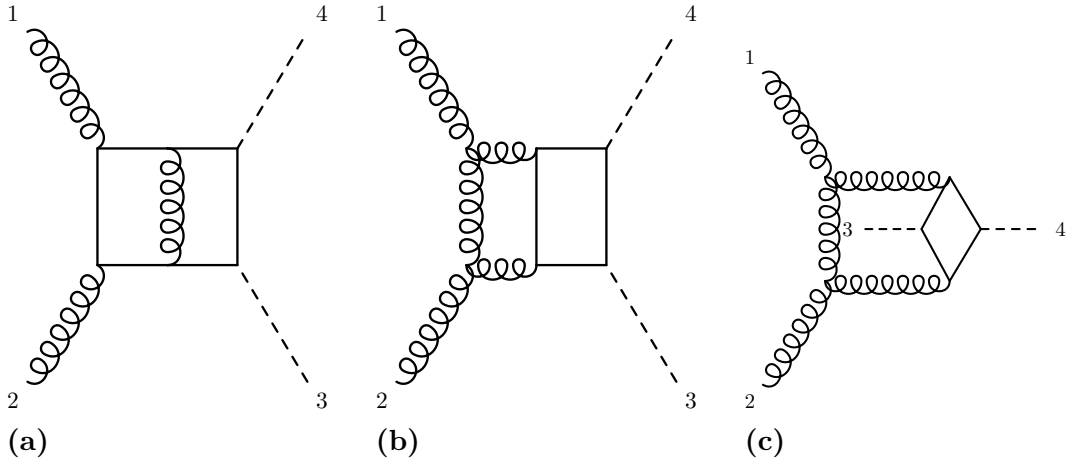


Figure 9.2: Representative planar and nonplanar diagrams contributing to the process $gg \rightarrow hh$.

REDUZE. For the remaining 6- and 7-propagator nonplanar integrals the tensor rank was reduced as far as possible by rewriting inverse propagators in terms of scalar products. This leads to 70 nonplanar integrals with tensor rank ≤ 4 . Another 112 integrals are related to the previous integrals by crossing. Fig. 9.2 shows examples of contributing 7-propagator planar and nonplanar integrals.

For most of the integrals no analytic expressions are known. Therefore we use the program SECDEC-3.0 [38] to integrate all of the appearing integrals numerically. The numerical stability could be improved by choosing a partially quasi-finite master integral basis, described in Subsection 6.2.1 [200, 201]. The numerical integration of the SECDEC functions is performed using the quasi-Monte Carlo method based on a rank-one lattice rule, as described in Section 7.7. The integrator is implemented in OPENCL1.1 and can be executed on a General Purpose Graphics Processing Unit (GPGPU). For the numerical results 913 phase-space points were calculated on ~ 16 dual NVIDIA TESLA K20X GPGPU nodes in ~ 6400 GPGPU hours.

The numerical integration error of the individual integrals is dynamically adjusted according to the contribution of the integral to the error estimate of the amplitude at a given phase-space point. To estimate the relative importance of the integrals a short integration run with a fixed number of points is performed. Considering the required time per integration point and the con-

tribution of the integral including its coefficient to the amplitude, the number of sampling points for the integral is set. This is repeated until the desired precision for the amplitude is reached. The method avoids calculating integrals to a high precision whose contribution to the overall error estimate is small, and automatically calculates important integrals more precisely.

Even with all of these improvements the numerical evaluation of the virtual amplitude at a single phase-space point is computationally expensive. For this reason unweighted events generated according to the LO matrix element are used for the phase-space integration of the virtual corrections. Using unweighted events it is possible to obtain the total cross section with an uncertainty of 0.25% due to the number of phase-space points by evaluating the virtual contribution only 913 times. More details on the numerical integration of the virtual correction can be found in [294, 295].

Several checks on the virtual contribution were performed. For every phase-space point the poles of the virtual corrections cancel against the integrated subtraction term given in (9.21) within the numerical uncertainty. For a set of randomly chosen phase-space points the pole coefficients were calculated with higher precision and a cancellation with a median of five digits was observed. The two-loop amplitude is invariant under exchange of the invariants \hat{s} and \hat{t} . This invariance was confirmed for 10 random phase-space points. Parts of the $gg \rightarrow hh$ amplitude correspond to single Higgs production. For these parts agreement was found with the results of [279].

9.4.4 Real radiation

The real radiation contribution $\sigma_{ij}^{\text{real}}$ consists of the four subprocesses $gg \rightarrow hh + g$, $gq \rightarrow hh + q$, $g\bar{q} \rightarrow hh + \bar{q}$, and $q\bar{q} \rightarrow hh + g$. The $q\bar{q}$ channel is infrared finite.

GoSAM [18, 19] is used for the calculation of the required $2 \rightarrow 3$ one-loop matrix elements. The most complicated appearing integrals are pentagons with internal top quark mass. After including Catani-Seymour dipole terms to subtract infrared divergences the real radiation contribution is finite. It is integrated with the VEGAS [296] integrator implemented in CUBA [261].

The total cross section is found to be independent of the phase-space restriction parameter of the dipole terms α_{dip} , which constitutes a check on the infrared subtraction.

To avoid numerical instabilities a technical cut on the real radiation of $p_T^{\text{min}} \geq$

$10^{-4}\sqrt{\hat{s}}$ is introduced. It is varied in the range $10^{-2} \leq p_T^{\min}/\sqrt{\hat{s}} \leq 10^{-6}$ and the cross section is found to be independent within the numerical uncertainty.

9.5 Top quark mass expansion

To obtain approximate results in the $m_t \rightarrow \infty$ limit, the partonic differential cross section can be expanded as

$$d\hat{\sigma}_{\text{exp},N} = \sum_{\rho=0}^N d\hat{\sigma}^{(\rho)} \left(\frac{\Lambda}{m_t^2} \right)^\rho \quad (9.26)$$

with $\Lambda \in \{\hat{s}, \hat{t}, \hat{u}, m_h^2\}$. The terms up to $N = 3$ are calculated using the programs QGRAF, Q2E/EXP [297, 298], and MATAD [299] as well as REDUZE and FORM.

The Higgs pair production cross section is peaked close to the top quark pair threshold $\hat{s} = 4m_t^2$. In this phase-space region the top quark mass m_t is not the highest scale in the problem, which means that the heavy top limit does not provide a good description of the process $gg \rightarrow hh$.

To improve the situation the calculation in the strict heavy top limit is rescaled with the LO full calculation. Here this is done by rescaling the virtual corrections differentially for each phase-space point via

$$d\hat{\sigma}^{\text{virt}} + d\hat{\sigma}^{\text{LO}}(\epsilon) \otimes \mathbf{I} \approx \left(d\hat{\sigma}_{\text{exp},N}^{\text{virt}} + d\hat{\sigma}_{\text{exp},N}^{\text{LO}}(\epsilon) \otimes \mathbf{I} \right) \frac{d\hat{\sigma}^{\text{LO}}(\epsilon)}{d\hat{\sigma}_{\text{exp},N}^{\text{LO}}(\epsilon)}. \quad (9.27)$$

The expression in brackets is kept infrared finite and ϵ can be set to zero in $d\hat{\sigma}^{\text{LO}}(\epsilon)/d\hat{\sigma}_{\text{exp},N}^{\text{LO}}(\epsilon)$.

9.6 Numerical results

Here numerical results for LHC collisions at a center of mass energy $\sqrt{s} = 14$ TeV are presented.

For LO as well as NLO predictions the PDF4LHC15_nlo_100_pdfas parton distribution functions together with their α_s value are used [300–303]. As central

	$\sigma(\sqrt{s} = 14 \text{ TeV})$
LO	$19.85^{+27.6\%}_{-20.5\%} \text{ fb}$
NLO	$32.91^{+13.6\%}_{-12.6\%} \text{ fb}$
NLO HEFT	$38.32^{+18.1\%}_{-14.9\%} \text{ fb}$
NLO FT _{approx}	$34.26^{+14.7\%}_{-13.2\%} \text{ fb}$

Table 9.1: Total cross section for various calculations at a center of mass energy of $\sqrt{s} = 14 \text{ TeV}$. The uncertainty due to the scale variation is given. The central scale is $m_{hh}/2$. We used $m_t = 173 \text{ GeV}$, $m_h = 125 \text{ GeV}$. The PDF set is PDF4LHC15_nlo_100_pdfas.

renormalization and factorization scale half of the invariant mass of the Higgs boson pair is chosen:

$$\mu_R = \mu_F = \frac{m_{hh}}{2}. \quad (9.28)$$

The numerical values of the Higgs boson and top quark masses are set to

$$m_h = 125 \text{ GeV} \quad \text{and} \quad m_t = 173 \text{ GeV}. \quad (9.29)$$

Without additional kinematical requirements on the final state particles the inclusive cross section is

$$\sigma^{\text{NLO}} = 32.91^{+13.6\%}_{-12.6\%} \text{ fb} \pm 0.25\%(\text{stat}) \pm 0.05\%(\text{int}). \quad (9.30)$$

The first uncertainty is due to a variation of μ_R and μ_F by a factor two around the central scale simultaneously. The second error estimate of $\pm 0.25\%(\text{stat})$ comes from the phase-space integration for which 913 unweighted events were used. Since the calculation of the virtual contribution for each individual phase-space point requires a numerical integration over the sector functions, there is a third error $\pm 0.05\%(\text{int})$ due to this integration.

Four phase-space points very close to the top quark threshold had to be excluded due to poor convergence of the numerical integration.

Tab.9.1 shows the cross section obtained at LO and NLO, and additionally results in the HEFT and FT_{approx} approximations. Comparing the LO cross section to the NLO result one finds a K -factor of ~ 1.66 . The K -factor can be reduced by 10% if LO PDF sets instead of NLO PDFs are used for the LO

cross section. The scale variation uncertainty is reduced by a factor of ~ 2 . Effects of the exact treatment of finite top quark contributions can be quantified by comparing to the HEFT approximation. One finds that these reduce the inclusive cross section by 16.5%. In the $\text{FT}_{\text{approx}}$ where the real radiation contributions are calculated with the full top quark mass dependence the difference is reduced.

The invariant mass distribution of the Higgs boson pair m_{hh} is shown in Fig. 9.3a. It is compared to the NLO Born-improved HEFT, i.e. the first term in (9.26) rescaled by the full LO cross section. While there is reasonable agreement for small invariant mass, the finite top quark mass corrections become important above $m_{hh} \gtrsim 600$ GeV. In the tail of the distribution they become as large as 50%.

The inclusion of finite top quark mass effects in the real radiation in the $\text{FT}_{\text{approx}}$ calculation leads to a better agreement with the full result. The difference grows for large invariant masses to 20 – 30% due to finite top quark contributions in the virtual correction.

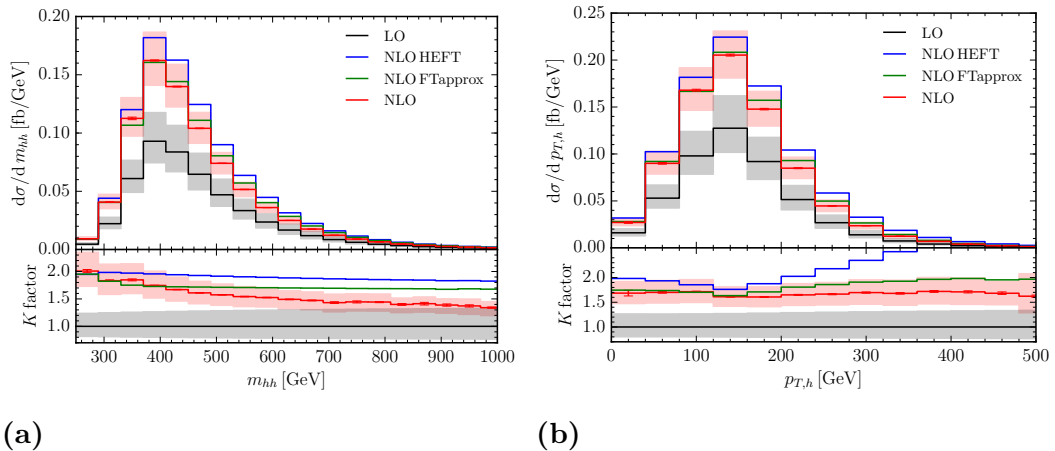


Figure 9.3: Comparison of the full calculation to various approximations for Higgs transverse momentum (9.3a) and Higgs pair invariant mass distributions (9.3b) at $\sqrt{s} = 14$ TeV. “NLO HEFT” denotes the Born-improved effective field theory result, while in “ $\text{FT}_{\text{approx}}$ ” the full top quark mass is taken into account in the real radiation part. The band results from scale variations by a factor of two around the central scale $\mu = m_{hh}/2$.

For the Higgs boson transverse momentum a similar behaviour can be observed. The $\text{FT}_{\text{approx}}$ agrees well with the full result up to $p_{T,h} \sim 160$ GeV, at large transverse momentum one finds differences of $\sim 40\%$. The HEFT leads to an even bigger increase of the cross section at large $p_{T,h}$. Compared to the invariant mass distribution, the K -factor of the transverse momentum is nearly flat for the full calculation.

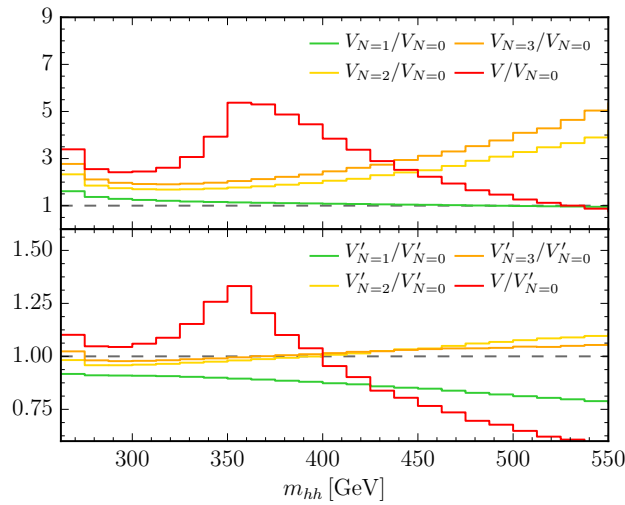


Figure 9.4: Comparison of the virtual amplitude with full top quark mass dependence to various orders in a $1/m_t^2$ expansion. V'_N denotes the Born-improved HEFT result to order N in the $1/m_t^2$ expansion, i.e. $V'_N = V_N B/B_N$.

In Fig. 9.4 the interference of the LO amplitude with the two-loop amplitude including the integrated subtraction terms is shown. It is compared to the results of the heavy top expansion introduced in Section 9.5. The upper panel shows the heavy top expansion up to the third order, while in the lower panel the expansion terms are rescaled with the LO cross section with full top quark mass dependence as described in (9.27). The expanded results agree with the full cross section only close to the Higgs pair production threshold. Around the top quark pair threshold and at high invariant mass large deviations are found.

To assess the sensitivity of the cross section to variations of the triple Higgs coupling λ_{3h} , a new parameter $\lambda = \lambda_{3h}/\lambda_{3h}^{\text{SM}}$ is introduced, where $\lambda = 1$ cor-

responds to the SM. The inclusive cross section is quadratically dependent on λ with a minimum at $\lambda \gtrsim 2$. In Fig. 9.5 the LO and NLO invariant mass distribution of the Higgs boson pair is shown for λ values in the range $[-1, 5]$. Besides the change in the total cross section with λ , there is also shift in the

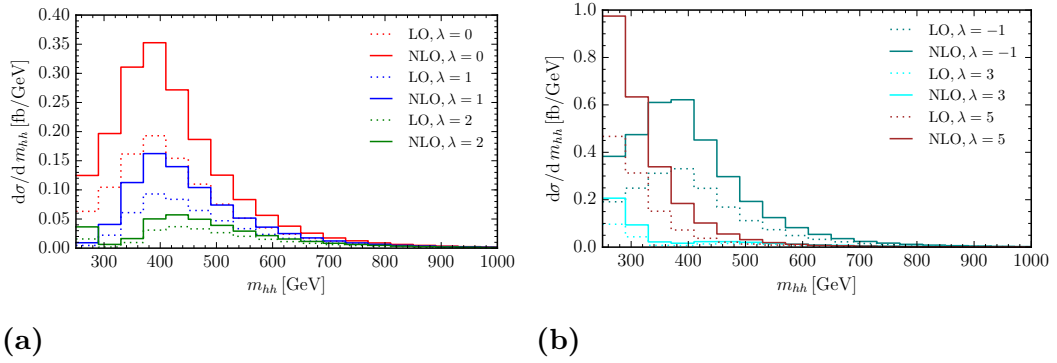


Figure 9.5: Invariant mass distribution of the Higgs boson pair at LO and NLO for several values of the triple Higgs coupling $\lambda = \lambda_{3h}/\lambda_{3h}^{\text{SM}}$.

peak position of the distribution. For small values of $\lambda \leq 1$ the distribution peaks at $m_{hh} \sim 400$ GeV, at larger λ values, a second peak close to the Higgs pair production threshold develops and finally at $\lambda = 5$ only the second peak is visible. This behaviour is due to destructive interference between self-coupling dependent and independent parts of the cross-section at $\hat{s} \sim 4m_h^2$ in the SM, which is softened for $\lambda \neq 1$. A more detailed study of the process $gg \rightarrow hh$ and its λ dependence for the high luminosity LHC and a future 100 TeV collider can be found in [270].

10 Conclusion and outlook

In the first part of the thesis the NLO QCD corrections to the process $pp \rightarrow W^+W^-b\bar{b} \rightarrow (e^+\nu_e)(\mu^-\bar{\nu}_\mu)b\bar{b}$ were presented. The process describes top quark pair production and subsequent decays including non-resonant contributions. For the calculation the automated one-loop amplitude provider GOSAM was used in combination with the Monte-Carlo generator SHERPA.

Significant differences to the calculation in the narrow width approximation with LO decays were found for the shape of the m_{lb} distribution.

A detailed study of effects of NLO and non-factorizable contributions on top quark mass measurements based on the m_{lb} observable was performed by reproducing an ATLAS template analysis at the parton level. It was found that the inclusion of NLO contributions leads to a larger shift in the measured top quark mass for the full $WWbb$ calculation than for the factorized calculation. Furthermore the scale variation uncertainty on the m_{lb} distribution leads to a higher uncertainty on the measured top quark mass of about 1 GeV for the full calculation than for the factorized calculation where it is only about 0.2 GeV. Further investigations using fully simulated events are required to give a reliable estimate of the theoretical uncertainties on the top quark mass measured with this approach. Since the factorized approach is used in experimental analyses it is possible that the theoretical uncertainty is underestimated.

It is also not clear if the observed differences between full and factorized calculation are due to NLO corrections to the top quark decays or due to non-resonant contributions. To answer this question a comparison to a strict narrow width calculation which includes NLO top quark decays is in progress, and a first comparison is shown. This will make it possible to study the impact of genuine non-resonant contributions.

While the first part of the thesis involves only one-loop calculations, in the second part higher loop orders are considered. The method of differential equations, which is used for the calculation of multi-loop Feynman integrals is introduced. A technique to simplify their form is presented and applied to the

calculation of two-loop QED vertex integrals.

Details on the sector decomposition method for the (numerical) integration of multi-loop Feynman integrals, and in particular on a decomposition algorithm based on convex geometry are given. The new algorithm provides a compact form for decomposed integrals, and suggests a connection to the theory of toric varieties. A better understanding of the appearing mathematical structures would be desirable, and could lead to further improvements of the sector decomposition method. Additionally the geometric algorithm is guaranteed to terminate, usually generates a smaller number of sectors, and is faster than other decomposition algorithms. Together with several other improvements and new features, the geometric algorithm is implemented in the most recent version of the program SECDEC. This, together with improvements such as the QMC integration method, makes it possible to use sector decomposition for the calculation of phenomenologically relevant multi-loop amplitudes.

Such an application is the calculation of the NLO QCD corrections to the production of a Higgs boson pair in gluon fusion including the full top quark mass dependence. In the calculation sector decomposition is used for the computation of the appearing two-loop Feynman integrals with four independent mass scales, and an extended version of GOSAM provides the two-loop amplitude. The program REDUZE is used for the partial integral reduction. For the total cross section a difference of 16.5% is found with respect to the Born-improved HEFT approximation. Differentially large deviations are also observed beyond $m_{hh} \gtrsim 600$ GeV even with respect to the $\text{FT}_{\text{approx}}$ calculation. This demonstrates that the inclusion of full top quark mass effects is required to get reliable predictions for the process $gg \rightarrow hh$ in all kinematic regions. The method used for the calculation is partially automated and process independent. It can be applied to the calculation of other multi-scale and multi-loop processes in the future.

Bibliography

- [1] ATLAS collaboration, G. Aad et al., *The ATLAS Experiment at the CERN Large Hadron Collider*, *JINST* **3** (2008) S08003.
- [2] CMS collaboration, S. Chatrchyan et al., *The CMS experiment at the CERN LHC*, *JINST* **3** (2008) S08004.
- [3] LHCb collaboration, J. Alves, A. Augusto et al., *The LHCb Detector at the LHC*, *JINST* **3** (2008) S08005.
- [4] ALICE collaboration, K. Aamodt et al., *The ALICE experiment at the CERN LHC*, *JINST* **3** (2008) S08002.
- [5] ATLAS collaboration, G. Aad et al., *Observation of a new particle in the search for the Standard Model Higgs boson with the ATLAS detector at the LHC*, *Phys.Lett.* **B716** (2012) 1–29, [1207.7214].
- [6] CMS collaboration, S. Chatrchyan et al., *Observation of a new boson at a mass of 125 GeV with the CMS experiment at the LHC*, *Phys.Lett.* **B716** (2012) 30–61, [1207.7235].
- [7] F. Englert and R. Brout, *Broken Symmetry and the Mass of Gauge Vector Mesons*, *Phys.Rev.Lett.* **13** (1964) 321–323.
- [8] P. W. Higgs, *Broken symmetries, massless particles and gauge fields*, *Phys.Lett.* **12** (1964) 132–133.
- [9] P. W. Higgs, *Broken Symmetries and the Masses of Gauge Bosons*, *Phys.Rev.Lett.* **13** (1964) 508–509.
- [10] G. Guralnik, C. Hagen and T. Kibble, *Global Conservation Laws and Massless Particles*, *Phys.Rev.Lett.* **13** (1964) 585–587.
- [11] P. W. Higgs, *Spontaneous Symmetry Breakdown without Massless Bosons*, *Phys.Rev.* **145** (1966) 1156–1163.

- [12] T. Kibble, *Symmetry breaking in nonabelian gauge theories*, *Phys.Rev.* **155** (1967) 1554–1561.
- [13] C. Buttar et al., *Les houches physics at TeV colliders 2005, standard model and Higgs working group: Summary report*, in *Physics at TeV colliders. Proceedings, Workshop, Les Houches, France, May 2-20, 2005*, 2006. hep-ph/0604120.
- [14] NLO MULTILEG WORKING GROUP collaboration, Z. Bern et al., *The NLO multileg working group: Summary report*, in *Physics at TeV colliders, La physique du TeV aux collisionneurs, Les Houches 2007 : 11-29 June 2007*, pp. 1–120, 2008. 0803.0494.
- [15] J. R. Andersen et al., *Les Houches 2013: Physics at TeV Colliders: Standard Model Working Group Report*, 1405.1067.
- [16] CDF collaboration, F. Abe et al., *Observation of top quark production in $\bar{p}p$ collisions*, *Phys.Rev.Lett.* **74** (1995) 2626–2631, [hep-ex/9503002].
- [17] D0 collaboration, S. Abachi et al., *Search for high mass top quark production in $p\bar{p}$ collisions at $\sqrt{s} = 1.8$ TeV*, *Phys.Rev.Lett.* **74** (1995) 2422–2426, [hep-ex/9411001].
- [18] G. Cullen, N. Greiner, G. Heinrich, G. Luisoni, P. Mastrolia et al., *Automated One-Loop Calculations with GoSam*, *Eur.Phys.J.* **C72** (2012) 1889, [1111.2034].
- [19] G. Cullen et al., *GOSAM-2.0: a tool for automated one-loop calculations within the Standard Model and beyond*, *Eur. Phys. J.* **C74** (2014) 3001, [1404.7096].
- [20] T. Gleisberg, S. Hoeche, F. Krauss, M. Schonherr, S. Schumann et al., *Event generation with SHERPA 1.1*, *JHEP* **0902** (2009) 007, [0811.4622].
- [21] G. Heinrich, A. Maier, R. Nisius, J. Schlenk and J. Winter, *NLO QCD corrections to $W^+W^-b\bar{b}$ production with leptonic decays in the light of top quark mass and asymmetry measurements*, *JHEP* **06** (2014) 158, [1312.6659].
- [22] A. Denner, S. Dittmaier, S. Kallweit and S. Pozzorini, *NLO QCD corrections to $WWb\bar{b}$ production at hadron colliders*, *Phys.Rev.Lett.* **106** (2011) 052001, [1012.3975].

-
- [23] G. Bevilacqua, M. Czakon, A. van Hameren, C. G. Papadopoulos and M. Worek, *Complete off-shell effects in top quark pair hadroproduction with leptonic decay at next-to-leading order*, *JHEP* **1102** (2011) 083, [1012.4230].
- [24] A. Denner, S. Dittmaier, S. Kallweit and S. Pozzorini, *NLO QCD corrections to off-shell top-antitop production with leptonic decays at hadron colliders*, *JHEP* **1210** (2012) 110, [1207.5018].
- [25] A. V. Kotikov, *Differential equations method: New technique for massive Feynman diagrams calculation*, *Phys. Lett.* **B254** (1991) 158–164.
- [26] E. Remiddi, *Differential equations for Feynman graph amplitudes*, *Nuovo Cim.* **A110** (1997) 1435–1452, [hep-th/9711188].
- [27] T. Gehrmann and E. Remiddi, *Differential equations for two loop four point functions*, *Nucl. Phys.* **B580** (2000) 485–518, [hep-ph/9912329].
- [28] J. M. Henn, *Multiloop integrals in dimensional regularization made simple*, *Phys. Rev. Lett.* **110** (2013) 251601, [1304.1806].
- [29] M. Argeri, S. Di Vita, P. Mastrolia, E. Mirabella, J. Schlenk, U. Schubert et al., *Magnus and Dyson Series for Master Integrals*, *JHEP* **03** (2014) 082, [1401.2979].
- [30] T. Binoth and G. Heinrich, *An automatized algorithm to compute infrared divergent multi-loop integrals*, *Nucl. Phys.* **B585** (2000) 741–759, [hep-ph/0004013].
- [31] T. Binoth and G. Heinrich, *Numerical evaluation of multi-loop integrals by sector decomposition*, *Nucl. Phys.* **B680** (2004) 375–388, [hep-ph/0305234].
- [32] T. Binoth and G. Heinrich, *Numerical evaluation of phase space integrals by sector decomposition*, *Nucl. Phys.* **B693** (2004) 134–148, [hep-ph/0402265].
- [33] G. Heinrich, *Sector Decomposition*, *Int. J. Mod. Phys.* **A23** (2008) 1457–1486, [0803.4177].
- [34] T. Ueda and J. Fujimoto, *New implementation of the sector decomposition on FORM*, *PoS ACAT08* (2008) 120, [0902.2656].

- [35] T. Kaneko and T. Ueda, *Sector Decomposition Via Computational Geometry*, *PoS ACAT2010* (2010) 082, [1004.5490].
- [36] J. Carter and G. Heinrich, *SecDec: A general program for sector decomposition*, *Comput.Phys.Commun.* **182** (2011) 1566–1581, [1011.5493].
- [37] S. Borowka, J. Carter and G. Heinrich, *Numerical Evaluation of Multi-Loop Integrals for Arbitrary Kinematics with SecDec 2.0*, *Comput.Phys.Commun.* **184** (2013) 396–408, [1204.4152].
- [38] S. Borowka, G. Heinrich, S. P. Jones, M. Kerner, J. Schlenk and T. Zirke, *SecDec-3.0: numerical evaluation of multi-scale integrals beyond one loop*, *Comput. Phys. Commun.* **196** (2015) 470–491, [1502.06595].
- [39] S. Borowka, N. Greiner, G. Heinrich, S. Jones, M. Kerner, J. Schlenk et al., *Higgs Boson Pair Production in Gluon Fusion at Next-to-Leading Order with Full Top-Quark Mass Dependence*, *Phys. Rev. Lett.* **117** (2016) 012001, [1604.06447].
- [40] E. W. N. Glover and J. J. van der Bij, *Higgs Boson Pair Production via Gluon Fusion*, *Nucl. Phys.* **B309** (1988) 282.
- [41] PARTICLE DATA GROUP collaboration, K. A. Olive et al., *Review of Particle Physics*, *Chin. Phys.* **C38** (2014) 090001.
- [42] J. C. Collins, D. E. Soper and G. F. Sterman, *Factorization of Hard Processes in QCD*, *Adv.Ser.Direct.High Energy Phys.* **5** (1988) 1–91, [hep-ph/0409313].
- [43] G. F. Sterman, *Partons, factorization and resummation*, *TASI 95*, hep-ph/9606312.
- [44] J. C. Collins and D. E. Soper, *Parton Distribution and Decay Functions*, *Nucl.Phys.* **B194** (1982) 445.
- [45] J. C. Collins, D. E. Soper and G. F. Sterman, *Transverse Momentum Distribution in Drell-Yan Pair and W and Z Boson Production*, *Nucl.Phys.* **B250** (1985) 199.
- [46] V. Gribov and L. Lipatov, *Deep inelastic e p scattering in perturbation theory*, *Sov.J.Nucl.Phys.* **15** (1972) 438–450.

-
- [47] Y. L. Dokshitzer, *Calculation of the Structure Functions for Deep Inelastic Scattering and $e^+ e^-$ Annihilation by Perturbation Theory in Quantum Chromodynamics.*, *Sov.Phys.JETP* **46** (1977) 641–653.
- [48] G. Altarelli and G. Parisi, *Asymptotic Freedom in Parton Language*, *Nucl.Phys.* **B126** (1977) 298.
- [49] A. Martin, W. Stirling, R. Thorne and G. Watt, *Parton distributions for the LHC*, *Eur.Phys.J.* **C63** (2009) 189–285, [0901.0002].
- [50] G. 't Hooft and M. J. G. Veltman, *Regularization and Renormalization of Gauge Fields*, *Nucl. Phys.* **B44** (1972) 189–213.
- [51] T. Kinoshita, *Mass singularities of Feynman amplitudes*, *J.Math.Phys.* **3** (1962) 650–677.
- [52] T. Lee and M. Nauenberg, *Degenerate Systems and Mass Singularities*, *Phys.Rev.* **133** (1964) B1549–B1562.
- [53] W. T. Giele and E. W. N. Glover, *Higher order corrections to jet cross-sections in $e^+ e^-$ annihilation*, *Phys. Rev.* **D46** (1992) 1980–2010.
- [54] W. T. Giele, E. W. N. Glover and D. A. Kosower, *Higher order corrections to jet cross-sections in hadron colliders*, *Nucl. Phys.* **B403** (1993) 633–670, [hep-ph/9302225].
- [55] S. Catani and M. Grazzini, *An NNLO subtraction formalism in hadron collisions and its application to Higgs boson production at the LHC*, *Phys. Rev. Lett.* **98** (2007) 222002, [hep-ph/0703012].
- [56] I. W. Stewart, F. J. Tackmann and W. J. Waalewijn, *N -Jettiness: An Inclusive Event Shape to Veto Jets*, *Phys. Rev. Lett.* **105** (2010) 092002, [1004.2489].
- [57] R. Boughezal, C. Focke, X. Liu and F. Petriello, *W -boson production in association with a jet at next-to-next-to-leading order in perturbative QCD*, *Phys. Rev. Lett.* **115** (2015) 062002, [1504.02131].
- [58] J. Gaunt, M. Stahlhofen, F. J. Tackmann and J. R. Walsh, *N -jettiness Subtractions for NNLO QCD Calculations*, *JHEP* **09** (2015) 058, [1505.04794].

- [59] S. Catani and M. Seymour, *A General algorithm for calculating jet cross-sections in NLO QCD*, *Nucl.Phys.* **B485** (1997) 291–419, [[hep-ph/9605323](#)].
- [60] T. Gleisberg and F. Krauss, *Automating dipole subtraction for QCD NLO calculations*, *Eur.Phys.J.* **C53** (2008) 501–523, [[0709.2881](#)].
- [61] R. Frederix, T. Gehrmann and N. Greiner, *Automation of the Dipole Subtraction Method in MadGraph/MadEvent*, *JHEP* **09** (2008) 122, [[0808.2128](#)].
- [62] S. Frixione, Z. Kunszt and A. Signer, *Three jet cross-sections to next-to-leading order*, *Nucl.Phys.* **B467** (1996) 399–442, [[hep-ph/9512328](#)].
- [63] R. Frederix, S. Frixione, F. Maltoni and T. Stelzer, *Automation of next-to-leading order computations in QCD: The FKS subtraction*, *JHEP* **10** (2009) 003, [[0908.4272](#)].
- [64] D. A. Kosower, *Antenna factorization of gauge theory amplitudes*, *Phys.Rev.* **D57** (1998) 5410–5416, [[hep-ph/9710213](#)].
- [65] A. Gehrmann-De Ridder, T. Gehrmann and E. N. Glover, *Antenna subtraction at NNLO*, *JHEP* **0509** (2005) 056, [[hep-ph/0505111](#)].
- [66] G. Heinrich, *A numerical method for NNLO calculations*, *Nucl. Phys. Proc. Suppl.* **116** (2003) 368–372, [[hep-ph/0211144](#)].
- [67] C. Anastasiou, K. Melnikov and F. Petriello, *A new method for real radiation at NNLO*, *Phys. Rev.* **D69** (2004) 076010, [[hep-ph/0311311](#)].
- [68] A. Gehrmann-De Ridder, T. Gehrmann and G. Heinrich, *Four particle phase space integrals in massless QCD*, *Nucl. Phys.* **B682** (2004) 265–288, [[hep-ph/0311276](#)].
- [69] M. Czakon, *A novel subtraction scheme for double-real radiation at NNLO*, *Phys.Lett.* **B693** (2010) 259–268, [[1005.0274](#)].
- [70] M. Czakon and D. Heymes, *Four-dimensional formulation of the sector-improved residue subtraction scheme*, *Nucl. Phys.* **B890** (2014) 152–227, [[1408.2500](#)].

-
- [71] G. Somogyi, Z. Trocsanyi and V. Del Duca, *A Subtraction scheme for computing QCD jet cross sections at NNLO: Regularization of doubly-real emissions*, *JHEP* **01** (2007) 070, [[hep-ph/0609042](#)].
- [72] V. Del Duca, C. Duhr, A. Kardos, G. Somogyi and Z. Trócsányi, *Three-jet production in electron-positron collisions using the CoLoRFulNNLO method*, [1603.08927](#).
- [73] M. Cacciari, F. A. Dreyer, A. Karlberg, G. P. Salam and G. Zanderighi, *Fully Differential Vector-Boson-Fusion Higgs Production at Next-to-Next-to-Leading Order*, *Phys. Rev. Lett.* **115** (2015) 082002, [[1506.02660](#)].
- [74] F. A. Dreyer and A. Karlberg, *Vector-boson fusion Higgs production at N^3LO in QCD*, [1606.00840](#).
- [75] X. Artru and G. Mennessier, *String model and multiproduction*, *Nucl.Phys.* **B70** (1974) 93–115.
- [76] B. Andersson, *The Lund model*, *Camb.Monogr.Part.Phys. Nucl.Phys.Cosmol.* **7** (1997) 1–471.
- [77] T. Sjostrand, S. Mrenna and P. Z. Skands, *PYTHIA 6.4 Physics and Manual*, *JHEP* **0605** (2006) 026, [[hep-ph/0603175](#)].
- [78] T. Sjostrand, S. Mrenna and P. Z. Skands, *A Brief Introduction to PYTHIA 8.1*, *Comput.Phys.Commun.* **178** (2008) 852–867, [[0710.3820](#)].
- [79] D. Amati and G. Veneziano, *Preconfinement as a Property of Perturbative QCD*, *Phys.Lett.* **B83** (1979) 87.
- [80] G. Corcella, I. Knowles, G. Marchesini, S. Moretti, K. Odagiri et al., *HERWIG 6: An Event generator for hadron emission reactions with interfering gluons (including supersymmetric processes)*, *JHEP* **0101** (2001) 010, [[hep-ph/0011363](#)].
- [81] J. Bellm et al., *Herwig 7.0/Herwig++ 3.0 release note*, *Eur. Phys. J.* **C76** (2016) 196, [[1512.01178](#)].
- [82] T. Binoth, J. P. Guillet and G. Heinrich, *Algebraic evaluation of rational polynomials in one-loop amplitudes*, *JHEP* **0702** (2007) 013, [[hep-ph/0609054](#)].

- [83] G. 't Hooft and M. Veltman, *Scalar One Loop Integrals*, *Nucl.Phys.* **B153** (1979) 365–401.
- [84] G. Cullen, J. P. Guillet, G. Heinrich, T. Kleinschmidt, E. Pilon et al., *Golem95C: A library for one-loop integrals with complex masses*, *Comput.Phys.Commun.* **182** (2011) 2276–2284, [1101.5595].
- [85] T. Hahn and M. Perez-Victoria, *Automatized one loop calculations in four-dimensions and D-dimensions*, *Comput.Phys.Commun.* **118** (1999) 153–165, [hep-ph/9807565].
- [86] A. van Hameren, *OneLOop: For the evaluation of one-loop scalar functions*, *Comput.Phys.Commun.* **182** (2011) 2427–2438, [1007.4716].
- [87] R. K. Ellis and G. Zanderighi, *Scalar one-loop integrals for QCD*, *JHEP* **0802** (2008) 002, [0712.1851].
- [88] S. Carrazza, R. K. Ellis and G. Zanderighi, *QCDLoop: a comprehensive framework for one-loop scalar integrals*, 1605.03181.
- [89] A. Denner, S. Dittmaier and L. Hofer, *Collier: a fortran-based Complex One-Loop Library in Extended Regularizations*, 1604.06792.
- [90] G. Passarino and M. Veltman, *One Loop Corrections for $e^+ e^-$ Annihilation Into $\mu^+ \mu^-$ in the Weinberg Model*, *Nucl.Phys.* **B160** (1979) 151.
- [91] T. Binoth, J.-P. Guillet, G. Heinrich, E. Pilon and T. Reiter, *Golem95: A Numerical program to calculate one-loop tensor integrals with up to six external legs*, *Comput.Phys.Commun.* **180** (2009) 2317–2330, [0810.0992].
- [92] T. Binoth, J. P. Guillet, G. Heinrich, E. Pilon and C. Schubert, *An Algebraic/numerical formalism for one-loop multi-leg amplitudes*, *JHEP* **0510** (2005) 015, [hep-ph/0504267].
- [93] G. Ossola, C. G. Papadopoulos and R. Pittau, *Reducing full one-loop amplitudes to scalar integrals at the integrand level*, *Nucl.Phys.* **B763** (2007) 147–169, [hep-ph/0609007].
- [94] W. T. Giele, Z. Kunszt and K. Melnikov, *Full one-loop amplitudes from tree amplitudes*, *JHEP* **0804** (2008) 049, [0801.2237].

-
- [95] R. K. Ellis, W. T. Giele, Z. Kunszt and K. Melnikov, *Masses, fermions and generalized D -dimensional unitarity*, *Nucl.Phys.* **B822** (2009) 270–282, [0806.3467].
- [96] C. Berger, Z. Bern, L. Dixon, F. Febres Cordero, D. Forde et al., *An Automated Implementation of On-Shell Methods for One-Loop Amplitudes*, *Phys.Rev.* **D78** (2008) 036003, [0803.4180].
- [97] G. Bevilacqua, M. Czakon, M. Garzelli, A. van Hameren, A. Kardos et al., *HELAC-NLO*, *Comput.Phys.Commun.* **184** (2013) 986–997, [1110.1499].
- [98] V. Hirschi, R. Frederix, S. Frixione, M. V. Garzelli, F. Maltoni et al., *Automation of one-loop QCD corrections*, *JHEP* **1105** (2011) 044, [1103.0621].
- [99] S. Badger, B. Biedermann, P. Uwer and V. Yundin, *Numerical evaluation of virtual corrections to multi-jet production in massless QCD*, 1209.0100.
- [100] F. Cascioli, P. Maierhofer and S. Pozzorini, *Scattering Amplitudes with Open Loops*, *Phys.Rev.Lett.* **108** (2012) 111601, [1111.5206].
- [101] S. Actis, A. Denner, L. Hofer, J.-N. Lang, A. Scharf and S. Uccirati, *RECOLA: REcursive Computation of One-Loop Amplitudes*, 1605.01090.
- [102] J. M. Campbell and R. K. Ellis, *An Update on vector boson pair production at hadron colliders*, *Phys.Rev.* **D60** (1999) 113006, [hep-ph/9905386].
- [103] J. M. Campbell, R. K. Ellis and W. T. Giele, *A Multi-Threaded Version of MCFM*, *Eur. Phys. J.* **C75** (2015) 246, [1503.06182].
- [104] K. Arnold, M. Bahr, G. Bozzi, F. Campanario, C. Englert et al., *VBFNLO: A Parton level Monte Carlo for processes with electroweak bosons*, *Comput.Phys.Commun.* **180** (2009) 1661–1670, [0811.4559].
- [105] S. Alioli, P. Nason, C. Oleari and E. Re, *A general framework for implementing NLO calculations in shower Monte Carlo programs: the POWHEG BOX*, *JHEP* **1006** (2010) 043, [1002.2581].
- [106] T. Binoth, F. Boudjema, G. Dissertori, A. Lazopoulos, A. Denner et al., *A Proposal for a standard interface between Monte Carlo tools and*

- one-loop programs*, *Comput.Phys.Commun.* **181** (2010) 1612–1622, [1001.1307].
- [107] S. Alioli et al., *Update of the Binoth Les Houches Accord for a standard interface between Monte Carlo tools and one-loop programs*, *Comput. Phys. Commun.* **185** (2014) 560–571, [1308.3462].
- [108] P. Nogueira, *Automatic Feynman graph generation*, *J.Comput.Phys.* **105** (1993) 279–289.
- [109] J. Vermaseren, *New features of FORM*, math-ph/0010025.
- [110] J. Kuipers, T. Ueda, J. Vermaseren and J. Vollinga, *FORM version 4.0*, 1203.6543.
- [111] G. Cullen, M. Koch-Janusz and T. Reiter, *Spinney: A Form Library for Helicity Spinors*, *Comput.Phys.Commun.* **182** (2011) 2368–2387, [1008.0803].
- [112] J. P. Guillet, G. Heinrich and J. von Soden-Fraunhofen, *Tools for NLO automation: extension of the golem95C integral library*, 1312.3887.
- [113] T. Peraro, *Ninja: Automated Integrand Reduction via Laurent Expansion for One-Loop Amplitudes*, *Comput. Phys. Commun.* **185** (2014) 2771–2797, [1403.1229].
- [114] V. Hirschi and T. Peraro, *Tensor integrand reduction via Laurent expansion*, *JHEP* **06** (2016) 060, [1604.01363].
- [115] P. Mastrolia, G. Ossola, T. Reiter and F. Tramontano, *Scattering Amplitudes from Unitarity-based Reduction Algorithm at the Integrand-level*, *JHEP* **1008** (2010) 080, [1006.0710].
- [116] P. Mastrolia, E. Mirabella and T. Peraro, *Integrand reduction of one-loop scattering amplitudes through Laurent series expansion*, *JHEP* **1206** (2012) 095, [1203.0291].
- [117] M. Chiesa, G. Montagna, L. Barzè, M. Moretti, O. Nicrosini, F. Piccinini et al., *Electroweak Sudakov Corrections to New Physics Searches at the LHC*, *Phys. Rev. Lett.* **111** (2013) 121801, [1305.6837].
- [118] M. Chiesa, N. Greiner and F. Tramontano, *Automation of electroweak corrections for LHC processes*, *J. Phys.* **G43** (2016) 013002, [1507.08579].

-
- [119] G. Cullen, N. Greiner and G. Heinrich, *Susy-QCD corrections to neutralino pair production in association with a jet*, *Eur. Phys. J.* **C73** (2013) 2388, [1212.5154].
- [120] A. Denner, S. Dittmaier, M. Roth and L. H. Wieders, *Electroweak corrections to charged-current $e^+e^- \rightarrow 4$ fermion processes: Technical details and further results*, *Nucl. Phys.* **B724** (2005) 247–294, [hep-ph/0505042].
- [121] G. Degrandi, S. Di Vita, J. Elias-Miro, J. R. Espinosa, G. F. Giudice, G. Isidori et al., *Higgs mass and vacuum stability in the Standard Model at NNLO*, *JHEP* **08** (2012) 098, [1205.6497].
- [122] ATLAS, CDF, CMS AND DØ collaboration, *First combination of Tevatron and LHC measurements of the top-quark mass*, 1403.4427.
- [123] P. Nason, S. Dawson and R. K. Ellis, *The Total Cross-Section for the Production of Heavy Quarks in Hadronic Collisions*, *Nucl.Phys.* **B303** (1988) 607.
- [124] P. Nason, S. Dawson and R. K. Ellis, *The One Particle Inclusive Differential Cross-Section for Heavy Quark Production in Hadronic Collisions*, *Nucl.Phys.* **B327** (1989) 49–92.
- [125] W. Beenakker, W. van Neerven, R. Meng, G. Schuler and J. Smith, *QCD corrections to heavy quark production in hadron hadron collisions*, *Nucl.Phys.* **B351** (1991) 507–560.
- [126] M. L. Mangano, P. Nason and G. Ridolfi, *Heavy quark correlations in hadron collisions at next-to-leading order*, *Nucl.Phys.* **B373** (1992) 295–345.
- [127] S. Frixione, M. L. Mangano, P. Nason and G. Ridolfi, *Top quark distributions in hadronic collisions*, *Phys.Lett.* **B351** (1995) 555–561, [hep-ph/9503213].
- [128] W. Beenakker, A. Denner, W. Hollik, R. Mertig, T. Sack et al., *Electroweak one loop contributions to top pair production in hadron colliders*, *Nucl.Phys.* **B411** (1994) 343–380.
- [129] W. Hollik and M. Kollar, *NLO QED contributions to top-pair production at hadron collider*, *Phys. Rev.* **D77** (2008) 014008, [0708.1697].

- [130] W. Bernreuther and Z.-G. Si, *Top quark and leptonic charge asymmetries for the Tevatron and LHC*, *Phys.Rev.* **D86** (2012) 034026, [1205.6580].
- [131] M. Czakon, P. Fiedler and A. Mitov, *The total top quark pair production cross-section at hadron colliders through $O(\alpha_s^4)$* , *Phys.Rev.Lett.* **110** (2013) 252004, [1303.6254].
- [132] M. Czakon, D. Heymes and A. Mitov, *High-precision differential predictions for top-quark pairs at the LHC*, *Phys. Rev. Lett.* **116** (2016) 082003, [1511.00549].
- [133] K. Melnikov and M. Schulze, *NLO QCD corrections to top quark pair production and decay at hadron colliders*, *JHEP* **0908** (2009) 049, [0907.3090].
- [134] S. Biswas, K. Melnikov and M. Schulze, *Next-to-leading order QCD effects and the top quark mass measurements at the LHC*, *JHEP* **1008** (2010) 048, [1006.0910].
- [135] K. Melnikov and M. Schulze, *Top quark spin correlations at the Tevatron and the LHC*, *Phys.Lett.* **B700** (2011) 17–20, [1103.2122].
- [136] R. Frederix, *The top induced backgrounds to Higgs production in the $WW \rightarrow ll\nu\nu$ decay channel at NLO in QCD*, 1311.4893.
- [137] F. Cascioli, S. Kallweit, P. Maierhöfer and S. Pozzorini, *A unified NLO description of top-pair and associated Wt production*, 1312.0546.
- [138] T. Ježo, J. M. Lindert, P. Nason, C. Oleari and S. Pozzorini, *An NLO+PS generator for $t\bar{t}$ and Wt production and decay including non-resonant and interference effects*, 1607.04538.
- [139] A. Denner and M. Pellen, *NLO electroweak corrections to off-shell top-antitop production with leptonic decays at the LHC*, 1607.05571.
- [140] J. Schlenk, G. Heinrich and J. Winter, *NLO QCD corrections to $W^+W^-b\bar{b}$ production and top quark observables*, *PoS RADCOR2013* (2013) 033, [1312.5666].
- [141] F. Krauss, R. Kuhn and G. Soff, *AMEGIC++ 1.0: A Matrix element generator in C++*, *JHEP* **0202** (2002) 044, [hep-ph/0109036].

-
- [142] T. Gleisberg and S. Hoeche, *Comix, a new matrix element generator*, *JHEP* **0812** (2008) 039, [0808.3674].
- [143] A. Buckley, J. Butterworth, L. Lonnblad, H. Hoeth, J. Monk et al., *Rivet user manual*, 1003.0694.
- [144] Z. Nagy, *Next-to-leading order calculation of three jet observables in hadron hadron collision*, *Phys. Rev.* **D68** (2003) 094002, [hep-ph/0307268].
- [145] M. Whalley, D. Bourilkov and R. Group, *The Les Houches accord PDFs (LHAPDF) and LHAGLUE*, hep-ph/0508110.
- [146] K. G. Chetyrkin, B. A. Kniehl and M. Steinhauser, *Strong coupling constant with flavor thresholds at four loops in the \overline{MS} scheme*, *Phys. Rev. Lett.* **79** (1997) 2184–2187, [hep-ph/9706430].
- [147] K. Nakamura and P. D. Group, *Review of particle physics*, *Journal of Physics G: Nuclear and Particle Physics* **37** (2010) 075021.
- [148] M. Jezabek and J. H. Kuhn, *QCD Corrections to Semileptonic Decays of Heavy Quarks*, *Nucl.Phys.* **B314** (1989) 1.
- [149] M. Cacciari and G. P. Salam, *Dispelling the N^3 myth for the k_t jet-finder*, *Phys.Lett.* **B641** (2006) 57–61, [hep-ph/0512210].
- [150] M. Cacciari, G. P. Salam and G. Soyez, *The Anti- $k(t)$ jet clustering algorithm*, *JHEP* **0804** (2008) 063, [0802.1189].
- [151] M. Cacciari, G. P. Salam and G. Soyez, *FastJet User Manual*, *Eur.Phys.J.* **C72** (2012) 1896, [1111.6097].
- [152] M. Czakon, D. Heymes and A. Mitov, *Dynamical scales for multi-TeV top-pair production at the LHC*, 1606.03350.
- [153] P. Marquard, A. V. Smirnov, V. A. Smirnov and M. Steinhauser, *Quark Mass Relations to Four-Loop Order in Perturbative QCD*, *Phys. Rev. Lett.* **114** (2015) 142002, [1502.01030].
- [154] M. Beneke, P. Marquard, P. Nason and M. Steinhauser, *On the ultimate uncertainty of the top quark pole mass*, 1605.03609.

- [155] M. Beneke and V. M. Braun, *Heavy quark effective theory beyond perturbation theory: Renormalons, the pole mass and the residual mass term*, *Nucl.Phys.* **B426** (1994) 301–343, [[hep-ph/9402364](#)].
- [156] M. Beneke, *Renormalons*, *Phys.Rept.* **317** (1999) 1–142, [[hep-ph/9807443](#)].
- [157] A. Buckley, J. Butterworth, S. Gieseke, D. Grellscheid, S. Hoche et al., *General-purpose event generators for LHC physics*, *Phys.Rept.* **504** (2011) 145–233, [[1101.2599](#)].
- [158] A. H. Hoang and I. W. Stewart, *Top Mass Measurements from Jets and the Tevatron Top-Quark Mass*, *Nucl.Phys.Proc.Suppl.* **185** (2008) 220–226, [[0808.0222](#)].
- [159] K. Agashe et al., *Snowmass 2013 Top quark working group report*, [1311.2028](#).
- [160] A. Juste, S. Mantry, A. Mitov, A. Penin, P. Skands et al., *Determination of the top quark mass circa 2013: methods, subtleties, perspectives*, [1310.0799](#).
- [161] R. Nisius, *QCD results from the LHC*, *Nucl.Phys.Proc.Suppl.* **222-224** (2012) 216–227, [[1202.3548](#)].
- [162] ATLAS collaboration, G. Aad et al., *Measurement of the top quark mass in the $t\bar{t} \rightarrow \text{lepton} + \text{jets}$ and $t\bar{t} \rightarrow \text{dilepton}$ channels using $\sqrt{s} = 7$ TeV ATLAS data*, *Eur. Phys. J.* **C75** (2015) 330, [[1503.05427](#)].
- [163] ATLAS collaboration, M. Aaboud et al., *Measurement of the top quark mass in the $t\bar{t} \rightarrow \text{dilepton}$ channel from $\sqrt{s} = 8$ TeV ATLAS data*, [1606.02179](#).
- [164] CMS collaboration, S. Chatrchyan et al., *Measurement of masses in the $t\bar{t}$ system by kinematic endpoints in pp collisions at $\sqrt{s} = 7$ TeV*, *Eur. Phys. J.* **C73** (2013) 2494, [[1304.5783](#)].
- [165] A. Maier, *Investigations towards a Measurement of the Top-Quark Mass in dileptonic Decay Channels of Top-Antitop Quark Pairs at ATLAS*, *Diplomarbeit, Max Planck Institute for Physics* (2012) .

-
- [166] A. Maier, *Precision measurements of the top quark mass in the dileptonic top quark pair decay channel at ATLAS, Dissertation, LMU Munich* (2016) .
- [167] M. Schulze. personal communication.
- [168] A. D. Kennedy, *Clifford Algebras in Two ω Dimensions*, *J. Math. Phys.* **22** (1981) 1330–1337.
- [169] T. Binoth, E. W. N. Glover, P. Marquard and J. J. van der Bij, *Two loop corrections to light by light scattering in supersymmetric QED*, *JHEP* **05** (2002) 060, [[hep-ph/0202266](#)].
- [170] F. V. Tkachov, *A Theorem on Analytical Calculability of Four Loop Renormalization Group Functions*, *Phys. Lett.* **B100** (1981) 65–68.
- [171] K. G. Chetyrkin and F. V. Tkachov, *Integration by Parts: The Algorithm to Calculate beta Functions in 4 Loops*, *Nucl. Phys.* **B192** (1981) 159–204.
- [172] S. Laporta and E. Remiddi, *The Analytical value of the electron ($g-2$) at order α^{*3} in QED*, *Phys. Lett.* **B379** (1996) 283–291, [[hep-ph/9602417](#)].
- [173] A. V. Smirnov, *FIRE5: a C++ implementation of Feynman Integral REDuction*, [1408.2372](#).
- [174] R. Lee, *Presenting LiteRed: a tool for the Loop InTEgrals REDuction*, [1212.2685](#).
- [175] C. Studerus, *Reduze-Feynman Integral Reduction in C++, Comput. Phys. Commun.* **181** (2010) 1293–1300, [[0912.2546](#)].
- [176] A. von Manteuffel and C. Studerus, *Reduze 2 - Distributed Feynman Integral Reduction*, [1201.4330](#).
- [177] J. Gluza, K. Kajda and D. A. Kosower, *Towards a Basis for Planar Two-Loop Integrals*, *Phys. Rev.* **D83** (2011) 045012, [[1009.0472](#)].
- [178] R. M. Schabinger, *A New Algorithm For The Generation Of Unitarity-Compatible Integration By Parts Relations*, *JHEP* **01** (2012) 077, [[1111.4220](#)].

- [179] H. Ita, *Two-loop Integrand Decomposition into Master Integrals and Surface Terms*, 1510.05626.
- [180] K. J. Larsen and Y. Zhang, *Integration-by-parts reductions from unitarity cuts and algebraic geometry*, *Phys. Rev.* **D93** (2016) 041701, [1511.01071].
- [181] P. A. Baikov, *Explicit solutions of the multiloop integral recurrence relations and its application*, *Nucl. Instrum. Meth.* **A389** (1997) 347–349, [hep-ph/9611449].
- [182] P. Kant, *Finding Linear Dependencies in Integration-By-Parts Equations: A Monte Carlo Approach*, *Comput. Phys. Commun.* **185** (2014) 1473–1476, [1309.7287].
- [183] A. von Manteuffel and R. M. Schabinger, *A novel approach to integration by parts reduction*, 1406.4513.
- [184] T. Peraro, *Scattering amplitudes over finite fields and multivariate functional reconstruction*, 1608.01902.
- [185] S. G. Gorishnii, S. A. Larin, L. R. Surguladze and F. V. Tkachov, *Mincer: Program for Multiloop Calculations in Quantum Field Theory for the Schoonschip System*, *Comput. Phys. Commun.* **55** (1989) 381–408.
- [186] S. Laporta, *High precision calculation of multiloop Feynman integrals by difference equations*, *Int. J. Mod. Phys.* **A15** (2000) 5087–5159, [hep-ph/0102033].
- [187] P. Mastrolia and G. Ossola, *On the Integrand-Reduction Method for Two-Loop Scattering Amplitudes*, *JHEP* **11** (2011) 014, [1107.6041].
- [188] S. Badger, H. Frellesvig and Y. Zhang, *Hepta-Cuts of Two-Loop Scattering Amplitudes*, *JHEP* **04** (2012) 055, [1202.2019].
- [189] Y. Zhang, *Integrand-Level Reduction of Loop Amplitudes by Computational Algebraic Geometry Methods*, *JHEP* **09** (2012) 042, [1205.5707].
- [190] P. Mastrolia, E. Mirabella, G. Ossola and T. Peraro, *Scattering Amplitudes from Multivariate Polynomial Division*, *Phys. Lett.* **B718** (2012) 173–177, [1205.7087].

-
- [191] D. A. Kosower and K. J. Larsen, *Maximal Unitarity at Two Loops*, *Phys. Rev.* **D85** (2012) 045017, [1108.1180].
- [192] S. Badger, H. Frellesvig and Y. Zhang, *A Two-Loop Five-Gluon Helicity Amplitude in QCD*, *JHEP* **12** (2013) 045, [1310.1051].
- [193] S. Badger, G. Mogull, A. Ochirov and D. O’Connell, *A Complete Two-Loop, Five-Gluon Helicity Amplitude in Yang-Mills Theory*, *JHEP* **10** (2015) 064, [1507.08797].
- [194] S. Badger, G. Mogull and T. Peraro, *Local integrands for two-loop all-plus Yang-Mills amplitudes*, 1606.02244.
- [195] F. Brown, *The Massless higher-loop two-point function*, *Commun. Math. Phys.* **287** (2009) 925–958, [0804.1660].
- [196] F. C. S. Brown, *On the periods of some Feynman integrals*, 0910.0114.
- [197] E. Panzer, *On the analytic computation of massless propagators in dimensional regularization*, *Nucl. Phys.* **B874** (2013) 567–593, [1305.2161].
- [198] E. Panzer, *On hyperlogarithms and Feynman integrals with divergences and many scales*, *JHEP* **1403** (2014) 071, [1401.4361].
- [199] E. Panzer, *Algorithms for the symbolic integration of hyperlogarithms with applications to Feynman integrals*, 1403.3385.
- [200] A. von Manteuffel, E. Panzer and R. M. Schabinger, *A quasi-finite basis for multi-loop Feynman integrals*, 1411.7392.
- [201] A. von Manteuffel, E. Panzer and R. M. Schabinger, *On the Computation of Form Factors in Massless QCD with Finite Master Integrals*, *Phys. Rev.* **D93** (2016) 125014, [1510.06758].
- [202] O. V. Tarasov, *Connection between Feynman integrals having different values of the space-time dimension*, *Phys. Rev.* **D54** (1996) 6479–6490, [hep-th/9606018].
- [203] R. N. Lee, *Space-time dimensionality D as complex variable: Calculating loop integrals using dimensional recurrence relation and analytical properties with respect to D* , *Nucl. Phys.* **B830** (2010) 474–492, [0911.0252].

- [204] R. N. Lee, *Calculating multiloop integrals using dimensional recurrence relation and D-analyticity*, *Nucl. Phys. Proc. Suppl.* **205-206** (2010) 135–140, [1007.2256].
- [205] S. Caron-Huot and J. M. Henn, *Iterative structure of finite loop integrals*, *JHEP* **06** (2014) 114, [1404.2922].
- [206] T. Gehrmann, A. von Manteuffel, L. Tancredi and E. Weihs, *The two-loop master integrals for $q\bar{q} \rightarrow VV$* , *JHEP* **06** (2014) 032, [1404.4853].
- [207] M. Höschele, J. Hoff and T. Ueda, *Adequate bases of phase space master integrals for $gg \rightarrow h$ at NNLO and beyond*, *JHEP* **09** (2014) 116, [1407.4049].
- [208] R. N. Lee, *Reducing differential equations for multiloop master integrals*, *JHEP* **04** (2015) 108, [1411.0911].
- [209] J. M. Henn, *Lectures on differential equations for Feynman integrals*, *J. Phys.* **A48** (2015) 153001, [1412.2296].
- [210] W. Magnus, *On the exponential solution of differential equations for a linear operator*, *Communications on Pure and Applied Mathematics* **7** (1954) 649–673.
- [211] S. Blanes, F. Casas, J. Oteo and J. Ros, *The magnus expansion and some of its applications*, *Physics Reports* **470** (2009) 151 – 238.
- [212] R. Bonciani, P. Mastrolia and E. Remiddi, *Vertex diagrams for the QED form-factors at the two loop level*, *Nucl. Phys.* **B661** (2003) 289–343, [hep-ph/0301170].
- [213] R. Bonciani, P. Mastrolia and E. Remiddi, *QED vertex form-factors at two loops*, *Nucl. Phys.* **B676** (2004) 399–452, [hep-ph/0307295].
- [214] J. Tausk, *Nonplanar massless two loop Feynman diagrams with four on-shell legs*, *Phys.Lett.* **B469** (1999) 225–234, [hep-ph/9909506].
- [215] C. Anastasiou, T. Gehrmann, C. Oleari, E. Remiddi and J. B. Tausk, *The Tensor reduction and master integrals of the two loop massless crossed box with lightlike legs*, *Nucl. Phys.* **B580** (2000) 577–601, [hep-ph/0003261].

-
- [216] S. Di Vita, P. Mastrolia, U. Schubert and V. Yundin, *Three-loop master integrals for ladder-box diagrams with one massive leg*, *JHEP* **09** (2014) 148, [1408.3107].
- [217] R. Bonciani, S. Di Vita, P. Mastrolia and U. Schubert, *Two-Loop Master Integrals for the mixed EW-QCD virtual corrections to Drell-Yan scattering*, 1604.08581.
- [218] K.-T. Chen, *Iterated path integrals*, *Bull. Amer. Math. Soc.* **83** (09, 1977) 831–879.
- [219] J. Lappo-Danilevsky, *Mémoires sur la théorie des systèmes des équations différentielles linéaires.*, *Travaux Inst. Physico-Math. Stekloff* **8** (1936) 5–206.
- [220] J. M. Henn, A. V. Smirnov and V. A. Smirnov, *Evaluating single-scale and/or non-planar diagrams by differential equations*, *JHEP* **03** (2014) 088, [1312.2588].
- [221] M. Argeri, P. Mastrolia and E. Remiddi, *The Analytic value of the sunrise selfmass with two equal masses and the external invariant equal to the third squared mass*, *Nucl. Phys.* **B631** (2002) 388–400, [hep-ph/0202123].
- [222] D. Maitre, *HPL, a mathematica implementation of the harmonic polylogarithms*, *Comput. Phys. Commun.* **174** (2006) 222–240, [hep-ph/0507152].
- [223] D. Maitre, *Extension of HPL to complex arguments*, *Comput. Phys. Commun.* **183** (2012) 846, [hep-ph/0703052].
- [224] C. Itzykson and J. B. Zuber, *Quantum Field Theory*. McGraw-Hill (International Series in Pure and Applied Physics), New York, 1980.
- [225] E. Panzer, *Feynman integrals and hyperlogarithms*. PhD thesis, Humboldt U., Berlin, Inst. Math., 2015. 1506.07243.
- [226] H. Cheng and T. Wu, *Expanding Protons: Scattering at High Energies*. The MIT Press, 1987.
- [227] N. Nakanishi, *Graph Theory and Feynman Integrals*. Gordon and Breach, New York, 1971.

- [228] L. D. Landau, *On analytic properties of vertex parts in quantum field theory*, *Nucl. Phys.* **13** (1959) 181–192.
- [229] R. J. Eden, P. V. Landshoff, D. I. Olive and J. C. Polkinghorne, *The Analytic S-Matrix*. Cambridge University Press, 1966.
- [230] K. Hepp, *Proof of the Bogolyubov-Parasiuk theorem on renormalization*, *Commun. Math. Phys.* **2** (1966) 301–326.
- [231] E. R. Speer, *The convergence of bph renormalization*, *Commun. Math. Phys.* **35** (1974) 151–154.
- [232] E. R. Speer, *Ultraviolet and infrared singularity structure of generic Feynman amplitudes*, *Annales Poincare Phys. Theor.* **23** (1975) 1–21.
- [233] E. R. Speer, *Mass Singularities of Generic Feynman Amplitudes*, *Annales Poincare Phys. Theor.* **26** (1977) 87–105.
- [234] M. Roth and A. Denner, *High-energy approximation of one-loop Feynman integrals*, *Nucl. Phys.* **B479** (1996) 495–514, [[hep-ph/9605420](#)].
- [235] C. Bogner and S. Weinzierl, *Resolution of singularities for multi-loop integrals*, *Comput.Phys.Commun.* **178** (2008) 596–610, [[0709.4092](#)].
- [236] A. Smirnov and M. Tentyukov, *Feynman Integral Evaluation by a Sector decomposition Approach (FIESTA)*, *Comput.Phys.Commun.* **180** (2009) 735–746, [[0807.4129](#)].
- [237] A. Smirnov, V. Smirnov and M. Tentyukov, *FIESTA 2: Parallelizeable multiloop numerical calculations*, *Comput.Phys.Commun.* **182** (2011) 790–803, [[0912.0158](#)].
- [238] A. V. Smirnov, *FIESTA 3: cluster-parallelizable multiloop numerical calculations in physical regions*, *Comput.Phys.Commun.* **185** (2014) 2090–2100, [[1312.3186](#)].
- [239] A. V. Smirnov, *FIESTA4: Optimized Feynman integral calculations with GPU support*, *Comput. Phys. Commun.* **204** (2016) 189–199, [[1511.03614](#)].
- [240] H. Hironaka, *Resolution of singularities of an algebraic variety over a field of characteristic zero: I*, *Annals of Mathematics* **79** (1964) 109–203.

-
- [241] A. V. Smirnov and V. A. Smirnov, *Hepp and Speer Sectors within Modern Strategies of Sector Decomposition*, *JHEP* **05** (2009) 004, [0812.4700].
- [242] T. Oda, *Convex bodies and algebraic geometry*. Springer, 1988.
- [243] W. Fulton, *Introduction to Toric Varieties*. Annals of mathematics studies. Princeton University Press, 1993.
- [244] B. Grünbaum, *Convex Polytopes*. Graduate Texts in Mathematics. Springer, 1967.
- [245] W. Bruns, B. Ichim, T. Römer and C. Söger, “Normaliz. Algorithms for rational cones and affine monoids. Available from <http://www.math.uos.de/normaliz>.”
- [246] D. Cox, *What is a toric variety?*, in *Topics in algebraic geometry and geometric modeling*, vol. 334 of *Contemp. Math.*, pp. 203–223. Amer. Math. Soc., Providence, RI, 2003. DOI.
- [247] J. Schlenk and T. Zirke, *Calculation of Multi-Loop Integrals with SecDec-3.0*, in *Proceedings, 12th International Symposium on Radiative Corrections (Radcor 2015) and LoopFest XIV (Radiative Corrections for the LHC and Future Colliders)*, 2016. 1601.03982.
- [248] D. Cox, J. Little and H. Schenck, *Toric Varieties*. Graduate studies in mathematics. American Mathematical Society, 2011.
- [249] I. Gelfand, M. Kapranov and A. Zelevinsky, *Generalized euler integrals and a-hypergeometric functions*, *Advances in Mathematics* **84** (1990) 255 – 271.
- [250] J. Stienstra, *GKZ hypergeometric structures*, in *Istanbul 2005: CIMPA Summer School on Arithmetic and Geometry Around Hypergeometric Functions Istanbul, Turkey, June 13-25, 2005*, 2005. math/0511351.
- [251] C. Berkesch, J. Forsgård and M. Passare, *Euler–Mellin integrals and A-hypergeometric functions*, *ArXiv e-prints* (Mar., 2011) , [1103.6273].
- [252] D. E. Soper, *Techniques for QCD calculations by numerical integration*, *Phys. Rev.* **D62** (2000) 014009, [hep-ph/9910292].

- [253] Z. Nagy and D. E. Soper, *Numerical integration of one-loop Feynman diagrams for N-photon amplitudes*, *Phys. Rev.* **D74** (2006) 093006, [[hep-ph/0610028](#)].
- [254] S. Borowka, *Evaluation of multi-loop multi-scale integrals and phenomenological two-loop applications*, *Ph.D. thesis, Max Planck Institute for Physics/Technical University Munich* (2014) , [[1410.7939](#)].
- [255] S. Beerli, *A New method for evaluating two-loop Feynman integrals and its application to Higgs production*. PhD thesis, ETH Zurich, 2008.
- [256] J. Carter, *Higher Order Corrections in Perturbative Quantum Field Theory via Sector Decomposition*. PhD thesis, Durham University, 2011.
- [257] J. Dick, F. Y. Kuo and I. H. Sloan, *High-dimensional integration: The quasi-monte carlo way*, *Acta Numerica* **22** (5, 2013) 133–288.
- [258] Z. Li, J. Wang, Q.-S. Yan and X. Zhao, *Efficient numerical evaluation of Feynman integrals*, *Chin. Phys.* **C40** (2016) 033103, [[1508.02512](#)].
- [259] D. Nuyens, *Fast construction of good lattice rules*. PhD thesis, KU Leuven, 2007.
- [260] G. Bell, R. Rahn and J. Talbert, *Automated Calculation of Dijet Soft Functions in Soft-Collinear Effective Theory*, in *Proceedings, 12th International Symposium on Radiative Corrections (Radcor 2015) and LoopFest XIV (Radiative Corrections for the LHC and Future Colliders): Los Angeles, CA, USA, June 15-19, 2015*, 2015. [1512.06100](#).
- [261] T. Hahn, *CUBA: A library for multidimensional numerical integration*, *Comput. Phys. Commun.* **168** (2005) 78–95, [[hep-ph/0404043](#)].
- [262] T. Hahn, *Concurrent Cuba*, [1408.6373](#).
- [263] Mathematica, Copyright by Wolfram Research.
- [264] P. Gonnet, *Increasing the reliability of adaptive quadrature using explicit interpolants*, *CoRR* **abs/1006.3962** (2010) .
- [265] S. Borowka, G. Heinrich, S. Jahn, S. P. Jones, M. Kerner, J. Schlenk et al., *Numerical multi-loop calculations: tools and applications*, in *17th International workshop on Advanced Computing and Analysis Techniques in physics research (ACAT 2016) Valparaiso, Chile, January 18-22, 2016*, 2016. [1604.00267](#).

-
- [266] W. Bruns, B. Ichim and C. Söger, *The power of pyramid decomposition in Normaliz*, *ArXiv e-prints* (June, 2012) , [1206.1916].
- [267] K. Fukuda and A. Prodon, *Double description method revisited*, in *Selected Papers from the 8th Franco-Japanese and 4th Franco-Chinese Conference on Combinatorics and Computer Science*, (London, UK, UK), pp. 91–111, Springer-Verlag, 1996.
- [268] D. Avis and K. Fukuda, *A pivoting algorithm for convex hulls and vertex enumeration of arrangements and polyhedra*, *Discrete & Computational Geometry* **8** (1992) 295–313.
- [269] C. B. Barber, D. P. Dobkin and H. Huhdanpaa, *The quickhull algorithm for convex hulls*, *ACM Trans. Math. Softw.* **22** (Dec., 1996) 469–483.
- [270] S. Borowka, N. Greiner, G. Heinrich, S. P. Jones, M. Kerner, J. Schlenk et al., *Full top quark mass dependence in Higgs boson pair production at NLO*, 1608.04798.
- [271] ATLAS collaboration, G. Aad et al., *Searches for Higgs boson pair production in the $hh \rightarrow bb\tau\tau, \gamma\gamma WW^*, \gamma\gamma bb, bbbb$ channels with the ATLAS detector*, *Phys. Rev.* **D92** (2015) 092004, [1509.04670].
- [272] CMS collaboration, V. Khachatryan et al., *Search for two Higgs bosons in final states containing two photons and two bottom quarks*, 1603.06896.
- [273] J. Baglio, A. Djouadi and J. Quevillon, *Prospects for Higgs physics at energies up to 100 TeV*, 1511.07853.
- [274] R. Contino et al., *Physics at a 100 TeV pp collider: Higgs and EW symmetry breaking studies*, 1606.09408.
- [275] M. L. Mangano et al., *Physics at a 100 TeV pp collider: Standard Model processes*, 1607.01831.
- [276] J. Baglio, A. Djouadi, R. Gröber, M. M. Mühlleitner, J. Quevillon and M. Spira, *The measurement of the Higgs self-coupling at the LHC: theoretical status*, *JHEP* **04** (2013) 151, [1212.5581].
- [277] T. Plehn, M. Spira and P. M. Zerwas, *Pair production of neutral Higgs particles in gluon-gluon collisions*, *Nucl. Phys.* **B479** (1996) 46–64, [hep-ph/9603205].

- [278] M. Spira, A. Djouadi, D. Graudenz and P. M. Zerwas, *Higgs boson production at the LHC*, *Nucl. Phys.* **B453** (1995) 17–82, [hep-ph/9504378].
- [279] R. Harlander and P. Kant, *Higgs production and decay: Analytic results at next-to-leading order QCD*, *JHEP* **12** (2005) 015, [hep-ph/0509189].
- [280] C. Anastasiou, S. Beerli, S. Bucherer, A. Daleo and Z. Kunszt, *Two-loop amplitudes and master integrals for the production of a Higgs boson via a massive quark and a scalar-quark loop*, *JHEP* **01** (2007) 082, [hep-ph/0611236].
- [281] T. Gehrmann, S. Guns and D. Kara, *The rare decay $H \rightarrow Z\gamma$ in perturbative QCD*, *JHEP* **09** (2015) 038, [1505.00561].
- [282] R. Bonciani, V. Del Duca, H. Frellesvig, J. M. Henn, F. Moriello and V. A. Smirnov, *Next-to-leading order QCD corrections to the decay width $H \rightarrow Z\gamma$* , *JHEP* **08** (2015) 108, [1505.00567].
- [283] S. Dawson, S. Dittmaier and M. Spira, *Neutral Higgs boson pair production at hadron colliders: QCD corrections*, *Phys. Rev.* **D58** (1998) 115012, [hep-ph/9805244].
- [284] D. de Florian and J. Mazzitelli, *Two-loop virtual corrections to Higgs pair production*, *Phys. Lett.* **B724** (2013) 306–309, [1305.5206].
- [285] D. de Florian and J. Mazzitelli, *Higgs Boson Pair Production at Next-to-Next-to-Leading Order in QCD*, *Phys. Rev. Lett.* **111** (2013) 201801, [1309.6594].
- [286] J. Grigo, K. Melnikov and M. Steinhauser, *Virtual corrections to Higgs boson pair production in the large top quark mass limit*, *Nucl. Phys.* **B888** (2014) 17–29, [1408.2422].
- [287] D. de Florian, M. Grazzini, C. Hanga, S. Kallweit, J. M. Lindert, P. Maierhöfer et al., *Differential Higgs Boson Pair Production at Next-to-Next-to-Leading Order in QCD*, 1606.09519.
- [288] D. de Florian and J. Mazzitelli, *Higgs pair production at next-to-next-to-leading logarithmic accuracy at the LHC*, 1505.07122.

-
- [289] R. Frederix, S. Frixione, V. Hirschi, F. Maltoni, O. Mattelaer, P. Torrielli et al., *Higgs pair production at the LHC with NLO and parton-shower effects*, *Phys. Lett.* **B732** (2014) 142–149, [1401.7340].
- [290] F. Maltoni, E. Vryonidou and M. Zaro, *Top-quark mass effects in double and triple Higgs production in gluon-gluon fusion at NLO*, *JHEP* **11** (2014) 079, [1408.6542].
- [291] J. Grigo, J. Hoff, K. Melnikov and M. Steinhauser, *On the Higgs boson pair production at the LHC*, *Nucl. Phys.* **B875** (2013) 1–17, [1305.7340].
- [292] J. Grigo, J. Hoff and M. Steinhauser, *Higgs boson pair production: top quark mass effects at NLO and NNLO*, 1508.00909.
- [293] G. Degrossi, P. P. Giardino and R. Gröber, *On the two-loop virtual QCD corrections to Higgs boson pair production in the Standard Model*, *Eur. Phys. J.* **C76** (2016) 411, [1603.00385].
- [294] M. Kerner, *Next-to-Leading Order Corrections to Higgs Boson Pair Production in Gluon Fusion*, in *13th DESY Workshop on Elementary Particle Physics: Loops and Legs in Quantum Field Theory (LL2016) Leipzig, Germany, April 24-29, 2016*, 2016. 1608.03851.
- [295] S. P. Jones, *Automation of 2-loop Amplitude Calculations*, in *13th DESY Workshop on Elementary Particle Physics: Loops and Legs in Quantum Field Theory (LL2016) Leipzig, Germany, April 24-29, 2016*, 2016. 1608.03846.
- [296] G. P. Lepage, *VEGAS: AN ADAPTIVE MULTIDIMENSIONAL INTEGRATION PROGRAM*, .
- [297] R. Harlander, T. Seidensticker and M. Steinhauser, *Complete corrections of $\mathcal{O}(\alpha\alpha_s)$ to the decay of the z boson into bottom quarks*, *Phys. Lett.* **B426** (1998) 125–132, [hep-ph/9712228].
- [298] T. Seidensticker, *Automatic application of successive asymptotic expansions of feynman diagrams*, hep-ph/9905298.
- [299] M. Steinhauser, *MATAD: A program package for the computation of massive tadpoles*, *Comput. Phys. Commun.* **134** (2001) 335–364, [hep-ph/0009029].

- [300] J. Butterworth et al., *PDF4LHC recommendations for LHC Run II*, 1510.03865.
- [301] S. Dulat, T.-J. Hou, J. Gao, M. Guzzi, J. Huston, P. Nadolsky et al., *New parton distribution functions from a global analysis of quantum chromodynamics*, *Phys. Rev.* **D93** (2016) 033006, [1506.07443].
- [302] L. A. Harland-Lang, A. D. Martin, P. Motylinski and R. S. Thorne, *Parton distributions in the LHC era: MMHT 2014 PDFs*, *Eur. Phys. J.* **C75** (2015) 204, [1412.3989].
- [303] NNPDF collaboration, R. D. Ball et al., *Parton distributions for the LHC Run II*, *JHEP* **04** (2015) 040, [1410.8849].

Acknowledgements

First of all, I want to thank Gudrun Heinrich for her guidance during my graduate studies, for providing me with exciting and challenging projects to work on, and for innumerable discussions and explanations.

I am also grateful to my official supervisor Prof. Wolfgang Hollik for giving me the opportunity to join the phenomenology group at the Max Planck Institute for Physics and to attend several conferences and summer schools.

I would like to thank all former and present members of the GOSAM collaboration, especially Nicolas Greiner, Gionata Luisoni, and Giovanni Ossola for interesting discussions. I am also grateful to the SECDEC team consisting of Sophia Borowka, Gudrun Heinrich, Stephan Jahn, Stephen Jones, Matthias Kerner, and Tom Zirke for the successful collaboration. Thank you to Jan Winter for sharing his knowledge of top quark physics and Monte-Carlo event generators with me.

For making my time at the Max Planck institute much more enjoyable, I thank all members of the phenomenology group, especially the PhD students Henning Bahl, Hans van Deurzen, Stephan Hessenberger, Stephan Jahn, Viktor Papara, Cyril Pietsch, Ulrich Schubert, Ludovic Scyboz, and Johann Felix Graf von Soden-Fraunhofen. In particular I am grateful to my office mates Sophia Borowka, Stephen Jones, Tiziano Peraro, and Tom Zirke for many interesting discussions and a friendly and productive office environment.

Finally, I want to thank my family for their continuous support during my studies.